NASA/TP—2002–210773

Charged Coupled Device Debris Telescope Observations of the Geosynchronous Orbital Debris Environment – Observing Year: 1998

K. S. Jarvis
T. L. Thumm
K. Jorgensen
J. L. Africano
P. F. Sydney
M. J. Matney
E. G. Stansbery
M. K. Mulrooney

April 2002

The NASA STI Program Office … in Profile

Since its founding, NASA has been dedicated to the advancement of aeronautics and space science. The NASA Scientific and Technical Information (STI) Program Office plays a key part in helping NASA maintain this important role.

The NASA STI Program Office is operated by Langley Research Center, the lead center for NASA's scientific and technical information. The NASA STI Program Office provides access to the NASA STI Database, the largest collection of aeronautical and space science STI in the world. The Program Office is also NASA's institutional mechanism for disseminating the results of its research and development activities. These results are published by NASA in the NASA STI Report Series, which includes the following report types:

- TECHNICAL PUBLICATION. Reports of completed research or a major significant phase of research that present the results of NASA programs and include extensive data or theoretical analysis. Includes compilations of significant scientific and technical data and information deemed to be of continuing reference value. NASA counterpart of peer-reviewed formal professional papers, but having less stringent limitations on manuscript length and extent of graphic presentations.

- TECHNICAL MEMORANDUM. Scientific and technical findings that are preliminary or of specialized interest, e.g., quick release reports, working papers, and bibliographies that contain minimal annotation. Does not contain extensive analysis.

- CONTRACTOR REPORT. Scientific and technical findings by NASA-sponsored contractors and grantees.

- CONFERENCE PUBLICATION. Collected papers from scientific and technical conferences, symposia, seminars, or other meetings sponsored or co-sponsored by NASA.

- SPECIAL PUBLICATION. Scientific, technical, or historical information from NASA programs, projects, and missions, often concerned with subjects having substantial public interest.

- TECHNICAL TRANSLATION. English-language translations of foreign scientific and technical material pertinent to NASA's mission.

Specialized services that complement the STI Program Office's diverse offerings include creating custom thesauri, building customized databases, organizing and publishing research results … even providing videos.

For more information about the NASA STI Program Office, see the following:

- Access the NASA STI Program Home Page at ***http://www.sti.nasa.gov***

- E-mail your question via the Internet to help@sti.nasa.gov

- Fax your question to the NASA STI Help Desk at (301) 621-0134

- Telephone the NASA STI Help Desk at (301) 621-0390

- Write to:
  NASA STI Help Desk
  NASA Center for AeroSpace Information
  7121 Standard Drive
  Hanover, MD 21076-1320

NASA/TP—2002–210773

Charged Coupled Device Debris Telescope Observationsof the Geosynchronous Orbital Debris Environment – Observing Year: 1998

K. S. Jarvis
T. L. Thumm
M. J. Matney
Lockheed Martin Space Operations
Houston, Texas

K. Jorgensen
E. G. Stansbery
Lyndon B. Johnson Space Center
Houston, Texas

J. L. Africano
P. F. Sydney
Boeing North American, Colorado Springs, Colorado

M. K. Mulrooney
Ariel Research Company, Houston, Texas

National Aeronautics and
Space Administration

Lyndon B. Johnson Space Center
Houston, Texas 77058

April 2002

Available from:

NASA Center for AeroSpace Information
7121 Standard Drive
Hanover, MD 21076-1320
301-621-0390

National Technical Information Service
5285 Port Royal Road
Springfield, VA 22161
703-605-6000

This report is also available in electronic form at http://techreports.larc.nasa.gov/cgi-bin/NTRS

Contents

Figures

Tables

Acronyms and Nomenclature

AFRL	[United States] Air Force Research Lab
CCD	charged coupled device
CDT	charged coupled device debris telescope
CIS	Commonwealth of Independent States
CT	correlated target
DEC	declination
DOY	day of year
FITS	Flexible Image Transport System
GEO	geosynchronous Earth orbit
GEODSS	Ground-Based Electro-Optical Deep Space Surveillance Systems
GSC	Guide Star Catalog
GTO	geostationary tracking orbit
HA	hour angle
IADC	Inter-Agency Space Debris Coordination Committee
IRAF	Image Reduction and Analysis Facility
LMT	liquid mirror telescope
LRIR	long-range imaging radar
LST	local sidereal time
NAVSTAR	navigation satellite tracking and ranging
NOAO	National Optical Astronomy Observatories
OTA	optical tube assembly
RA	right ascension
RAAN	right ascension of the ascending node
SGP4	simplified general perturbation code
SSN	Space Surveillance Network
UCT	uncorrelated target
UT	universal time

Summary

NASA has been using the charged coupled device (CCD) debris telescope (CDT)—a transportable 32-cm Schmidt telescope located near Cloudcroft, New Mexico—to help characterize the debris environment in geosynchronous Earth orbit (GEO). The CDT is equipped with a SITe 512 × 512 CCD camera whose 576 μm^2 (12.5 arc sec) pixels produce a 1.7 × 1.7-deg field of view. The CDT system can detect 17th-magnitude objects in a 20-sec integration corresponding to an ~0.6-m diameter, 0.20 albedo object at 36,000 km. The telescope pointing and CCD operation are computer controlled to collect data automatically for an entire night. The CDT has collected more than 1500 hrs of data since November 1997. This report describes the collection and analysis of 58 nights (~420 hrs) of data acquired in 1998.

The CDT uses a search strategy optimized to collect data at a low solar phase angle where satellites, including debris, should be brightest. The strategy also makes use of the fact that all objects must pass over the Earth's equator at some point in their orbit. By observing near the GEO belt, all uncontrolled objects will sooner or later pass through the field of view. Specifically, the search strategy used by the CDT observed a strip of GEO space that was 8 deg tall and was centered at –5 deg declination (DEC) (the GEO belt as viewed from Cloudcroft). This strip either leads or follows the Earth's shadow by about 10 deg. The actual length of the strip depends on the length of the night and the elevation of the Earth's shadow. The search pattern starts in the east at the beginning of the night and gradually moves to the west during the remainder of the night, tracking the Earth's shadow.

Studies have shown that the orbits of uncontrolled GEO objects oscillate around the stable Laplacian plane, which has an inclination of 7.5 deg with respect to the equatorial plane. This oscillation is dominated by the combined effects of the Earth's oblateness (J2 term) and the solar and lunar perturbations. The inclination oscillation period is about 50 years. Plots of the daily motion for cataloged GEO objects in right ascension (RA) versus DEC as viewed from Cloudcroft show that most objects are grouped on one side or other of the GEO belt at any given time. By applying this knowledge, the search strategy can be altered to provide higher object counts per observation.

The telescope is pointed to a position in the sky (a search field) and parked during each exposure. The stars leave streaks in the east-west direction due to the Earth's rotation. Objects orbiting the Earth will appear as streaks or points depending on their altitude and inclination. The actual observing sequence consists of a series of four exposures taken of approximately the same field. Each exposure is 20 sec in duration with a 15-sec "dead time" between exposures used to read out the CCD and reposition the telescope. On average, 250 fields are collected per night, or 1000 individual images.

Data from the CDT are processed using a software package originally developed by the [United States] Air Force Research Laboratory for the Raven-class telescope. This software has been ex-tensively modified to account for instrumental differences between Raven and the CDT. The software package performs the following steps:

1) Images are calibrated for dark, bias, and flat-field effects.
2) The sky background is determined and subtracted.
3) The x, y pixel positions for the center of each star streak are determined.
4) The magnitude of each star streak is determined.
5) The x, y pixel positions of the centroid of each satellite are determined.
6) A table of Hubble Guide Star Catalog stars is created that is based on commanded pointing.
7) Gauss's triangles method for field matching
   a) determines true pointing (as opposed to "commanded").
   b) maps the x, y pixel locations to RA, DEC using a 6th-order plate solution.

8) The location and magnitude of each satellite is determined.

Subsequent processing steps performed are:

1) Objects are identified as either Space Surveillance Network-cataloged objects (correlated targets (CTs)) or uncorrelated targets (UCTs).
2) Orbital elements are estimated assuming a circular orbit.
3) Identified UCTs that appear in multiple fields within a night but are the same object are associated with themselves. (No attempt has been made to correlate UCTs from night to night.)
4) Sizes of detected objects are estimated, assuming an average albedo of 0.2.

Figure 1 shows the size distribution of 4900 objects detected in data processed for 1998. The peak of absolute magnitude distribution for CTs corresponds to objects with average diameters of 4.5 m and generally agrees with the known sizes of intact satellites. The peak of the absolute magnitude distribution for UCTs, before it starts to roll off, corresponds to objects with 1.1-m diameters. About 17 % of the UCTs detected have diameters of 1.1 m or smaller. The roll off in distribution reflects the detection capability of the CDT, not the true nature of the population.

1 Introduction

Orbital debris is a concern to all nations that use satellites or launch space vehicles. The debris field scattered near Earth's geosynchronous orbit poses a threat to anything passing through it. In order to mitigate risk and minimize expansion, this debris must be understood. To this end, NASA has been using the charged coupled device (CCD) debris telescope (CDT)—a transportable 32-cm Schmidt telescope located near Cloudcroft, New Mexico—to help characterize the debris environment in geosynchronous Earth orbit (GEO).

Researchers currently are using the CDT to conduct systematic searches of the GEO environment as part of an international measurement campaign under the auspices of the Inter-Agency Space Debris Coordination Committee (IADC). Objectives of the IADC survey are to determine the extent and character of debris in GEO, specifically by obtaining distributions for the brightness, inclination, right ascension (RA) of the ascending node (RAAN), and to determine mean motion for the debris. Tests using the CDT took place in late 1997. Data collection began in January 1998. This report describes data taken during 1998 (a total of ~420 hrs), including 68 hrs of data published in the previous CDT report for NASA, document JSC-28884[1].

2 Background

The GEO environment's debris population has a high potential for collision with operational satellites due to the extremely long lifetimes of the debris. Space-faring nations have been placing both operational satellites and debris in GEO since the mid-to-late 1960s. The debris consists of dead satellites, rocket body upper stages, deployment hardware, small debris, etc. To date, two breakups have been reported in GEO. The 1978 breakup of an EKRAN 2 satellite, Space Surveillance Network (SSN) 10365, went unreported prior to its identification in 1992 by the Commonwealth of Independent States (CIS)[2]. In 1992 a Titan 3C Transtage, SSN 3432, breakup[2,3] produced at least 20 pieces. The Ground-Based Electro-Optical Deep Space Surveillance (GEODSS) telescopes tracked these objects for a few days after the event, but the objects have since been lost.

The CDT was transported to the Hawaiian island of Maui for a survey of the GEO environment conducted by NASA from 1992 through 1994[4]. Results from this survey indicate that, to a limiting apparent magnitude of 17 (~70 cm in diameter), about 27% of all objects in GEO are debris. The actual debris population will be much larger due to the presence of objects smaller than 70 cm in diameter.

3 Observation Overview

3.1 Charged Coupled Device Debris Telescope

The CDT is supported on a massive, three-axis mount designed and built by SciTech Astronomical Research specifically to address orbital debris acquisition and tracking. This three-axis altitude-altitude optical tube assembly (OTA) rotation mount allows for positioning in hour angle (HA) (site-based pointing angle) and DEC (star-based pointing angle), RA (star-based pointing angle) and DEC, or azimuth and elevation (site-based pointing angles). The OTA can be rotated to accommodate motion along any position angle (site-based pointing angle). Depending on specific mission requirements, the mount permits fixed pointing aligned with the satellite track for drift-scan CCD camera operation, programmable tracking for active satellite tracking, and sidereal rate tracking modes. The CDT is shown in Figure 2.

The CDT is equipped with a SITe 512×512 CCD camera. Its pixels are 576 μm^2 (12.5 arc sec), which translate to a 1.7×1.7-deg field of view. Output from the CDT's CCD detector system is an electronic image that is stored as a Flexible Image Transport System (FITS) image file. The CDT system can detect 17th-magnitude objects in a
20-sec integration; this corresponds to an ~0.6-m diameter, 0.20 albedo object at 36,000 km. Telescope pointing and CCD operation are computer controlled to automatically collect data for an entire night. Control files for telescope pointing and data acquisition are created at NASA for each night's observing and are uploaded remotely to the telescope control computer.

3.2 Search Strategy

Numerous studies[5,6] provide compelling arguments that most uncontrolled debris objects in GEO should be at inclinations ≤ 15 deg. Orbits of uncontrolled GEO objects oscillate around the stable Laplacian plane, which has an inclination of 7.5 deg with respect to the equatorial plane. This oscillation is dominated by the combined effects of Earth oblateness (J2 term) and solar and lunar perturbations. The inclination oscillation period is about 50 years. During the first 25 years, an uncontrolled object with an initial inclination of 0 deg will gradually increase in inclination until its inclination has peaked at 15 deg. During the next 25 years, inclination will gradually decrease until the uncontrolled object has returned to its original inclination—in this case, 0 deg. After this the uncontrolled object will begin its oscillation cycle again. Most uncontrolled objects with a different initial inclination will follow the same 50-year pattern of increasing inclination to 15 deg, decreasing to 0 deg, and returning to the original inclination. (There are some cases where inclination will first decrease to zero.) Depending on the insertion RAAN, an uncontrolled object's oscillation can be out of phase with other objects, although these examples are few. Figure 3 shows the inclination of objects in GEO plotted against their launch date. These data, which were taken from the element set file as of day 312, year 1999; plot 804 objects. All objects plotted have mean motions of <1.70 rev/day. The oldest have already peaked in inclination and are now approaching 0 deg inclination again.

There is also a strong correlation between an object's inclination and its RAAN, as illustrated in Figure 4. As a result of the systematic orientation of the orbital planes, objects with a given inclination will be above (or below) the Earth's equator at the same time.

Figure 5 illustrates the daily motion for a set of objects that have mean motions < 1.1 rev/day and inclinations < 17 deg. Notice that the vast majority of the objects are all above or below the equator at the same time. Since most orbital debris will be associated with operational satellites, searches need to be made above or below the equator at appropriate times to maximize the detection rate of the debris. While there may be a few very interesting objects outside of this envelope, most debris will be found near or inside of it.

To detect the smallest debris possible, it is best to observe the debris under nearly face-on (small phase angle) solar illumination. This

condition is most closely obtained for objects near the anti-solar point. Since the Earth's shadow projected into space has a finite angular diameter—on the order of 17 deg at geosynchronous distances—it is impossible to meet the condition of exact face-on illumination (phase angle = 0 deg). Because of problems with the CDT telescope's pointing, which will be described in section 3.5.1, an angular displacement of about 10 deg from the anti-solar point is required to stay clear of the shadow.

Objects detected from any observing station that is more than ~3 hrs from the meridian begin to suffer noticeable atmospheric extinction. Since the objective of this project is to observe small and intrinsically faint debris objects, there is little point in observing outside this window of ±3 hrs from the meridian. Figure 6 illustrates the viewing geometry from Cloudcroft. The solid, nearly straight lines in the figure indicate the extent of the GEO belt as seen from Cloudcroft. Note that while the GEO belt is centered over the Earth's equator, the center is shifted about 5 deg to the south of the equator, at –5 deg DEC. The dashed parabolic curves in the figure indicate constant elevation angles of 60, 30, and 0 deg for a given HA and DEC.

With any search technique, compromises are made. By searching near the Earth's equator, objects will have their largest north-south space motion as they pass through the CDT field of view. Objects at 0-deg inclinations appear motionless in the north-south direction. For objects with 15-deg inclinations, the rates of motion are about 80 sec of arc in 20 sec of time (integration time used for observations). Since each pixel for the CDT is about 12.5 arc sec, the objects leave a trail almost 6 to 7 pixels long. This produces the same effect as decreasing the integration time would, which results in a sensitivity loss. If we were to observe at higher or lower DECs to decrease the north-south space motion of the objects, all objects with inclinations less than the absolute value of the DEC would never be seen.

The search strategy used by the CDT for this dataset is to observe a strip of GEO space 8 deg tall, centered at –5 deg DEC (i.e., the GEO belt as viewed from Cloudcroft). All object ground tracks must pass over the Earth's equator. By observing near the GEO belt, all uncontrolled objects will eventually pass through the field of view. This strip either leads or follows the Earth's shadow by about 10 deg. The actual length of the strip depends on the length of the night and the elevation of the Earth's shadow. The search pattern used by the CDT is shown in Figure 7. Each block represents a field (also known as a "frameset"), and is comprised of four exposure frames. The search pattern starts in the east at the beginning of the night and gradually moves to the west during the remainder of the night, tracking the Earth's shadow.

3.3 Data Collection

The CDT is pointed to a position in the sky (a search field) and parked during each exposure. The stars, because of the Earth's rotation, leave streaks in the east-west direction. Objects orbiting the Earth will appear as streaks or points depending on their altitude and inclination. The actual observing sequence consists of a series of four exposures taken of approximately the same field. Exposures 1 and 2 (see Figure 8) are taken 35 sec apart at the same RA and DEC. If the CDT pointed perfectly, the stars will be in exactly the same positions on exposures 1 and 2. In these exposures the stars appear in roughly the same left-right (east-west) positions but have moved down (north-south) slightly. Encircled are two GEO objects in exposure 1. Three GEO objects (circled) can be seen in exposure 2. While the telescope is at the same RA and DEC, the azimuth and elevation of the two exposures differ slightly, giving a different view of GEO space.

Exposure 3 is taken 35 sec later at the same HA and DEC as exposure 2. The stars now move between exposures 2 and 3 while the GEO objects are detected at the same location. Exposure 4 is taken 35 sec later at the same RA and DEC as exposure 3. Notice that during exposure 4, a bright object (streak) either entered or exited during the exposure. With only one exposure of this object, its direction of motion is unknown.

The exposure pairs at the same RA and DEC (exposures 1, 2 and 3, 4) allow for easy identification of moving GEO objects since the star trails are at the same location on the image and the GEO objects will move to the east (left). The reason for measuring two such pairs is to observe the GEO objects for a longer time, which results in a longer observed arc. This longer arc helps determine the orbital parameters better. Cosmic rays will appear randomly on images. Sometimes two successive frames will have cosmic ray events that mimic a possible detection. Observing two pairs also helps eliminate these false alarms. On average, 1000 fields are collected per night, or 4000 individual images. Appendix A lists a subset of positions and times from a CDT pointing file.

Table 1 provides some details for the data used in this report. Column one lists the month and year of data. The asterisk indicates a day chosen as part of an 11-day sample of the year; these days were selected for more detailed analyses. When the 11-day sample is discussed, it is this subset that is referenced. Subset results have been compared to the complete dataset, which appears to be representative. No bias went into selecting this subset other than to choose days spread across the year and to avoid nights with bad weather. Column two provides the total number of nights observed each month. Columns three and four display the day of year (DOY) of the observations and the hours observed each night. Columns five, six, and seven are the number of objects detected during each night of observation. Column five has the total number of objects detected each night; columns six and seven show the subsets of correlated targets (CTs) and uncorrelated targets (UCTs) making up that total.

The term unique per night (UPN) is associated with both the total number of detections and the CTs. This indicates that, regardless of how many frames or framesets the same object appeared in, that object is counted only once. The UCTs are not UPN. Obvious repeat appearances have been eliminated; but if there are multiple framesets between appearances, each object's RA and DEC must be plotted and examined, as must its multiple associated inferred parameters, in order to eliminate duplicates. This has been done for a select set of data (the sample of 11 nights); specific results are listed later in this report. Although the "number of detections" column (column five) is indicated as UPN, it is actually only UPN with regard to the CTs.

Column eight provides the number of fields. Recall that there are four frames to a frameset. (Frameset and field are used interchangeably in this report.) Column nine lists the number of UPN "nosees." A nosee is a satellite that is predicted (based on orbital parameters) to be in the field of view but which, for a variety of possible reasons, is not seen. An object may be a nosee in one frameset but be seen in the next. If an object is seen at any time during the night of observing, it is not classified as a nosee. Two criteria will eliminate an object from the count:

1) That it was seen but no data could be gathered on it. This can occur if it is a partial streak (only one end of its movement trail is visible) or if it is too close to the edge of the field of view for analysis. In either case, accurate orbital or positional data cannot be gathered on it. It is neither a CT nor a nosee.

2) That it was removed from the nosee list during bad weather. Since bad weather frames are not included in the count, any predicted objects are also removed from the data.

3.4 Data Processing

Over the past 5 years the [United States] Air Force Research Lab (AFRL), located on the Hawaiian island of Maui[7], has developed image reduction software for the Raven small telescope systems project. This software started with the basic Image Reduction and Analysis Facility (IRAF) code developed by the National Optical Astronomy Observatories (NOAO). The main IRAF distribution has a good selection of programs for general image processing and

graphics as well as a large number of programs that reduce and analyze optical and IR astronomy data (the NOAO packages). The IRAF system also contains a complete programming environment for scientific applications that includes a programmable command language scripting facility and a Fortran and C programming interface. By using applications written with these tools, the Raven systems automatically perform the astrometry and photometry required to determine satellite positions and magnitudes.

This code, named "astro," has been transferred from AFRL to NASA for use with CDT data. Instrumental details between the Raven systems used on Maui and the CDT differ significantly; therefore the astro code has been extensively modified to accommodate the CDT data. When astro was first used to reduce CDT data, a large number of "detections" were actually false alarms. Much of this problem has been eliminated through additional code modification. Some code modification is still necessary to increase detection sensitivity for the faintest objects and to enable astro to correctly identify the endpoints of objects that appear as streaks.

Astro works by first reading an image file. The image is divided into 32×32 tiles; a sky background is determined for each tile; and a spline function is fit to the background for the tiles. The functional form of the sky is then subtracted from the image. By knowing the integration time and pixel size, a template can be generated for star streaks. The template is moved over the images; all of the stars, which appear as same-length streaks, are found. The x, y pixel position for the center of the streak is determined, and the integrated intensity along the streak is converted to an instrumental magnitude. Results are stored in a table for later use.

All non-streaked or non-template matching objects, "satellites," are found. The centroid x, y pixel positions and the instrumental magnitudes are determined for the "satellites." A table of reference stars from the Hubble Guide Star Catalog (GSC), which is based on the RA and DEC contained in the FITS header information, is created. The 25 brightest reference star positions are overlain onto the image. The Gauss triangles method for field matching[8] is used to determine any RA and DEC pointing biases (the difference between the observed and commanded position) and any instrument rotation. Using this telescope pointing information, a new reference star table is created; the field matching step is repeated until overall plate solution errors are below a specified threshold of 15 arc sec. Typically astro matches 50 to 100 Hubble guide stars per image with accuracies of about 6 sec of arc or 0.5 pixels. From these stars a final 6th-order plate solution is obtained for converting pixel x, y positions to RA and DEC. This plate solution is used to determine the RA and DEC for the satellites. RA and DEC are in terms of the mean equator and mean equinox of J2000 for the topocentric location of the CDT. Since some of the Hubble guide stars are also photometric standards, they can be used to determine the transformation from the instrumental magnitude to the standard Johnson V (visual) magnitude. This transformation is applied to the satellite instrumental magnitudes to determine Johnson V magnitude. Finally an output file, referred to as an "ast" file, is created that contains the time of observation, positions, and magnitudes for all satellites. This process can take less than 120 sec per image to complete.

Appendix B lists the output file for exposure 1 in Figure 8. This file contains details of the observation including date, time, and length of exposure; filters used (typically no filter is used); commanded RA and DEC of the CDT; number of stars detected; number of Hubble GSC stars used in the plate solution; telescope pointing errors; cataloged and observed RA, DEC, and magnitude for all stars used in the plate solution; and the positions and magnitudes for any detected objects of interest. For exposure 1, 201 stars were detected in the field of view. For this field of view and based on the image header RA and DEC, 100 Hubble guide stars were selected for use in the plate solution. Of these cataloged stars, 57 were used for the final plate solution. Two objects of

interest detected in the field of view were identified as objects 90001 and 90002. There are actually two positions for each object; these are based on the start and stop time of the exposure.

3.5 Data Analysis

This section describes the process of converting the lists of observations (date, universal time (UT), RA, DEC, and magnitude) from astro into lists of catalogued objects (i.e., CTs) and UCTs, as well as into their derivable orbital parameters.

3.5.1 CDT pointing errors

First attempts to reduce the CDT data using astro indicated there were some severe pointing errors associated with the telescope. The Raven systems can point to within several arc minutes, but the CDT is only pointing to tens of arc minutes and sometimes much worse. Astro was modified to track the pointing errors associated with the CDT. Figure 9 shows the pointing error for DOY 93 of year 1998. The RA and DEC biases are computed as the difference in the actual position of the telescope as determined from the background stars minus the commanded position.

In this figure, time increases to the right. For several weeks the CDT pointing errors followed this basic curve. As shown in Figure 10, sometimes the pointing in RA jumps by hundreds of arc minutes. This makes it extremely difficult to find where the telescope was actually pointed. A simple analysis has shown that the trend throughout a night is temperature- and HA-dependent. The large jumps in pointing from one night to the next are due to something slipping or binding in the telescope mount. The CDT was serviced in late November 1999, at which time several problems were found and fixed. Figure 11 shows that the general trend of pointing errors is similar from night to night.

3.5.2 Correlation of detections

For each exposure, the day, year, UT, and true center of the field of view are determined. Then, using the United States Space Command's (USSPACECOM) Simplified General Perturbation (SGP4) code, the satellite catalog is "flown past" the field of view. Any satellites within a 1-deg radius of the center of the field of view are correlated with the detected objects. Results are then output to a file containing all information for all exposures within a given night. Appendix C lists a subset of the file for exposure 1 in Figure 8. The two objects detected in the exposure are correlated and identified with SSN 21041 and 13637. Notice that a third object, SSN 13652, is predicted to be at pixel location 525.4, 309.7. Since the CCD array is 512×512, this third object is just out of the field of view. SSN 13652 is the new satellite that appears to the far right in exposure 2 of Figure 8.

Figure 12 shows the distribution function of the miss-distance. Miss-distance is defined as the absolute value of the difference between observed and predicted RA and DEC positions. Of the correlated satellites, 92% are within 10 arc min of their predicted position while 80% are within 5 arc min. This indicates that the correlation software is working properly. Epoch dates (age of an element set) are known to impact the accuracy of where an object is predicted versus where it is actually located on a given night. Epoch date impact was not evaluated for this chart.

Another way of examining the accuracy of the predicted and actual location is relative to the images in terms of the x, y pixel locations. This is also useful in refining the list of actual nosees versus the list of potential nosees. If a satellite is predicted to be near the edge of a field of view but is not seen, the x, y pixel location errors provide a possible explanation as to why the satellite was not seen.

Fifty-eight nights of data for 1998 were examined, and absolute values were calculated for the observed x, y pixel locations of every object detected in each frameset minus the predicted x, y pixel locations of these objects. These absolute values were then averaged to provide an average x, y pixel location error value for each night of data (Figure 13). There is a biasing of these average values in the datasets used to calculate these averages; every detected

Table 1: Data Log

Month	Total Nights	DOY	Total Hours	Number of Detections UPN	Number of CTs	Number of UCTs	Number of Fields Observed	Numbers of NoSees UPN	Obsered Area Square Degree
March 98									
		60	7:18:35	90	66	24	188.25	14	
*		***61***	***7:15:06***	***95***	***68***	***27***	***187.25***	***16***	
		62	7:36:05	88	66	22	195.75	21	
		63	7:37:50	87	66	21	197	26	
		84	1:08:15	10	8	2	29.5	1	
		88	6:30:11	90	82	8	167.25	5	
Total	**6**		**37:26:02**	**460**	**356**	**104**	**965**	**83**	**2789**
April 98									
		91	8:36:09	114	96	18	221.5	25	
		92	4:56:17	54	49	5	128	27	
		93	9:09:24	100	79	21	235.5	31	
		94	9:28:04	110	84	26	244	40	
*		***95***	***8:16:20***	***118***	***90***	***28***	***213.25***	***25***	
		96	8:33:50	115	89	26	217	27	
		113	8:04:05	137	99	38	207.25	8	
		114	6:30:45	95	75	20	165.25	7	
		115	7:59:25	121	85	36	199.75	4	
		119	5:02:41	71	63	8	130.25	9	
Total	**10**		**76:37:00**	**1035**	**809**	**226**	**1961.75**	**203**	**5669**
May 98									
*		***122***	***8:35:36***	***133***	***108***	***25***	***221.5***	***13***	
		123	5:18:06	82	69	13	136.25	5	
		125	8:21:00	130	99	31	215.25	5	
		126	1:23:24	13	11	2	26.75	3	
		144	7:09:15	90	72	18	184	17	
		146	7:22:06	78	62	16	190.25	14	
		147	7:55:20	102	81	21	204	15	
		148	7:27:55	81	61	20	192	18	
		149	7:02:51	75	60	15	181.75	16	
Total	**9**		**60:35:33**	**784**	**623**	**161**	**1551.75**	**106**	**4485**
June 98									
*		***152***	***7:24:02***	***73***	***62***	***11***	***190.25***	***11***	
		154	7:23:50	74	61	13	190.5	13	
		156	7:11:01	72	59	13	185.25	13	
*		***167***	***6:49:26***	***59***	***53***	***6***	***176***	***10***	
		170	5:34:11	49	45	4	143.25	9	
		174	6:48:16	51	43	8	158.25	10	
		175	6:06:17	55	45	10	157.25	11	
		177	5:18:00	54	43	11	136.5	16	
		179	5:50:37	57	54	3	150.5	15	
		181	6:06:16	60	52	8	148.5	8	
Total	**10**		**64:31:56**	**604**	**517**	**87**	**1636.25**	**116**	**4729**

(Table 1: continued)

Month	Total Nights	DOY	Total Hours	Number of Detections UPN	Number of CTs	Number of UCTs	Number of Fields Observed	Numbers of NoSees UPN	Obsered Area Square Degree
July 98									
*****		***200***	***7:19:10***	***67***	***50***	***17***	***188.25***	***8***	
Total	**1**		**7:19:10**	**67**	**50**	**17**	**188.25**	**8**	**544**
August 98									
*		227	7:33:45	65	49	16	195	10	
		229	8:02:55	82	56	26	190.25	9	
		237	4:06:13	39	31	8	105.75	15	
		243	8:58:39	76	52	24	223.25	18	
Total	**4**		**28:41:32**	**262**	**188**	**74**	**714.25**	**52**	**2064**
Septmber 98									
		255	9:13:29	48	36	12	180	29	
		257	2:23:28	17	12	5	58.75	6	
*****		***265***	***9:13:29***	***71***	***49***	***22***	***229.5***	***21***	
		270	9:17:00	99	62	37	232	16	
Total	**4**	**30:07:26**	**235**	**159**	**76**	**700.25**	**72**	**2024**	
October 98									
		284	3:24:08	28	19	9	87.75	6	
		285	4:04:22	24	18	6	97.5	14	
		288	9:15:15	101	84	17	236.75	19	
*****		***291***	***9:35:39***	***110***	***91***	***19***	***247***	***19***	
		302	5:49:22	101	84	17	150	8	
Total	**5**	**32:08:46**	**364**	**296**	**68**	**819**	**66**	**2367**	
November 98									
		315	9:35:04	145	109	36	247	9	
		318	5:54:36	94	80	14	141.25	2	
*****		***320***	***9:35:38***	***141***	***111***	***30***	***245.5***	***15***	
		326	9:24:34	118	104	14	238.5	8	
		328	8:28:01	121	99	22	218	21	
		330	9:08:49	122	104	18	234.75	18	
Total	**6**	**52:06:42**	**741**	**607**	**134**	**1325**	**73**	**3829**	
December 98									
*****		***347***	***9:35:40***	***124***	***110***	***14***	***251***	***8***	
		350	10:08:19	114	99	15	259.75	12	
		353	10:52:39	110	95	15	248.5	25	
Total	**3**		**30:36:38**	**348**	**304**	**44**	**759.25**	**45**	**2194**
Total	**58**	**58**	**420:10:45**	**4900**	**3909**	**991**	**10620.75**	**824**	**30694**

CT was used. If an object is detected four times in one frame set versus an object that is detected only twice, the result will be weighted toward the object that was detected more often. Improvements are planned for the data reduction code to eliminate this bias in future datasets.

Figure 14 gives an example of the x, y pixel location error seen in a single night, DOY 229. The averaged absolute value for DOY 229 is 7.8 (x) pixels, and 3.9 (y) pixels. While each satellite two-line element set (elset) is independent for an average night, overall this average error value represents the bulk of elsets for that night. Figure 14 illustrates that the error in predicted x, y pixel locations has improved, in part due to improvements to the astro code and its ability to detect endpoints of objects more accurately. The y pixel location error tends to be smaller; this is reasonable given that the preponderance of satellite movement is in the east-west (x) direction rather than in the north-south (y) direction. The error for the y pixel location has been reduced to a little less than 5 pixels (62.5 arc sec). The error in the x pixel location is larger, but it also decreased throughout the year until the average error was reduced to ~15 pixels (187.5 arc sec).

The solid lines in Figure 15 represent the dataset with high-eccentricity objects removed. The dashed lines represent complete datasets, including high-eccentricity objects. High-eccentricity objects do impact the results. Once the weighting bias is removed from the datasets, the removal of objects with high eccentricity is anticipated to have a more apparent effect on the averages and standard deviation calculations. High-eccentricity objects impact y difference results less than x difference results.

3.5.3 Comparison of derived orbital quantities with known objects

The accuracy of the orbital parameters, mean motion, inclination, and RAAN for debris can be inferred from the CTs. The viewing geometry for computing the orbit of an object that passes through the field of view is shown in Figure 16. The rectangular geocentric equatorial coordinate system is used. The X-axis points in the direction of the vernal equinox; the Y-axis, which lies in the plane of the equator, points towards longitude 90 deg; and the Z-axis points toward the celestial North Pole. Both orbital inclination i and the RAAN can be calculated using the spherical triangles in Figure 16. From the spherical triangle defined by points A – the RAAN; B – the sub-Earth satellite position; and P – the Earth's pole,

$$i = \cos^{-1}[\sin(CBA)\cos(BC)]$$

$$\Delta\lambda = \sin^{-1}[\tan(BC)/\tan(i)]$$

$$RAAN = LST + \Delta\lambda$$

where CBA is the angle at which the object crosses the field of view, BC is the sub-satellite latitude, $\Delta\lambda$ (angle CA) is the longitude difference between the sub-satellite longitude and the orbit's ascending node, and LST is the local sidereal time. The proper quadrant for the longitude difference can be determined by inspection.

A reasonable estimate of the altitude of an observed debris object can be obtained from the distance that object moves along arc AB during the exposure sequence, and by assuming the object is in a circular orbit. By knowing the altitude, the mean motion can be determined.

Since some objects only appear in one exposure, the actual time between data points is equivalent to the exposure time, typically 20 sec. Some objects appear in several exposures or fields; the total duration between the first and last observation may be as much as 120 min. Errors associated with determining orbital parameters depend on the time span over which the observations were obtained, inclination and eccentricity of the orbit, and actual pixel size of the CCD.

Two objects, SSN 11635 and SSN 22911, were observed one night over a 30-min interval. These observations can help illustrate the magnitude of errors in determining the inclination, range, and RAAN. These errors are a function of the observation time interval. Additionally, the RAAN error can be impacted

by the inclination while the range error can be affected by the eccentricity of the orbit.

Figure 17 shows the error in inclination, defined as the difference between the observed and known inclination, as a function of the observation time. SSN 11635 has an inclination of 9.8 deg while SSN 22911 has an inclination of 0.03 deg. For objects observed on only one exposure (20-sec duration), the inclination error could be as large as 10 deg. Typically objects are observed over four exposures (140-sec duration), where the inclination error approaches a few degrees.

Figure 18 illustrates the range error as a function of the observation time. SSN 11635 has an eccentricity of 0.481908, and SSN 22911 has an eccentricity of 0.0002154. As can be seen from the figure, the range error can be large, measuring thousands of kilometers for objects with large eccentricities. Large range errors are not unexpected for objects with large eccentricities. These objects spend most of their time at apogee where their space motions are the slowest. By assuming a circular orbit, the determined altitude is overestimated if the object is at apogee, or under-estimated when the object is observed at perigee. Range errors for objects in near-circular orbits tend to be much smaller, measuring in tens to hundreds of kilometers.

Figure 19 illustrates the RAAN error as a function of observation time. For objects with small inclinations, < 1 deg or so, the RAAN is basically undefined. This is because at small inclinations determining where the two planes cross is difficult as the planes are nearly parallel. This can generate very large errors for the RAAN. The RAAN error for SSN 22911 is about 120 deg, but SN 22911 has an inclination of 0.03 deg. For SSN 11635, with a 9.8-deg inclination, the RAAN error is < 5 deg.

3.5.3.1 Inclination determination

Inclination errors that are based on UPN observations for the 11-day sample are shown in Figures 20 and 21. The straight line in these figures shows the trend where the observed inclination equals the known inclination. The observed inclination is being under-determined for the largest inclinations. This is better illustrated in Figures 22 and 23, where the error in inclination (observed inclination minus known inclination) is shown as a function of observed inclination. The average error is 0.03 deg with a standard deviation of 6.3 deg, while the median error is –0.01 deg.

To characterize the effect of the assumptions of a circular orbit on observations, objects with high eccentricities were removed from error measurements (see Table 2).

Table 2: Inclination Errors

Types of Error (reported in degrees)	All Objects	All Objects with eccentricities < 0.04
Average	0.03	–0.2
Standard Deviation	6.3	1.6
Median	–0.01	–0.01

The standard deviation improves while the average error worsens. The average error worsens because the average error for the high-eccentricity objects only is ~2. These data appear to have three linear trends (see Figure 22) and in the smaller range (see Figure 23). One theory was that the correlation of the object was incorrect. However when the right ascension and declination as well as the rate of motion through the field of view were plotted, it was found that the correlations were accurate. A second theory was that the inclination was being affected by the circular orbit assumption, thereby lending a higher inclination error to satellites with higher eccentricities. This is the most plausible. Objects with high eccentricities travel at different velocities at different points in their orbits. Depending on the point in their orbit where the object is observed, that object will generate vastly differing ranges and inclinations.

Rocket bodies and the 80,000s series satellites are marked on the figures, as are the two Delta rocket bodies that were observed.

The 80,000s series satellites are observed satellites that have yet to be assigned a permanent number in the USSPACECOM catalog. This is because they are assigned permanent satellite numbers only after several observations occur so that dependable element sets can be established. In many cases, 80,000s series satellites have few observations; old epoch dates can contribute to large errors associated with their element sets.

Note that only two objects were observed with eccentricities > 0.04 and < 0.2. These objects, which had eccentricities of 0.139 and 0.184, were included in the > 0.2 eccentricity group.

3.5.3.2 Range determination

Range errors based on UPN observations from the 11-day sample can be seen in Figures 24 and 25. The straight line represents the points where the inferred range would equal the known range. Determination of the inferred range is close to the actual range. The average error is 973 km, the median error is 62 km, and the standard deviation is about 4103 km. These errors can be seen in Table 3.

Table 3: Range Errors

Types of Error (reported in km)	All Objects	All Objects with eccentricities < 0.04
Average	973	–23
Standard Deviation	4103	774
Median	62	56

Notice that within the "true" GEO range in Figure 25 no CTs have eccentricities > 0.04. Figures 26 and 27 show the error in range (inferred range minus known range) as a function of inferred range. As with Figure 24, no high-eccentricity objects plot in the true GEO range for Figure 27. As mentioned previously, only two objects were observed with eccentricities > 0.04 and < 0.2, and these had eccentricities of 0.139 and 0.184. These objects were included in the > 0.2 eccentricity group.

Figures 28 and 29 demonstrate the effect of eccentricity on range error. In general, objects with the largest eccentricity have the largest range errors. If objects with eccentricities larger than 0.04 are removed from the calculations for range errors and the average range error is –23 km, the median is 56 km and the standard deviation is 774 km (Table 3).

3.5.3.3 Right ascension of the ascending node determination

RAAN errors based on observations from the 11-day sample, totaling 824 objects, can be seen in Figure 30. The straight line shows the trend line where the observed RAAN would equal the known RAAN. RAAN is meaningless for objects that have inclinations near 0 deg. Scatter in the determination of the RAAN (Figure 30) is mostly due to this fact.

Figures 31 and 32 illustrate the error in RAAN as a function of inclination. In these figures it is clearly seen that the largest errors are associated with the smallest inclinations. For all objects with inclinations > 1 deg, the average error is 9 deg and the median is 4 deg (Table 4). The same effect is seen when objects with eccentricities > 0.2 are removed but the low inclinations are left in. The average error for the whole dataset is 27 deg while the median is 7 deg. A few objects with inclinations > 3 deg have fairly large errors (> 50 deg). These objects were observed for very short times and appeared on only one or two exposures. As explained in section 3.5.3, observations from a single frame will have the largest errors; this is the believed cause for the large errors seen in these few cases.

Table 4: RAAN Errors

Type of Error (reported in degrees)	All Objects	Inclinations > 1 deg	Eccentricity > 0.2
Average	24	9	9
Median	7	4	6
Standard Deviation	91	56	99

3.5.4 Linking UCT observations between search fields within one night

The search pattern used by the CDT occasionally allows for objects to be observed between overlapping adjacent fields. Our code, which uses SGP4, predicts the objects that should be in the field of view. The process for identifying fields with the same UCT is a little more difficult, however.

UCTs typically will be in adjacent search fields or every fifth search field. This is because every sixth field is at the same declination and at roughly 90% of the field of view to the west. When UCTs are in adjacent search fields, association of the same object is easily achieved. When there are several fields between sightings, RA and DEC (as well as other inferred parameters) must be plotted and examined. Figures 33 and 34 show the RA and DEC variation as a function of time, respectively, for two unknown objects observed five search fields apart. If this were the same object, the rate of change of both RA and DEC would be constant over this interval of time and all points would lie on a straight line. This is obviously not the case for these two objects.

Figures 35 and 36 show the RA and DEC variation as a function of time for one object observed over 42 fields, over about 1 hr 45 min. Notice how the points line up over the entire time interval. This is the same object.

A comparison of the repeatability of objects within a given night for the 11-day sample (Table 5) was conducted. The process described above was used to compare the UCTs within a given night to determine whether the object was seen multiple times in the night but given different identification numbers. In order to compare similar type objects, the station-kept CTs were removed from the nightly totals and repeatability was calculated on the remaining objects. As expected, a larger percentage of CTs repeat than of UCTs. Although the objects are similar in the sense of not being station kept, the UCTs are most likely smaller than the CTs; this makes them more difficult to observe repeatedly. The numbers calculated are shown in Table 5; these are the totals and errors associated with the 11-day sample.

Table 5: Repeatability of UCT and CTs Within a Given Night for the 11-day Sample

Object	Numbers	Repeats	Unique Objects	Repeatability (%)
CT	Totals	120	382	31.4
	Average	10.9	36.8	29.6
	Median	8	24	33.3
	Standard Deviation	6.5	21.7	30.0
UCT	Totals	19	199	9.5
	Average	1.7	18.1	9.5
	Median	1	17	5.9
	Standard Deviation	1.7	6.5	25.8

4 Results

4.1 Detection Rates

Fifty-eight days' data were reduced for 1998, starting with DOY 60 and ending with DOY 353. An average of ~7.2 hrs of data was gathered every night, totaling 10,620 fields (with four frames per field). A total of 3909 UPN CTs and 991 UCTs was found, totaling 4900 objects with 20% of the total objects for the year being identified as UCTs. UPN indicates that regardless of how many frames within a night an object appeared in, that object was counted only once. No comparisons were made between nights. Figure 37 provides a pie chart for the two populations. A total of 30,694 square degrees was observed. The number of nosees was 824. Of the 10,620 fields, 56% had no detections while 44% had at least one object detected per field. See Table 6 for totals.

As the repeatability study revealed, CTs had a 31% repeatability while UCTs had a 9.5% repeatability. When the full dataset for 1998 was examined, a 30 to 40% repeatability of CTs was found to occur. It seems reasonable then to

Table 6: Percentage of Fields with Objects

Number of Objects in Field	Number of Fields	Percentage
0	5864	56
1	2764	26
2	1101	11
3	454	4
4	165	2
5	43	< 1
6	50	< 1
7+	31	< 1

assume that approximately 9.5% of the UCTs for the full dataset were unrecognized repeaters. This would reduce the number of actual UPN UCTs to about 900. No data have been removed from the results that follow, but any perceived clustering or spikes may be due in part to the 9.5% repeaters. We expect that future investigations into repeaters will show either a magnitude or an orbital element bias. By understanding the causes behind repeating UCTs, we can better judge our percent chance of seeing objects based on whatever biases may apply (i.e., magnitude, orbital elements, etc.), thus enhancing our population modeling. We can also improve our understanding of the limits of our investigations and generate better projections of what objects we expect to view and what we will not view.

4.2 Location of Detections in Azimuth and Elevation

The location for all observed objects in the Earth-fixed frame of azimuth and elevation is shown in Figure 38. The plotted objects are 3909 UPN CTs and 991 UCTs for 1998 data. An azimuth of 180 deg is due south of the observatory, objects to the east of the observatory will have azimuths < 180 deg, while objects to the west of the observatory will have azimuths > 180 deg. According to CDT report JSC-28884[1], which consists of a subset of 10 nights of the 1998 58-night dataset, there were more observations to the east of Cloudcroft than to the west. If we look at Figure 38, we can see this density change of objects is less apparent when the 58-night dataset for 1998 is plotted. The change is due to increased observational coverage across the year.

There are subtle density changes in both the CT and UCT plots. The plot of the CTs (see Figure 39) shows a minor density decrease in observations around azimuth 150 deg and decreased density from azimuth 210 deg and west. The plot of the UCTs (see Figure 40) shows a relatively even density distribution to the east of due south (< 180 deg), but to the west of due south the density decreases, increases, and then decreases again. This could be due to uneven sampling, bad weather, or generally reduced seeing on some nights, but it may also indicate actual object density differences. As more data are taken and reduced, this question can be resolved.

4.3 Angular Momentum Vector

As previously discussed, the orbits of GEO and near-GEO objects undergo precession under the influence of the Earth's oblateness and the gravity of the Sun and the Moon. As this precession occurs, the ascending node also precesses such that (to the first order for "perfect" GEO objects) there is a one-to-one correspondence of inclination to ascending node. A simple formula to show the relationship between inclination i and RAAN is given by

$$Cos(i) \approx \frac{1 - [x\ Cos(\text{RAAN})]^2}{1 + [x\ Cos(\text{RAAN})]^2}$$

where

$$x = \frac{Sin(7.5°)}{\text{Cos}(7.5°)}$$

This behavior can best be seen by the path of the angular momentum vector of the orbit, which traces an arc during this precession cycle centered about a line tilted 7.5 deg with respect to the North Pole as shown in Figure 41.

An easy way to show the angular momentum vector for measured objects is to plot the orbital data in a polar graph with the ascending node as the polar angle and the inclination as the radius. In Cartesian terms,

$$x = i\ Cos(\text{RAAN})$$
$$y = i\ Sin(\text{RAAN}).$$

In these coordinates, the path traced out during the precession cycle is a loop. Objects found to reside on or near this idealized loop represent GEO or near-GEO objects at various stages in their orbital evolution. Debris from energetic breakups may stray farther from this idealized path, depending on how strong the delta-velocity was that they received at breakup. As can be seen from Figure 42, much of the GEO debris falls along this idealized path.

Figure 43 shows a concise range. Clumping of UCTs around known objects could indicate that the CT is the parent body of the UCT. If we look at Figure 42, we can see some overall clumping as well as a secondary outside ring beginning to form.

4.4 Nosees

Data reduction includes predicting which known satellites from the USSPACECOM catalog will be seen in which frame. If a satellite is predicted to be present but evidence for its presence is not found, it is listed as a nosee. There are many potential reasons for an object's non-detection; e.g., too faint a visual magnitude or speed of drift through a field of view. It is therefore important to understand why an object is not seen because it aids in our understanding of the debris environment and the limits of this method of analysis. Lack of detection of an object does not necessarily mean the object isn't present. It can as easily indicate a change in the orbital elements as it can a breakup. We examined 1998 data to help us better understand the significance of nosees in the debris environment.

The first step was to eliminate any nosees that, while not seen on one night, were seen on a different night. There are several reasons why an object may not have been observed on one night while it was observed on another. (These reasons are applied to the final list of nosees that have no tangible explanation.) For example, an object may have only been predicted in one frame. In that frame it may have been concealed by the track of a star. It may have been beyond the detector's limiting magnitude due to phase angle. It may have been in shadow. Geometry of reflective surfaces for viewing at that particular time may have been such that its visual magnitude was reduced and exceeded the CDT's detection limit. It may have been traveling too quickly through the field of view and timing was such that it was not seen. But since it was seen on a separate evening of data, the object exists; and one of the above explanations is offered for its absence for that night of data where it was predicted but not seen.

Also removed were any objects that, while no data was gathered on their orbits, were seen as a streak. When satellites are moving rapidly through a field of view, they appear as streaks. If both the start and the end of the streak are not visible, any arc calculation and derivable orbital parameters are inaccurate. In rare instances, this is the case. So the object can be removed from the nosee list because it was detected; orbital data simply cannot be calculated.

The USSPACECOM catalog is brought up to date constantly using radar and optical observations to reconfirm an object's location and update its element set. An epoch date is associated with the newest orbital calculations for an object. If USSPACECOM is unable to locate an object for 30 consecutive days, that object is classified as "lost". In other words, its calculated orbital elements are no longer trustworthy. An analysis of epoch dates for seen objects and nosees on 11 nights strongly suggests that this, or even 20 to 25 days, is a reasonable limit to adopt. USSPACECOM's 30-day epoch limit, which errs on the side of caution, seems reasonable to apply to the data. Any predicted satellite with an epoch date older than 30 days has been removed from the nosee count.

As seen in Figures 44, 45, and 46, only one object with an epoch date greater than 30 days is observed. Note that Figure 44 is reported in years, while Figures 45 and 46 are reported in days. If we set a 30-day epoch limit, we would potentially recategorize a very small percentage (< 1%) of objects as UCTs when in fact they would be CTs. To prevent this error, all satellites predicted to be in the field of view are considered and correlated if possible. If the object is not seen, its epoch date age can be offered as a reason for its absence. Figure 46 shows epoch dates for the 11-day sample. These nosees have been shifted by 5 days for visual clarity.

As an aside, an examination of Figure 46 would reveal that DOY 61 is apparently lacking nosees. In fact DOY 61 did have nosees, but two factors contributed to its apparent lack of nosees. First, we eliminated any nosees that were seen on another night. Second, since "astro" uses more than one 2-line element set to generate the predicted satellite list, some of the objects in the prediction file do not appear in the two-line element used by researchers to generate the data for the specific DOY. Therefore, days such as DOY 61 will be missing information on a small number of nosees.

The field of view of the CDT is 512×512 pixels. Analysis of the error in predicted x, y pixel location versus actual x, y pixel location varied from night to night. Any satellite was eliminated that, when the average absolute value of the error for that night was applied, potentially could fall outside of the field of view.

In some instances bad weather made object detection difficult. For frames with bad weather, the limiting magnitude is dramatically decreased. Nosees reported for these frames were thus eliminated from the count. For the 11-night sample, there were 89 nosees (UPN). Of these, 25 (~28%) had potential explanations for the lack of detection of these objects. Of those remaining, only eight (~9%) nosees have GEO orbits. Of those eight, all but one had inclinations between 11.55 and 12.66 deg, and the mean motions of all but one were between 1.07 and 1.1. When compared to the total number of CTs (UPN) in GEO orbit seen in the 11-day sample (759), the nosee rate is ~1%.

Through 58 nights of data collection, 416 (or 513, counting the 80,000s) unique nosees were noted. (As mentioned previously, in many cases 80,000s series satellites have few observations. Old epoch dates can contribute to large errors associated with their element sets.) After eliminating nosees for the above reasons, the number was reduced to 139 (229, counting the 80,000s). Of the 139, an additional 24 can potentially be eliminated due to being a fast-moving object or being predicted close to the edge of the field of view. Of the remaining 115 nosees, limiting magnitude (for any number of reasons such as viewing geometry, albedo, and size) is likely one of the primary reasons for the lack of object detection. Details of the nosees, such as their mean motions, inclinations, etc., will be covered in those sections where the topics are addressed for the CTs and UCTs.

4.5 Mean Motion Distribution

The mean motion distribution for both CTs and UCTs in the true GEO range is shown in Figure 47. The objects in this plot are UPN for the 11-day sample, yielding 89 nosees, 199 UCTs, and 840 CTs. Of the nosees shown in the following plots, 28% have reasons for why the object was not seen. "True" GEO objects have a mean motion near one, while navigational satellite tracking and ranging (NAVSTAR) and many geostationary transfer orbit (GTO) objects have mean motions that are near two. We are observing most objects with mean motions of two or less (see Figure 48). This is encouraging. Objects with mean motions greater than four are dominated by nosees. As shown in Figure 49, the chance of seeing an object decreases greatly as the mean motion of the object increases.

4.6 Inclination Distribution

The UCTs in GEO seem to be fairly well distributed with inclination while the known objects have a strong peak at 0 deg inclination (see Figure 50). In both Figures 50 and 51,

objects plotted were UPN for the 11-day sample. This yielded 89 nosees, 199 UCTs, and 840 CTs. Also in the following plots, 28% of the nosees have reasons for why we did not see the objects. The nosees show a stronger trend toward higher inclinations than both the UCTs and the CTs. In addition, there are three peaks worth noting near 8, 30, and 70 deg. These groupings occur due to high-eccentricity objects such as US GTO and Molniya objects. Moreover, many of the nosees in the three peaks are 80,000s series, which are SSN numbers given to new satellites that have been used over and over for various satellites. This makes the information on these orbits unreliable.

4.7 Visual Magnitude Distribution

The visual magnitude for all objects detected is determined from the background stars within a frame. The CTs peak at about 13th (between 12th and 13th magnitude) magnitude while the UCTs peak at about 16th magnitude. We do note that here, the 11-day sample shows some discrepancy with the full 58-day dataset. For the full dataset, the peak for the year is between 15th and 16th magnitude; but for the 11-day sample, which is Figure 52, it is between 13th and 14th magnitude. The roll off in distribution reflects the detection capability of the CDT, not the nature of the population. Objects used in the visual magnitude charts are UPN for the 11-day sample, yielding 838 CTs and 199 UCTs.

4.8 Absolute Magnitude Distribution and Derived Diameters

Even if all detected objects are identical, they would not all appear to be the same brightness (visual magnitude) because they are at different distances from the CDT. This is because the brightness recorded by the CDT for each object is inversely proportional to the square of the object's distance (range) and directly related to the surface area of the object. Range dependence must be removed to compare the sizes of objects. Brightness (absolute magnitude) for all objects was determined from visual magnitude and range. The standard distance used was 36,000 km. Phase angle was corrected to 0 deg. The absolute magnitude distribution is shown in Figure 53. The roll off in the distribution reflects the detection capability of the CDT, not the true nature of the population.

Diameters can be derived from these observations. To do so, an object's albedo must be known or a reasonable assumption concerning it must be made. Talent et al.[4] determined that a 0.2 albedo is appropriate to use for most GEO objects. If we use this assumed albedo, the corresponding diameters are shown in Figure 53. It can be seen from Figure 53 that the CDT is detecting objects smaller than 70 cm in diameter. The peak of distribution for the CTs corresponds to objects with average diameters of 4.5 m. These results generally agree with the known sizes of intact satellites.

4.9 RAAN versus Inclination Distribution

Figure 54 illustrates the distribution of inclination with respect to the RAAN for CT, UCT, and nosees observations for the entire range. Figure 56 shows the "true" GEO range for just the CT and UCT observations where the nosees were not plotted for emphasis. As expected, this distribution matches the catalog distribution as shown in Figure 4. Also as expected, the UCTs are found at all inclinations. In Figure 54 objects are UPN for the 11 nights listed in Table 1, producing 89 nosees, 199 UCTs, and 840 CTs, where 28% of the nosees have reasons why we did not see them. Most of the CT objects (Figure 55) are, as expected, near zero inclination. Furthermore, the nosees seemed to be grouped into three regions as mentioned in section 4.6.

4.10 Range versus Inclination Distribution

Figure 56 shows the inferred range versus (inferred) inclination distribution for CT, UCT, and nosee observations. Figure 57 depicts the same distribution, but only for CTs and UCTs in the "true" GEO range. Notice the hard break in correlated objects that occurs at about 14 deg. This break, which is to be expected, is related to the oscillation in the inclination discussed previously. Again the three groupings of nosee inclinations are apparent.

4.11 Phase Angle

Figure 58 displays the phase angle for observed CTs as well as the predicted values for the nosee objects for the 11 nights. It is interesting to note that the phase angle does not seem to be a factor as to why we are not seeing the object predicted.

5 Conclusion

By today's standards of 8- and 10-m-class telescopes, the CDT is a very small telescope. The limiting magnitude is only about 17th magnitude in a 20-sec integration, yet 20% of the objects detected are UCTs. Assuming an albedo of 0.2, the CDT is detecting objects down to about 60 cm in diameter at GEO. Of the frames, 46% have at least one object in the field of view.

CDT data are processed using a software package called "astro" that was originally developed for the Raven-class telescope by the AFRL. Software has been extensively modified to account for instrumental differences between Raven and the CDT. Serious pointing errors were detected during the initial data reduction runs. These errors were both large jumps (e.g., as much as three fields of view) from night to night and smaller systematic trends throughout a night. Manual procedures were developed to determine where the telescope was actually pointing at the beginning of each night based on star background. Procedures were also developed to automatically track the pointing error trends throughout the night. Since an investigation into the cause of these problems resulted in both software and hardware problems being found and fixed, data collected since November 1999 should be much better behaved.

Correlation software was written to determine which of the detections correlated with catalog objects. This software automatically processes the results from astro. For this dataset, 80% of all detections were within 5 arc min of the predicted position while 92% of all detections were within 10 arc min of the predicted position. Since November 1999, the astro code has been modified to include correlation software written by the Space Warfare Center. Now detections are correlated to the catalog as astro finds them in individual frames.

From the correlated objects, estimates can be made as to the errors associated with the derived quantities of range, inclination, and RAAN. For objects in near-circular orbits and with inclinations > 1 deg, the average range error is –23 km, the average inclination error is –0.2 deg, and the average RAAN error is 9 deg. Some of the error in each quantity is also due to the length of time the object was observed. The largest errors occur for objects observed on only one frame where the total length of the observation is only 20 sec. Overall these are good results that lend credibility to the UCT results.

The UCT results are not surprising. Distributions for mean motion, inclination, and RAAN are very similar to the correlated population. The peak of the absolute magnitude distribution for the CTs corresponds to objects with average diameters of 4.5 m. This result generally agrees with the known sizes of intact satellites. The peak of the absolute magnitude distribution for the UCTs corresponds to objects with 1.1-m diameters and then starts to roll off. About 17% of the detected UCTs have diameters 1.1 m or smaller. The roll off in distribution reflects the detection capability of the CDT, not the true nature of the population. Repeatability studies suggest that ~9.5% of the reported UCTs may be the same object identified as two separate objects within the same night. For the CTs, a repeatability of ~30% within a night appears typical. Satellites with element sets with epoch dates older than 30 days are unlikely to be found; in general, epoch dates younger than 20 days appear to be necessary. Logical reasons for nosees to occur can be provided for most of the predicted-but-not-seen objects. For those without explanations, it is believed that limiting magnitude is the primary factor. For this observing strategy, the chance of seeing an object drops off significantly if that object's mean motion is > 1.06.

In summary, the CDT technology, like other small telescope programs[9,10], has proven itself to

be a cost-effective way of providing large amounts of data on objects as small as 60 cm in diameter in GEO. Data collection is automated and very efficient. Data processing, on the other hand, is time-consuming at this point. However, the time to process data is improving and has been dramatically reduced—by more than 60%—since February 1999. Steady improvements are being made to the reduction code in order to increase the detection sensitivity, reduce the number of false detections, and increase the speed of processing.

References

1. Africano, J. L., et al., *CCD Debris Telescope Observations of the Geosynchronous Orbital Debris Environment*, JSC-28884, January 2000.
2. Orbital Debris Program Office, *History of On-Orbit Satellite Fragmentations*, JSC-28383, Houston, TX, 2001.
3. Pensa, A. F., et al., "Debris in Geosynchronous Orbit," *Space Forum*, Vol. 1, 1996, pp 23-27.
4. Talent, D. L. et al., "A Search for Debris in GEO," *Proceedings of the Second European Conference on Space Debris*, Darmstadt, Germany, March 17-19, 1997, pp 99-104.
5. Friesen, L. et al., "Results in Orbital Evolution of Objects in the Geosynchronous Region," AIAA 90-1362, AIAA/NASA/DOD Orbital Debris Conference: Technical Issues and Future Directions, Baltimore, MD, April 16-19, 1990.
6. Vaughan, S. H. and Mullikin, T. L., "Long Term Behavior of Inactive Satellites and Debris Near Geosynchronous Orbits." AIAA 95-200, AAS/AIAA Spaceflight Mechanics Meeting, Albuquerque, NM, February 13-16, 1995.
7. Sydney, P. et al., "Near Earth Object (NEO) Characterization at the Maui Space Surveillance System (MSSS)," Space Control Conference. Lexington, MA, March 25-27, 1997.
8. Groth, E. J., "A Pattern-Matching Algorithm for Two-Dimensional Coordinate Lists," *AJ*, Vol. 91, No. 5, May 1986.
9. Nishimoto, D. L., et al., "Raven: The Evolution of Small Telescopes," *1999 AMOS Technical Conference.* Wailea, HI, September 1999, pp 389-394.
10. Bisque M. and Bisque S., "Leveraging Software to Make Highly Productive Robotic Telescope Systems," *1999 AMOS Technical Conference.* Wailea, HI, September 1999, pp 395-400.

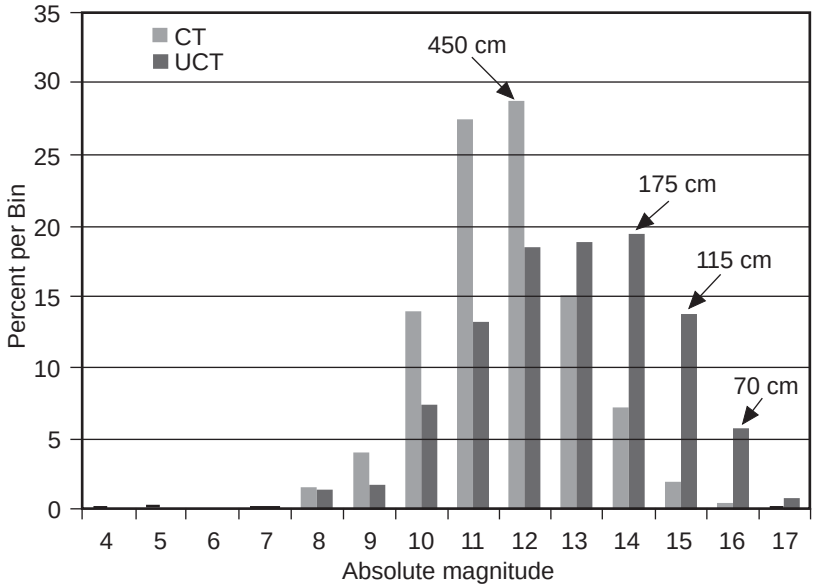

Figure 1: Absolute magnitude and derived size distribution.

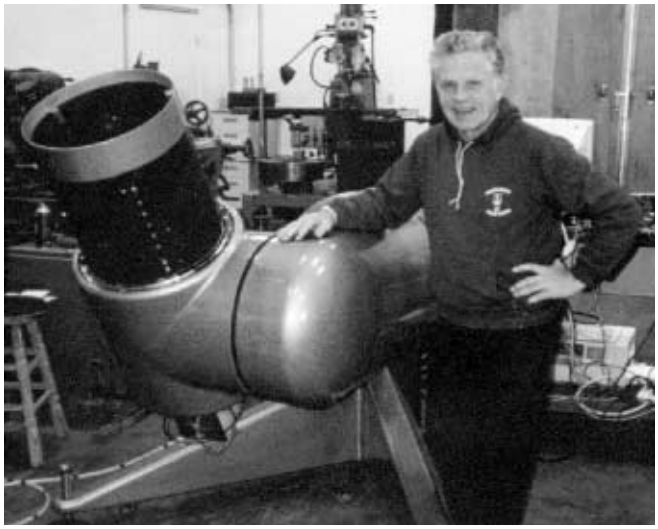

Figure 2: The CDT and Karl Henize.

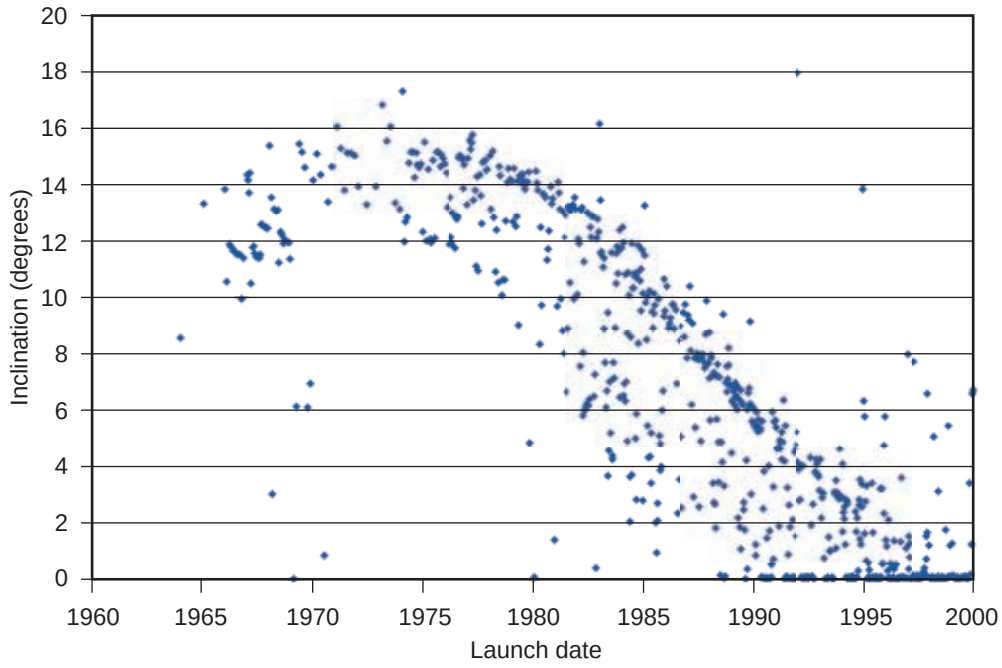

Figure 3: Inclination vs. launch date.

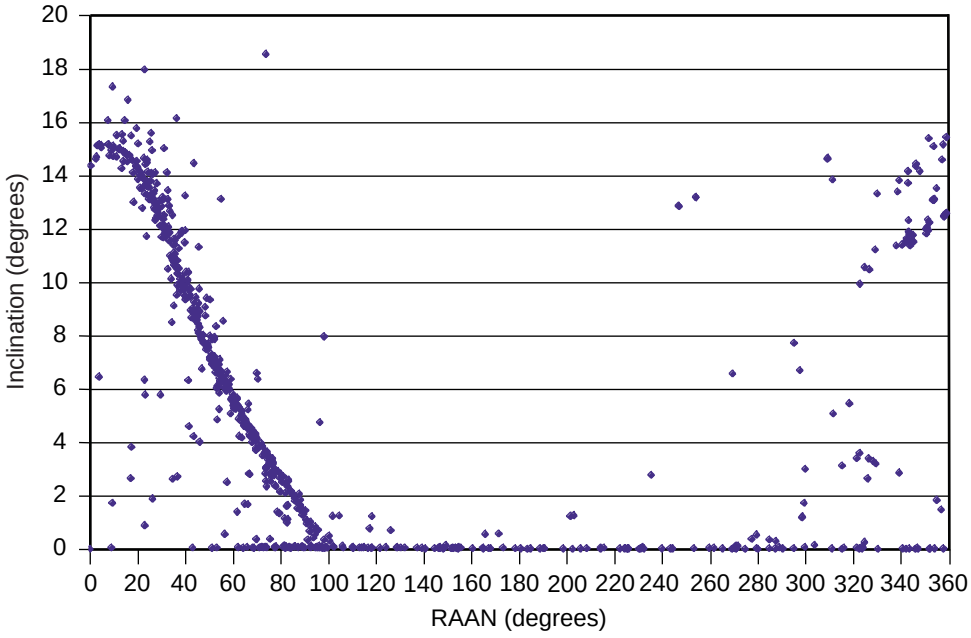

Figure 4: RAAN vs. inclination for near-GEO objects.

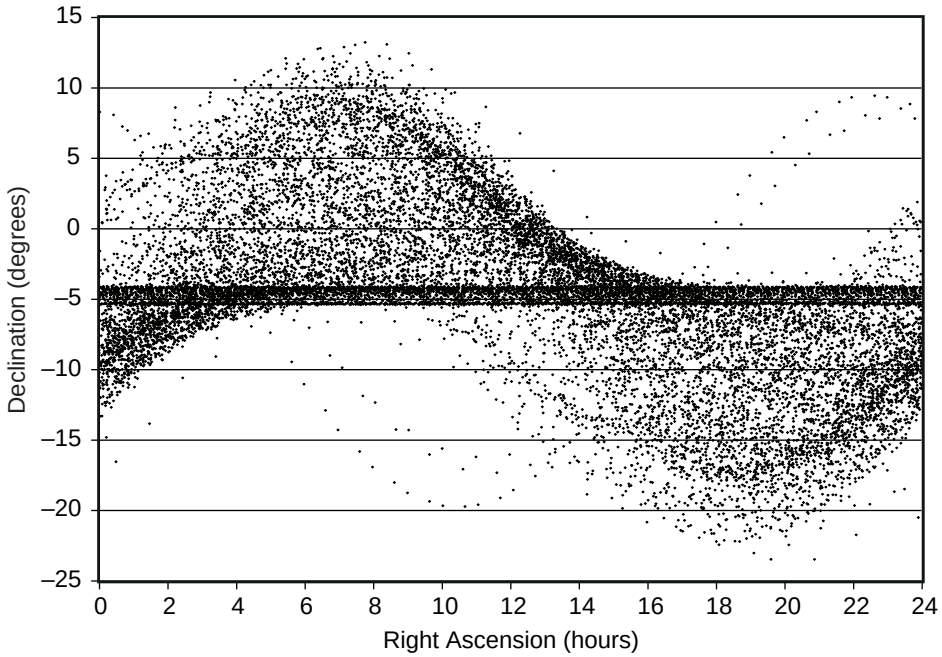

Figure 5: Daily motion for GEO objects (RA vs. DEC) as viewed from Cloudcroft.

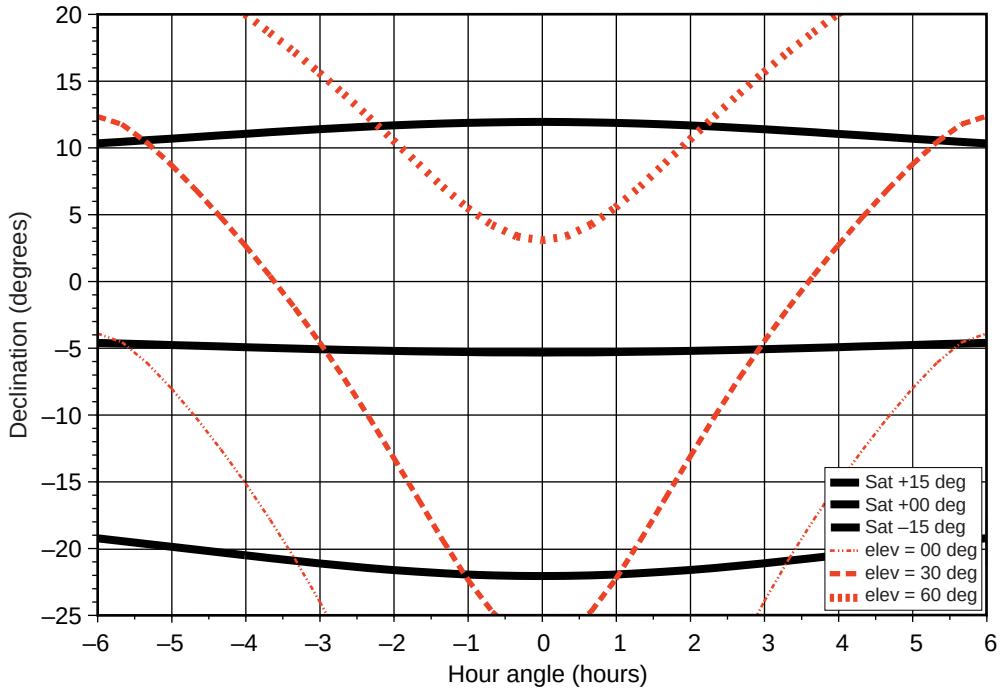

Figure 6: Geosynchronous objects as viewed from Cloudcroft.

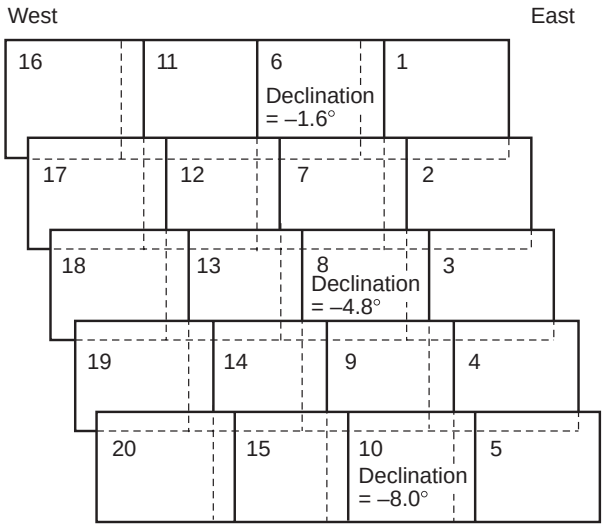

Figure 7: Search pattern used by the CDT.

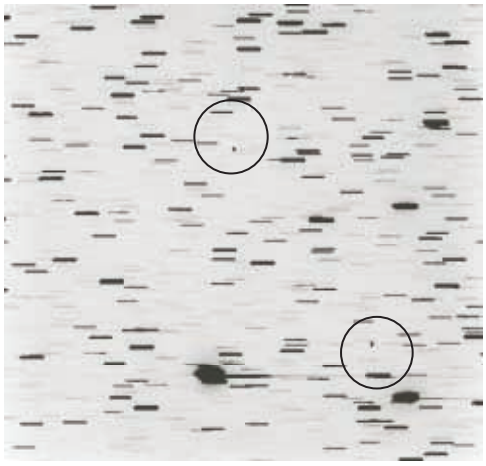

Exposure 1

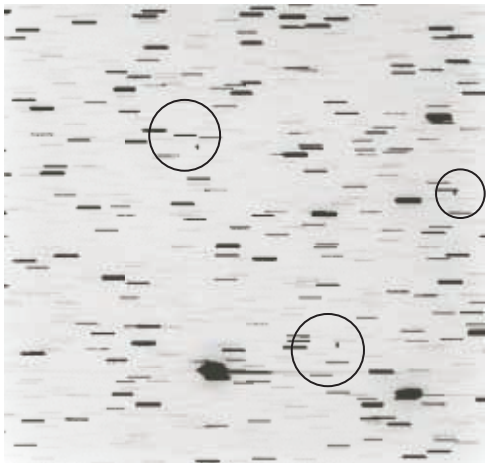

Exposure 2

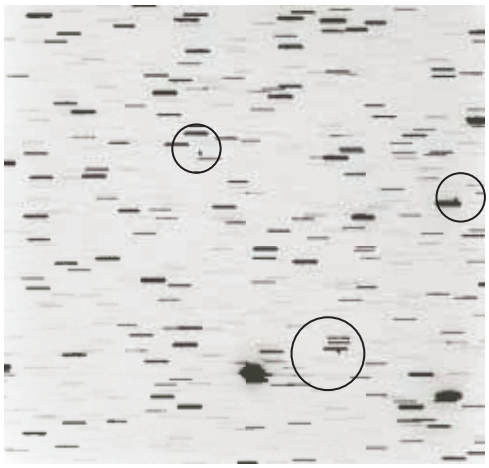

Exposure 3

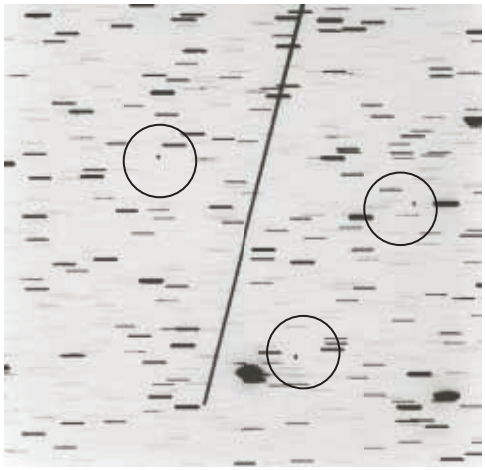

Exposure 4

Figure 8: Exposures 1, 2, 3, and 4 from a typical observing sequence.

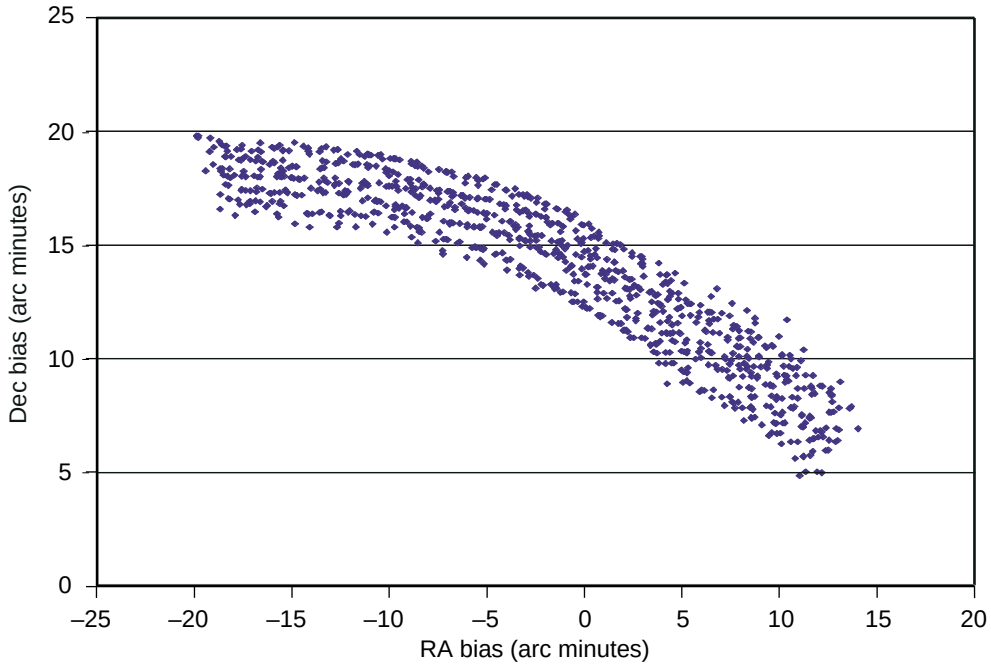

Figure 9: RA and DEC pointing biases for DOY 93, 1998.

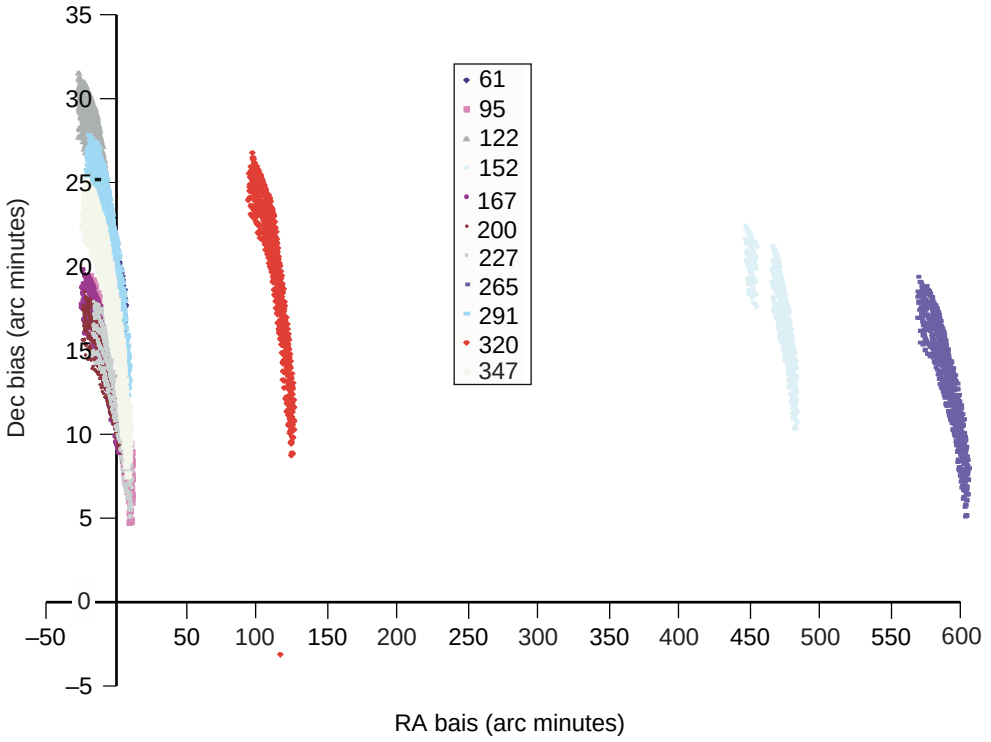

Figure 10: CDT pointing errors from several nights in 1998.

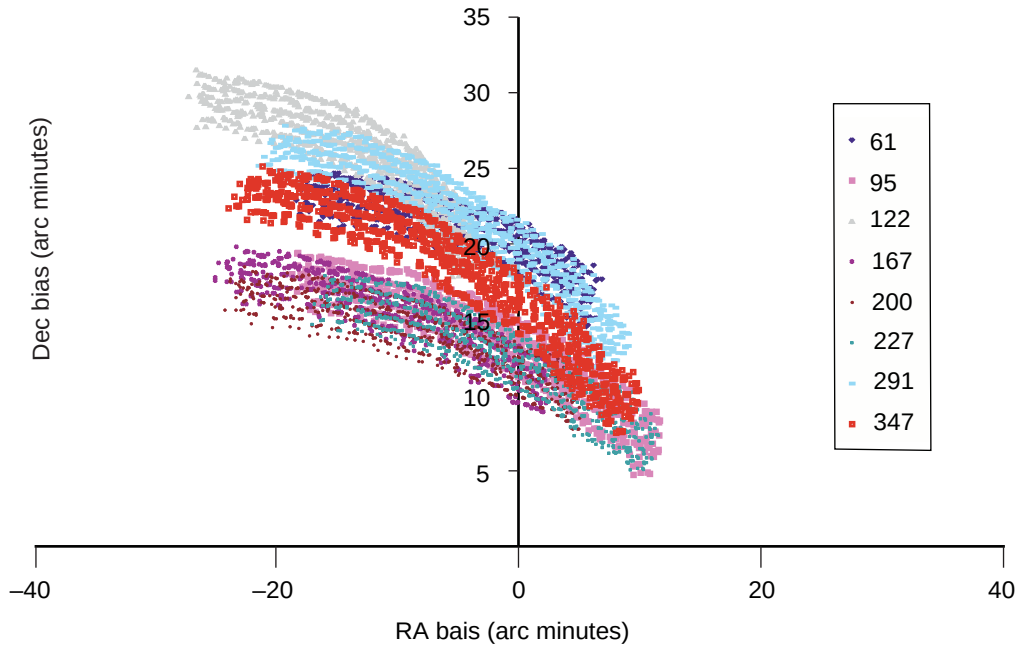

Figure 11: CDT pointing errors for subgroup of select days.

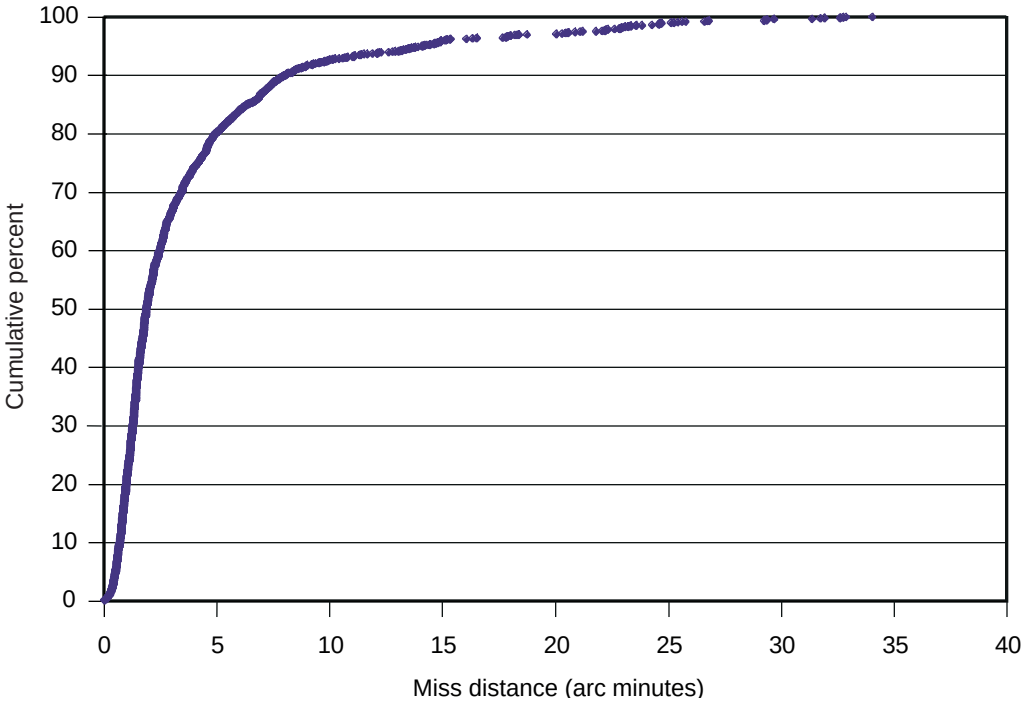

Figure 12: Distribution function of miss-distance for the correlated objects.

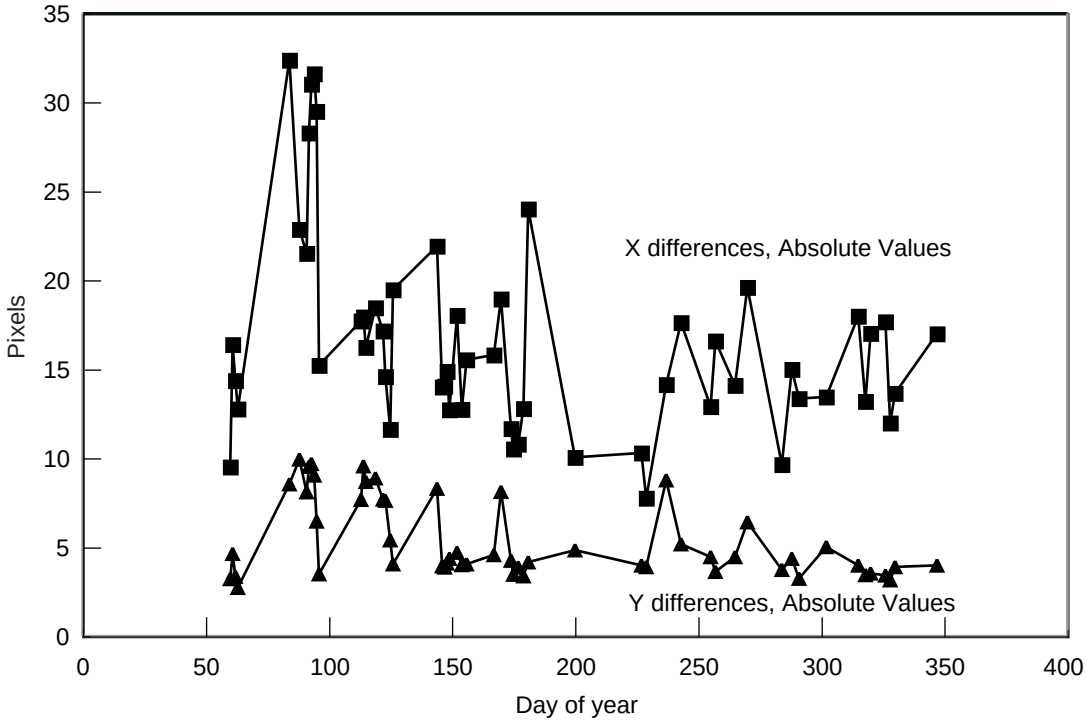

Figure 13: Average displacement of pixels per night.

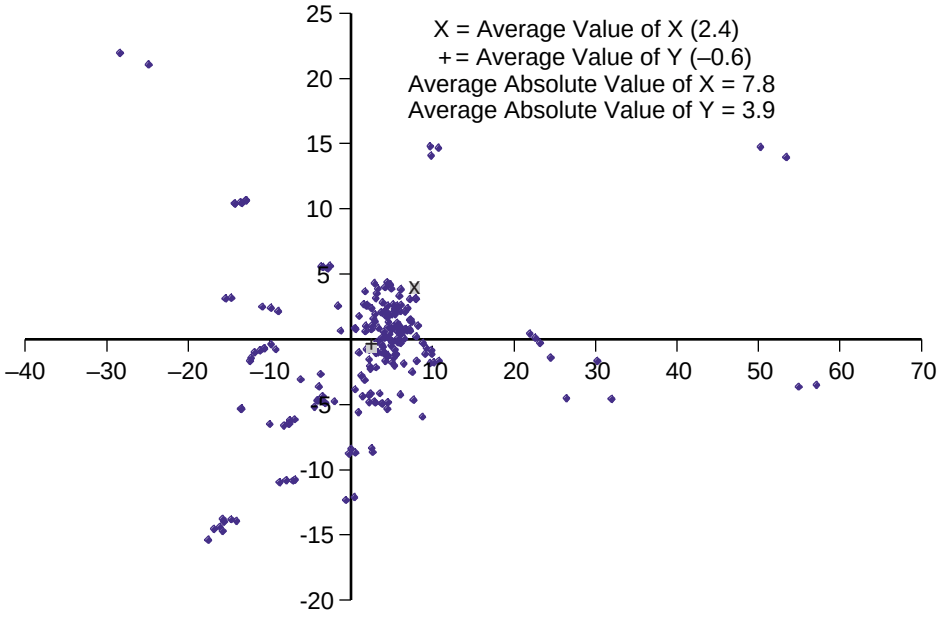

Figure 14: Average displacement of every CT for DOY 229.

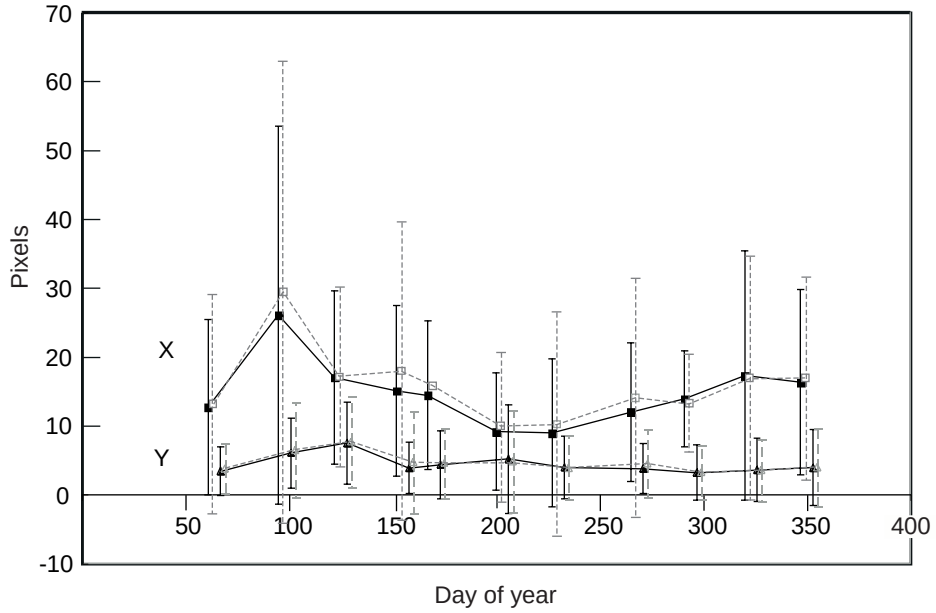

Figure 15: Standard deviation of x, y pixel location differences.

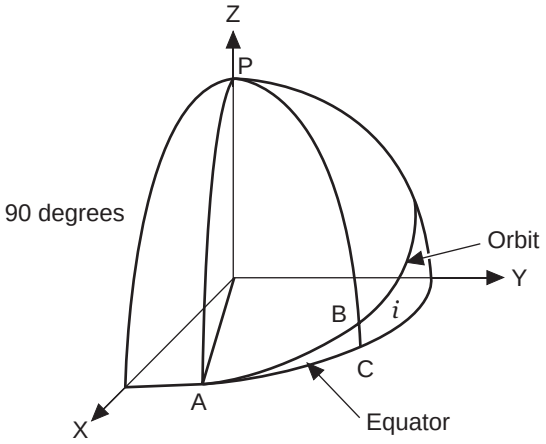

Figure 16: Geometry for computing orbital parameters.

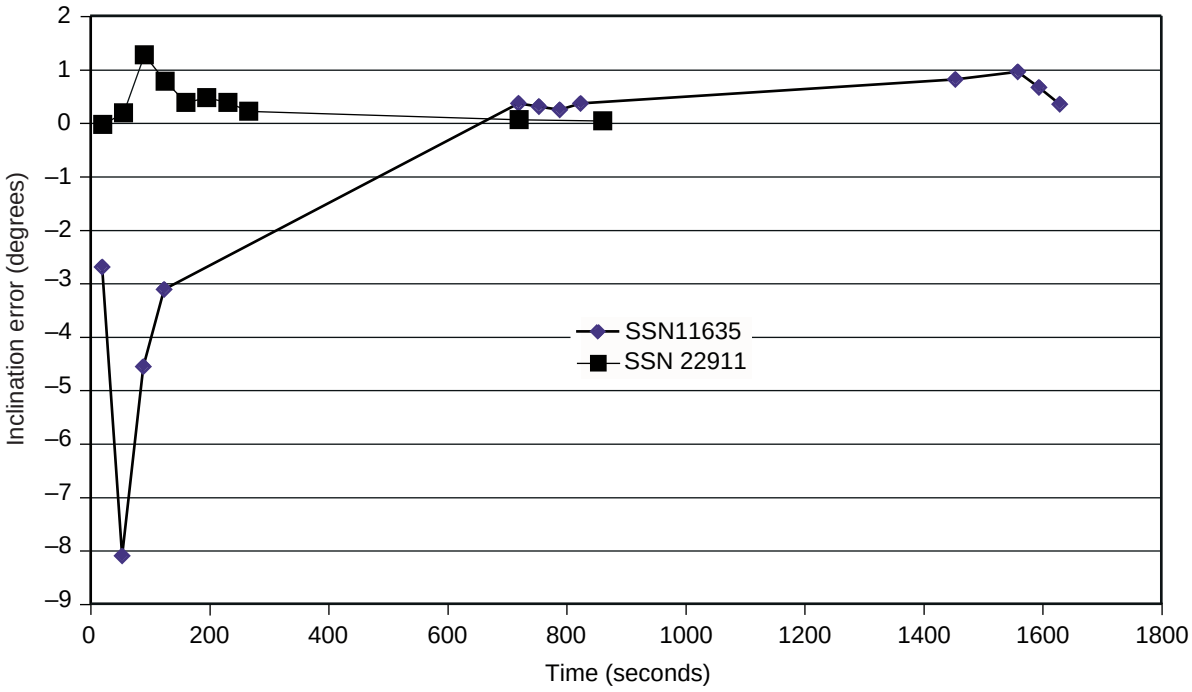

Figure 17: Inclination error as a function of observation time.

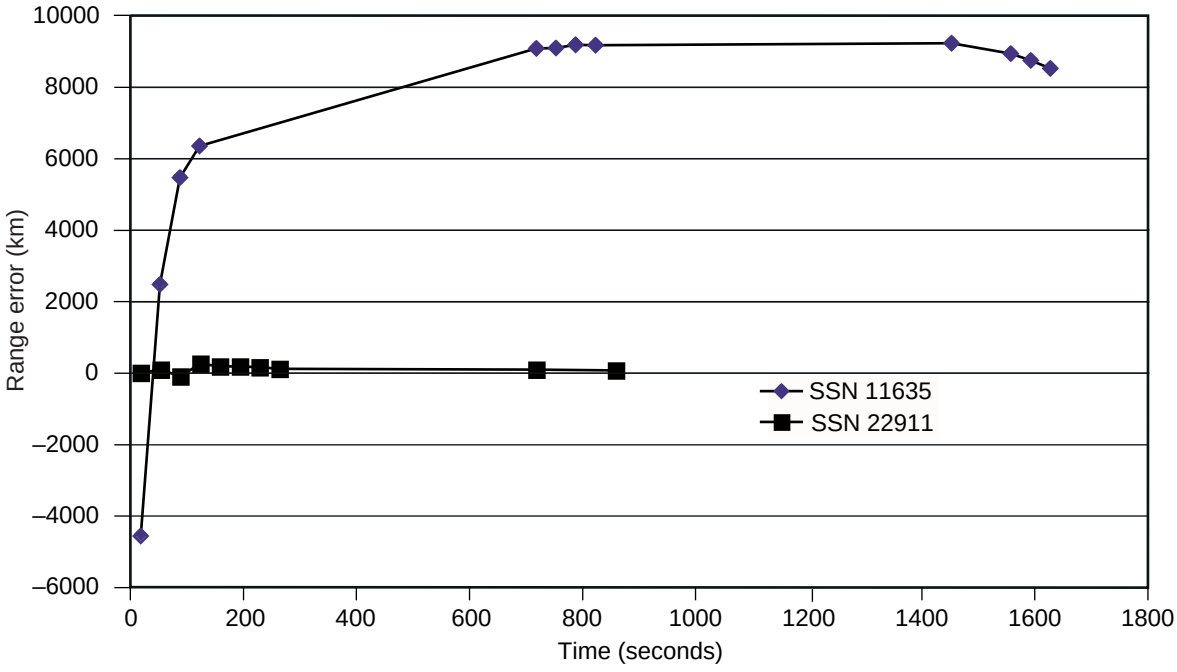

Figure 18: Range error as a function of observation time.

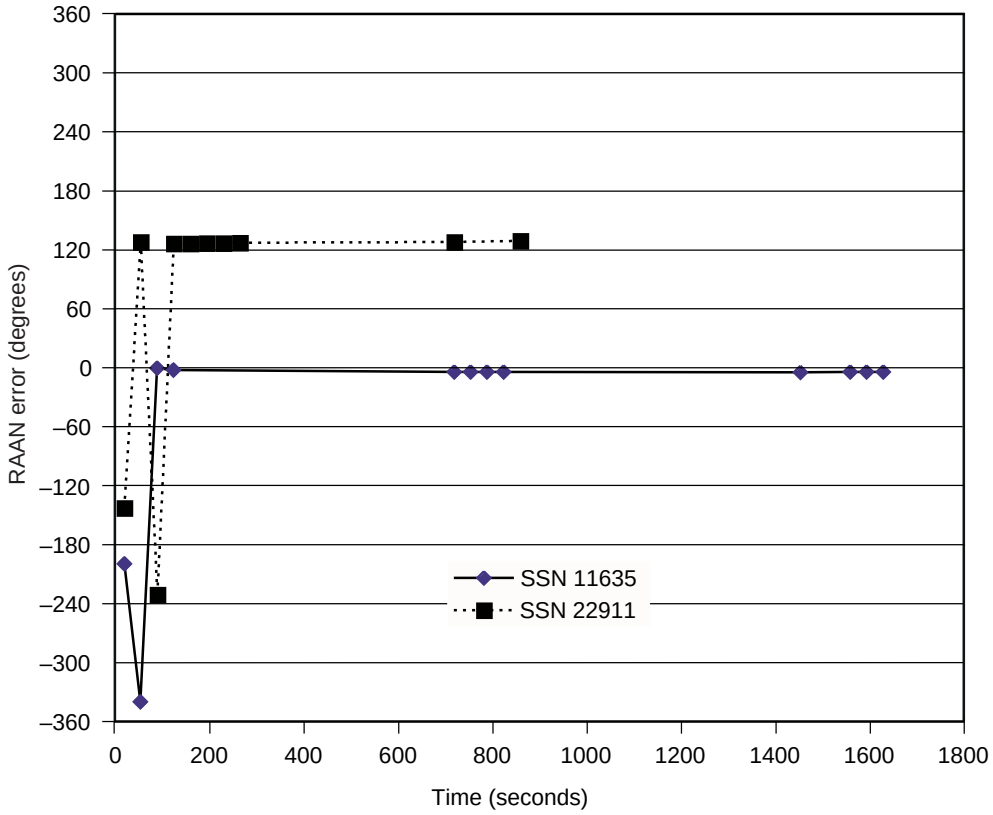

Figure 19: RAAN error as a function of observation time.

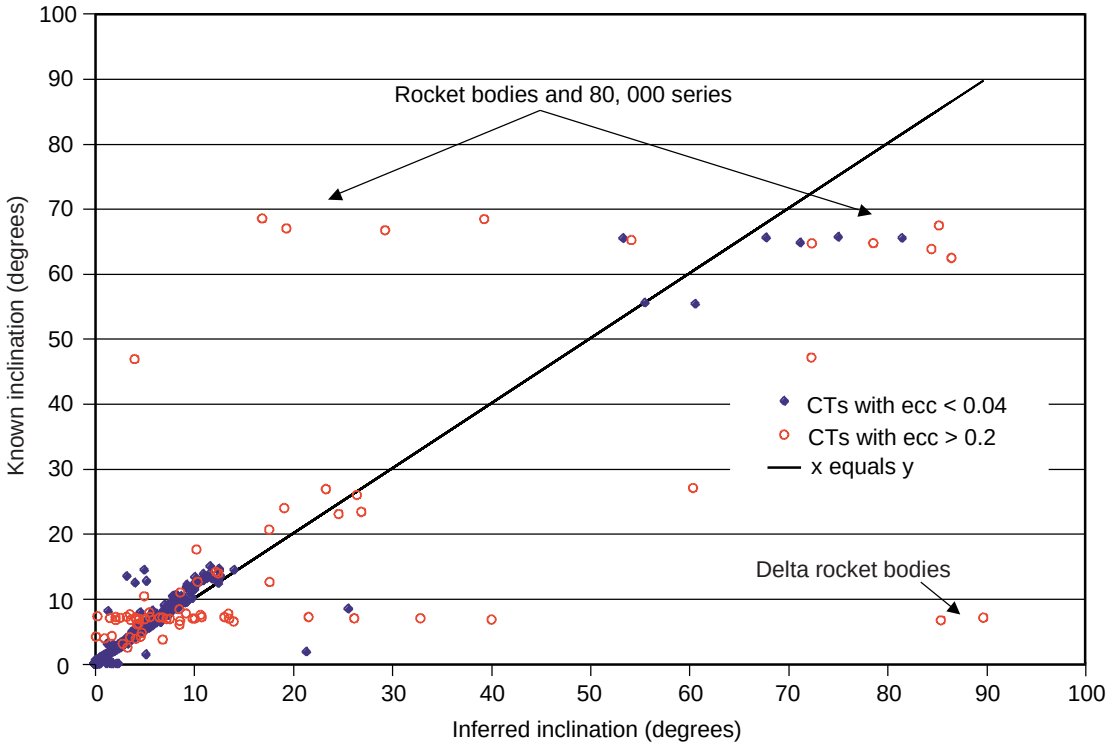

Figure 20: Inclination comparison for correlated satellites, entire range.

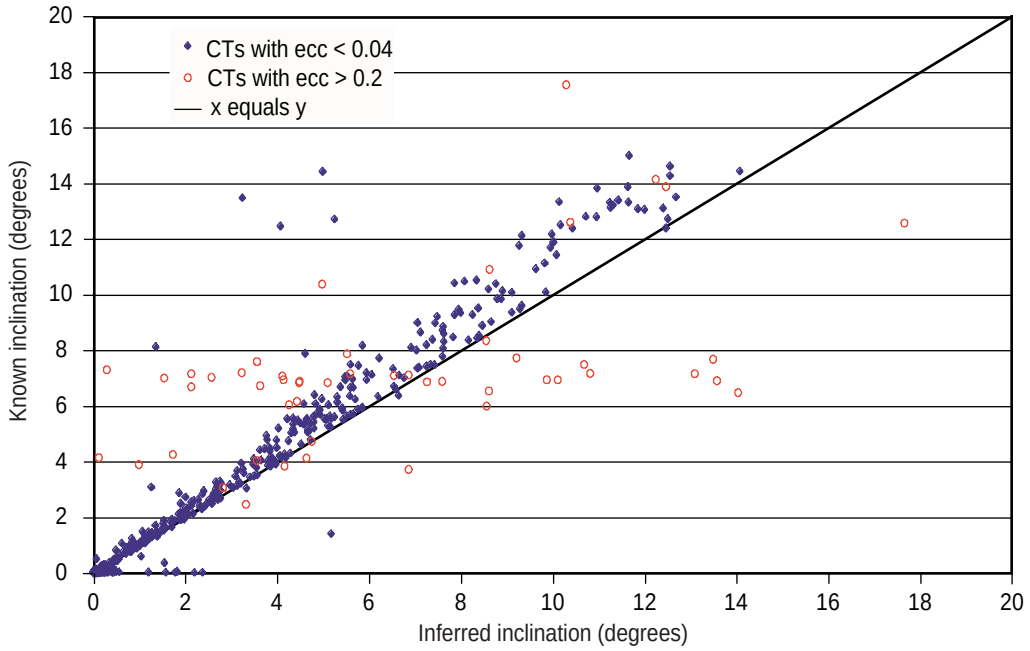

Figure 21: Inclination comparison for correlated satellites, concise range.

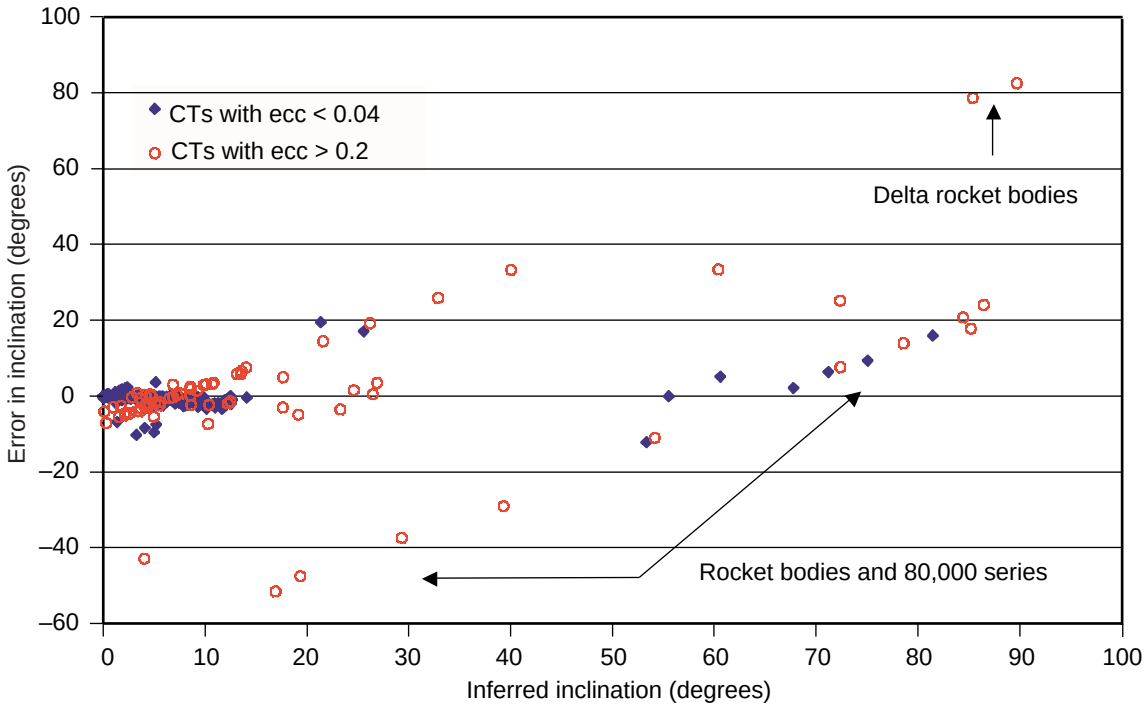

Figure 22: Inclination error as a function of inclination, entire range.

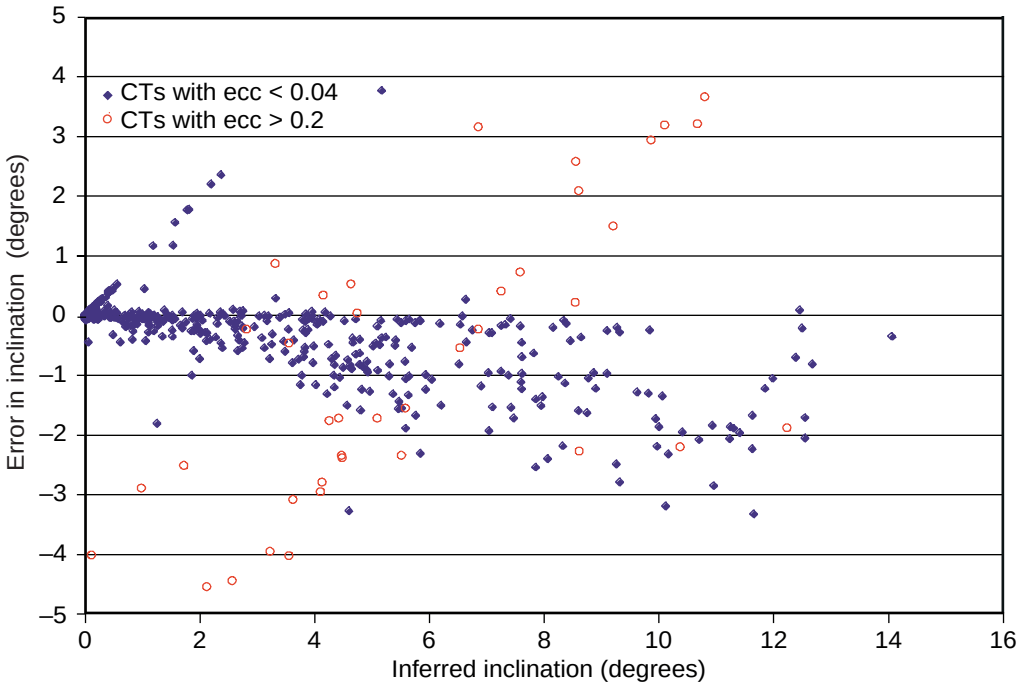

Figure 23: Inclination error as a function of inclination, concise range.

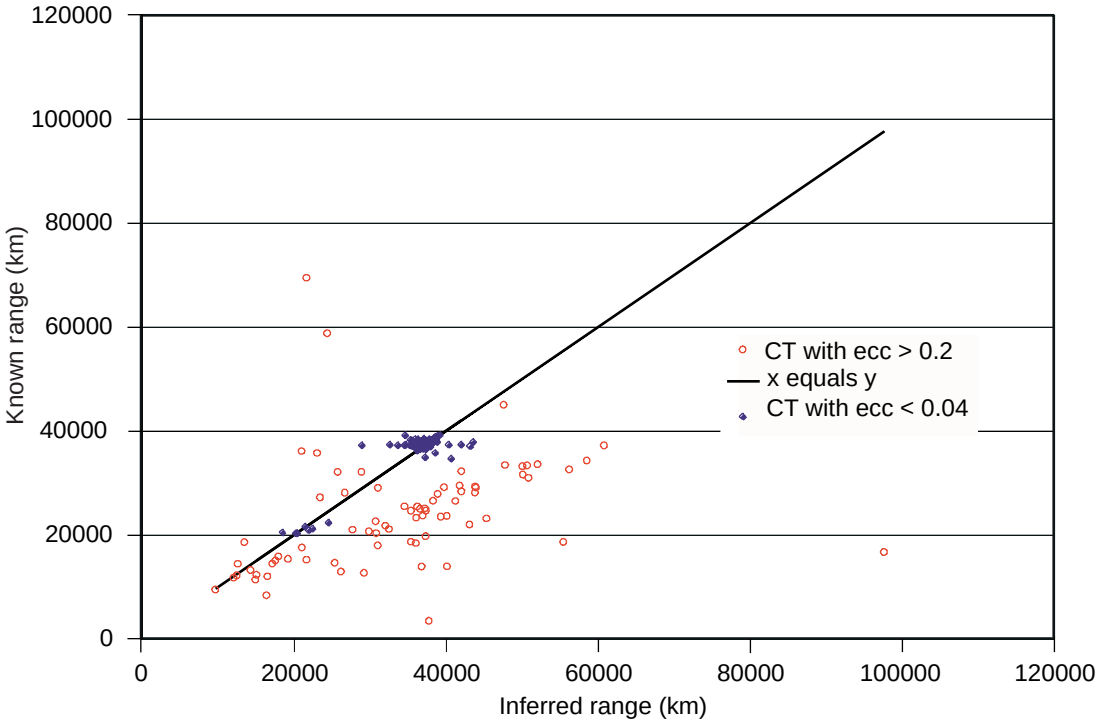

Figure 24: Comparison of inferred and known ranges, entire range.

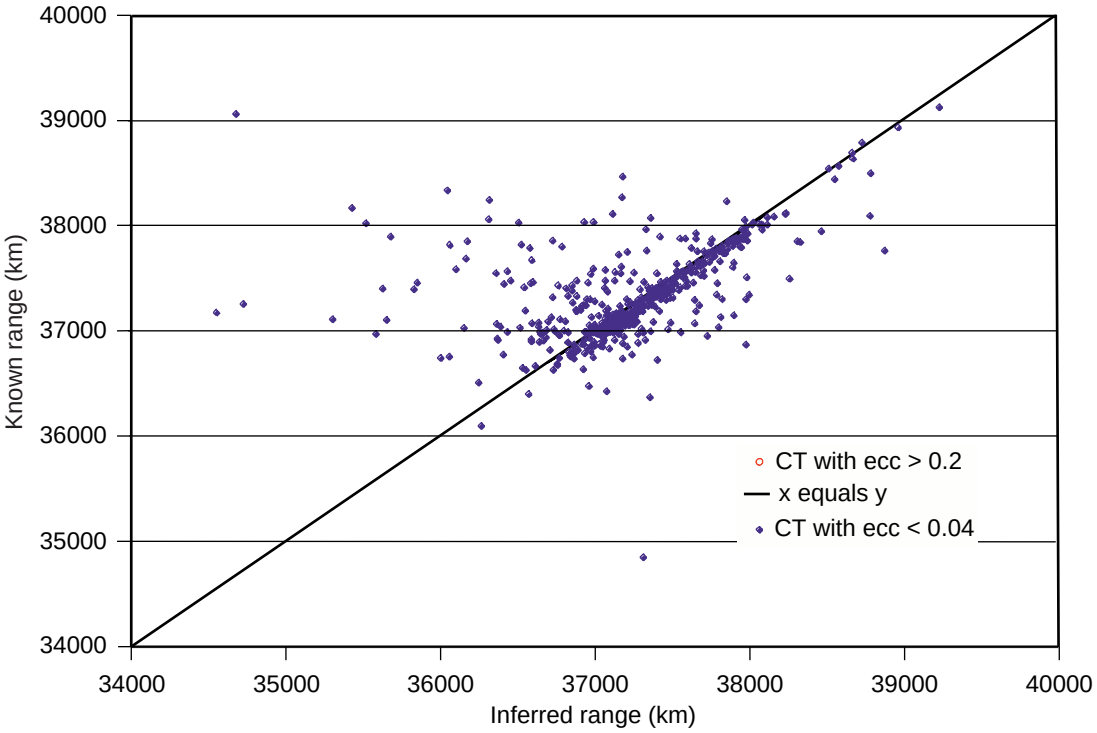

Figure 25: Comparison of inferred and known ranges, concise view.

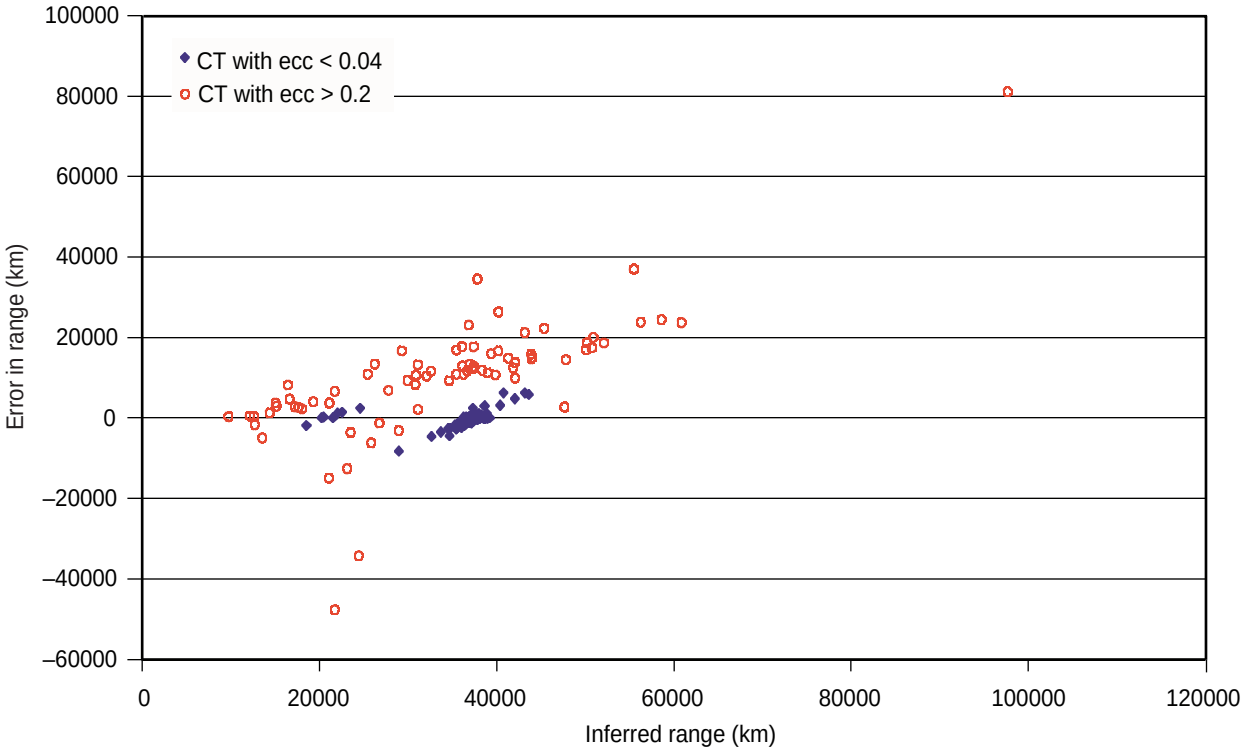

Figure 26: Range error, entire range.

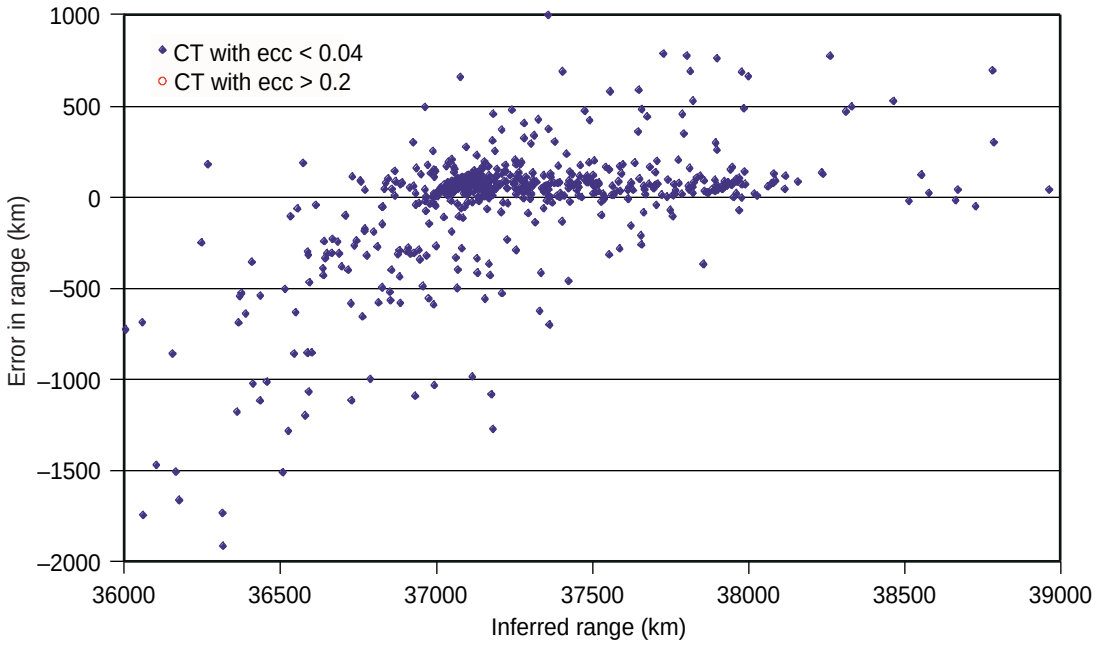

Figure 27: Range error, concise range.

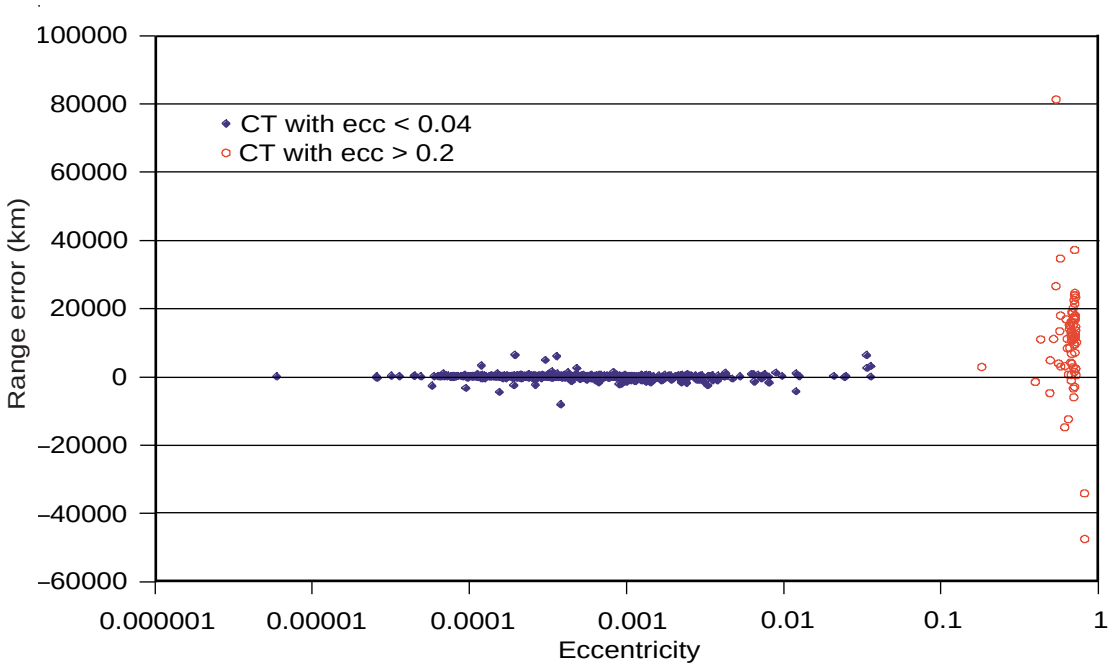

Figure 28: Range error as a function of eccentricity, entire range.

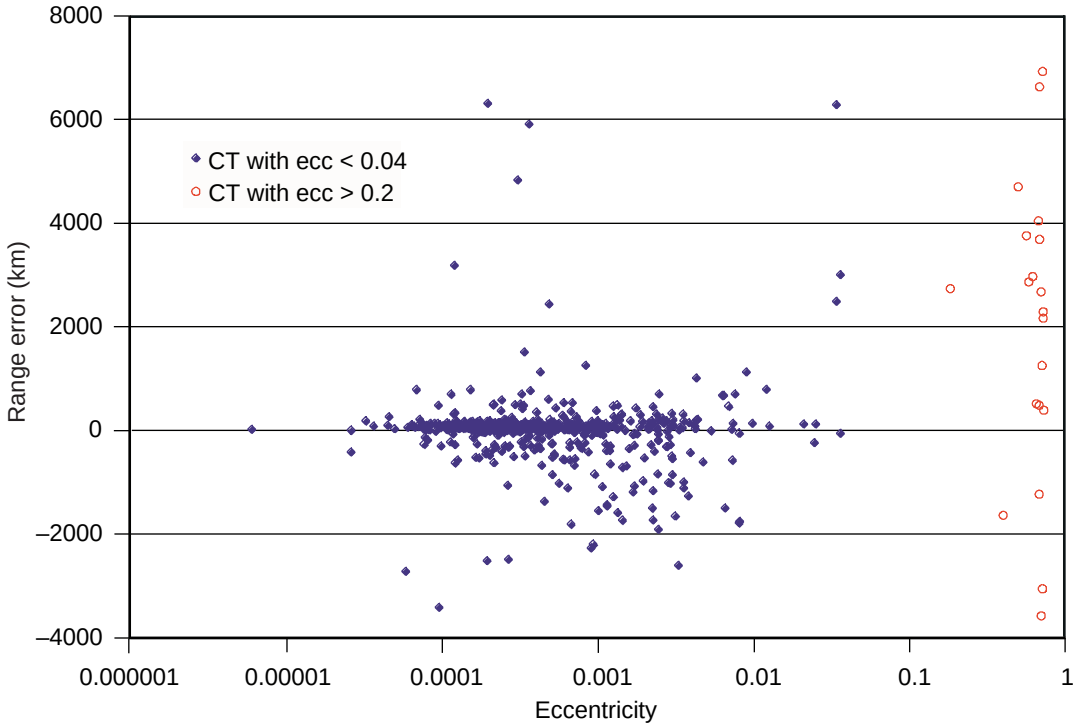

Figure 29: Range error as a function of eccentricity, concise range.

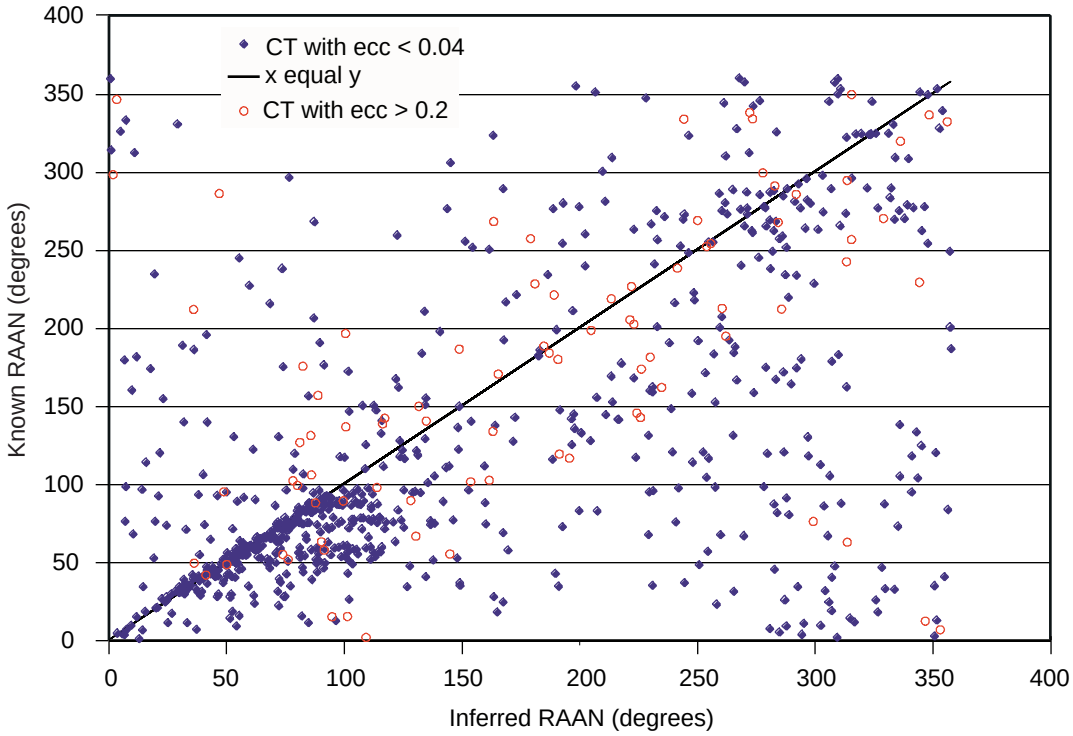

Figure 30: Comparison of inferred and known RAAN, entire range.

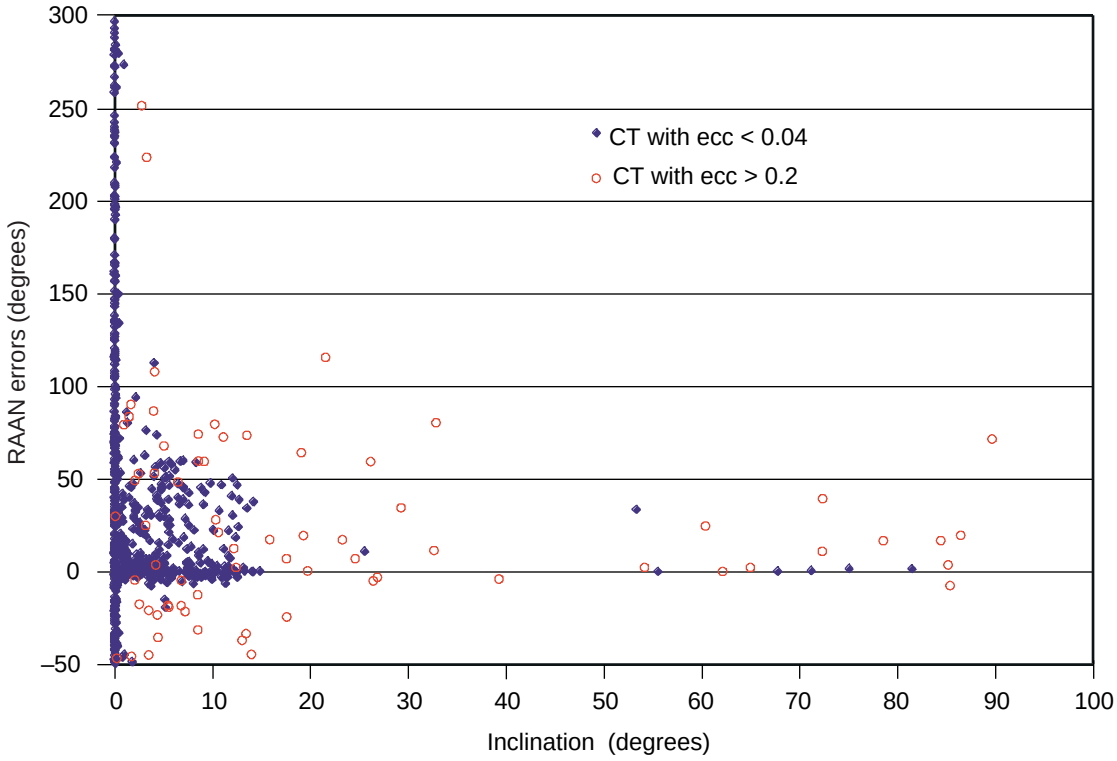

Figure 31: RAAN error as a function of inclination, entire range.

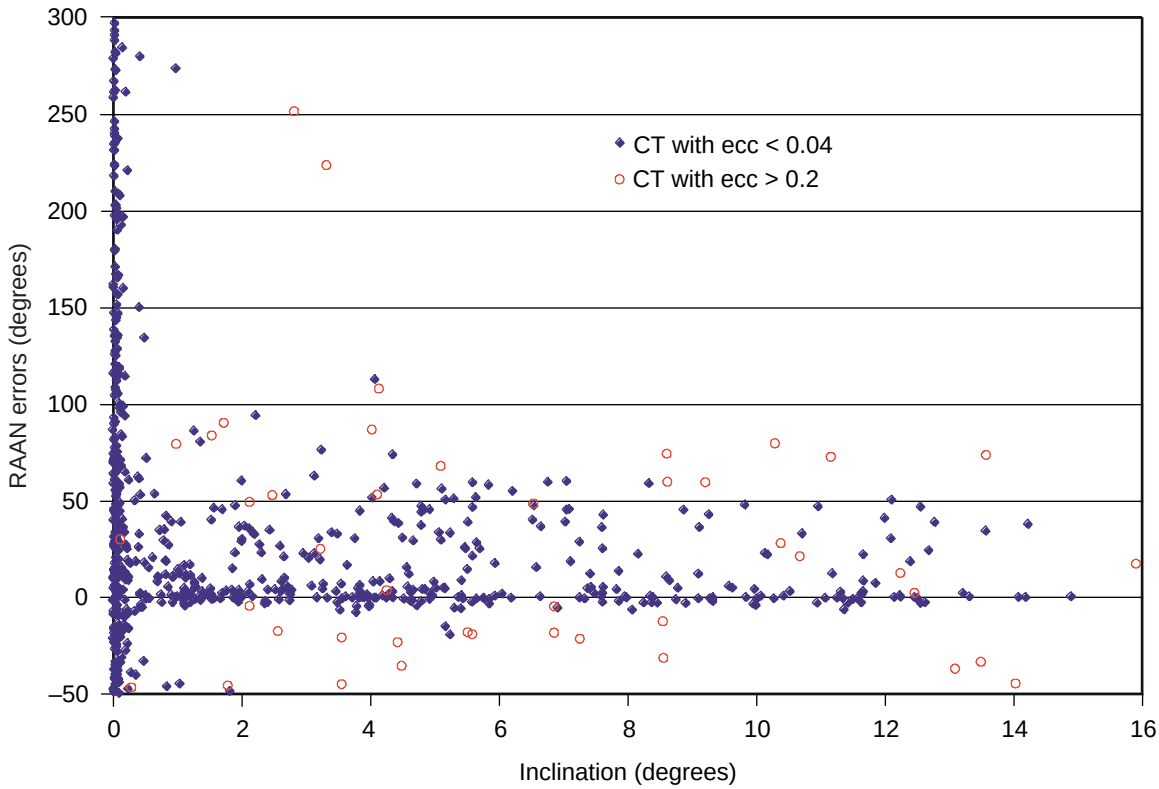

Figure 32: RAAN error as a function of incination, concise range.

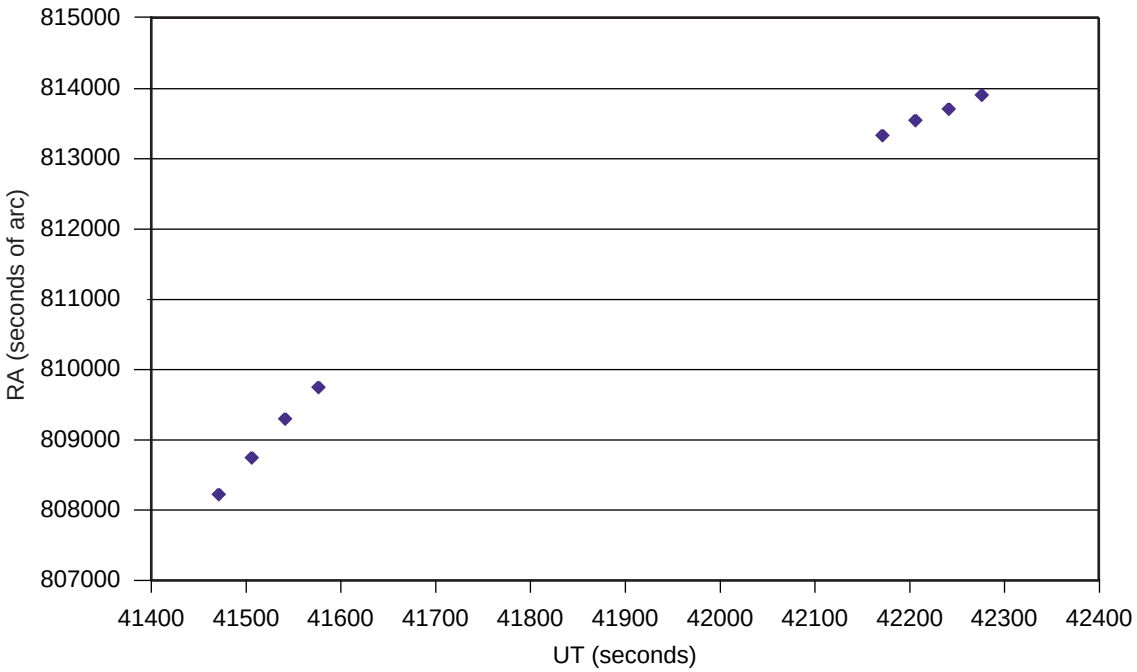

Figure 33: RA rate of change for two different objects.

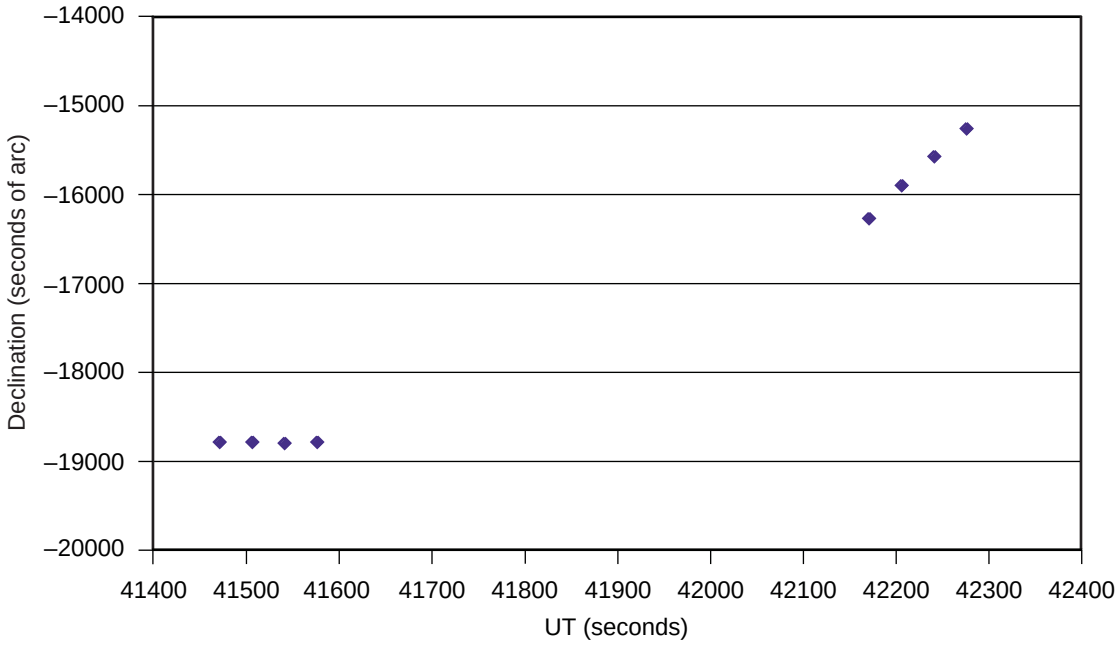

Figure 34: Declination rate of change for two different objects.

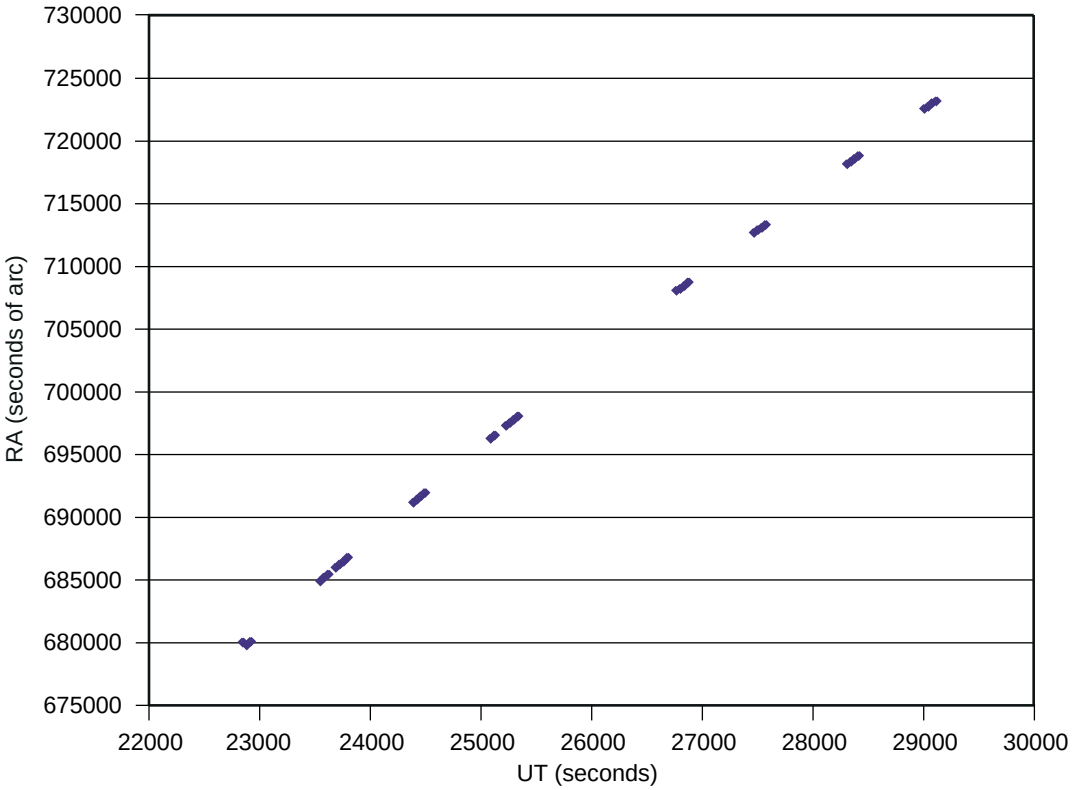

Figure 35: RA rate of change for a long UCT track.

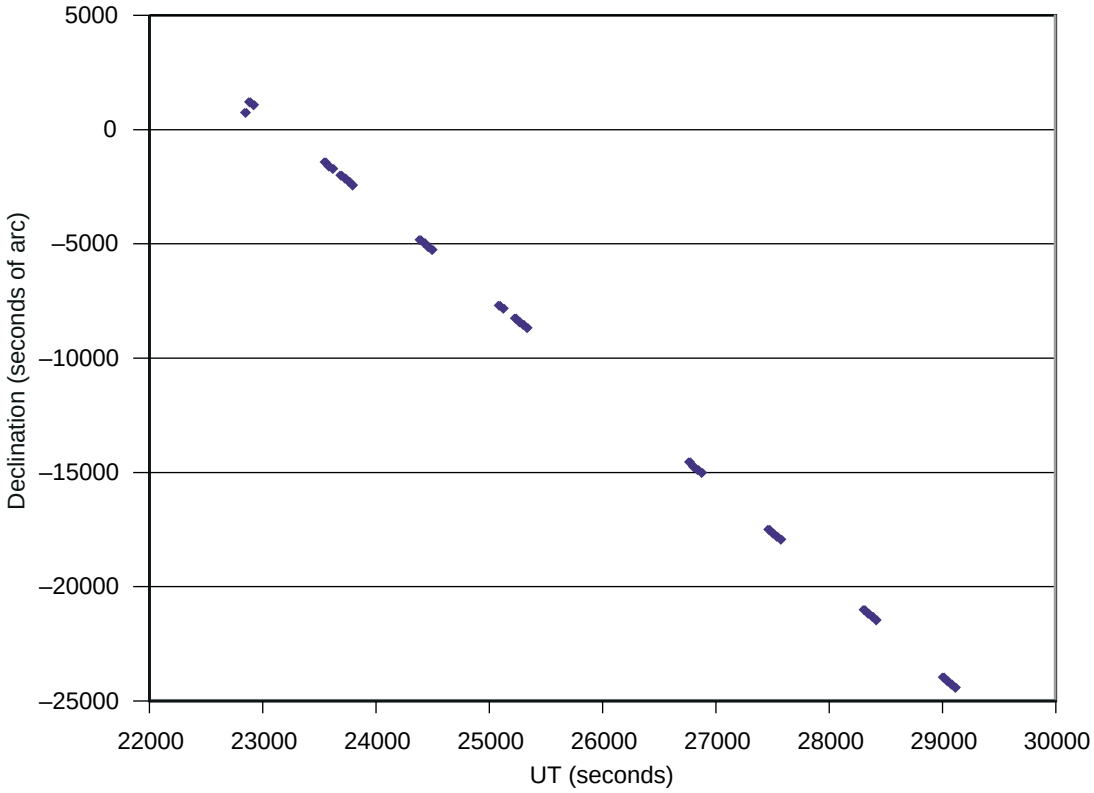

Figure 36: Declination rate of change for a long UCT track.

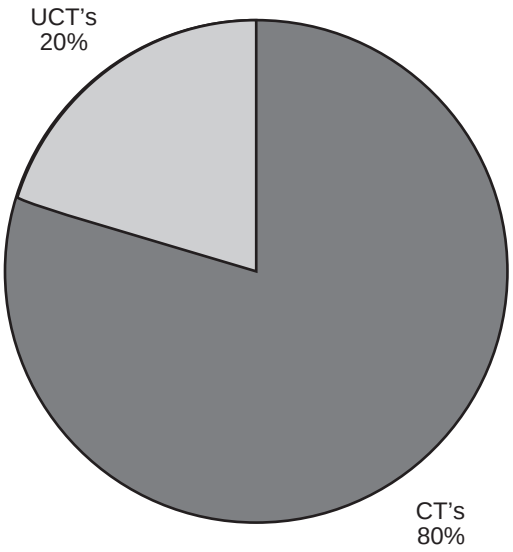

Figure 37: Pie chart for detections.

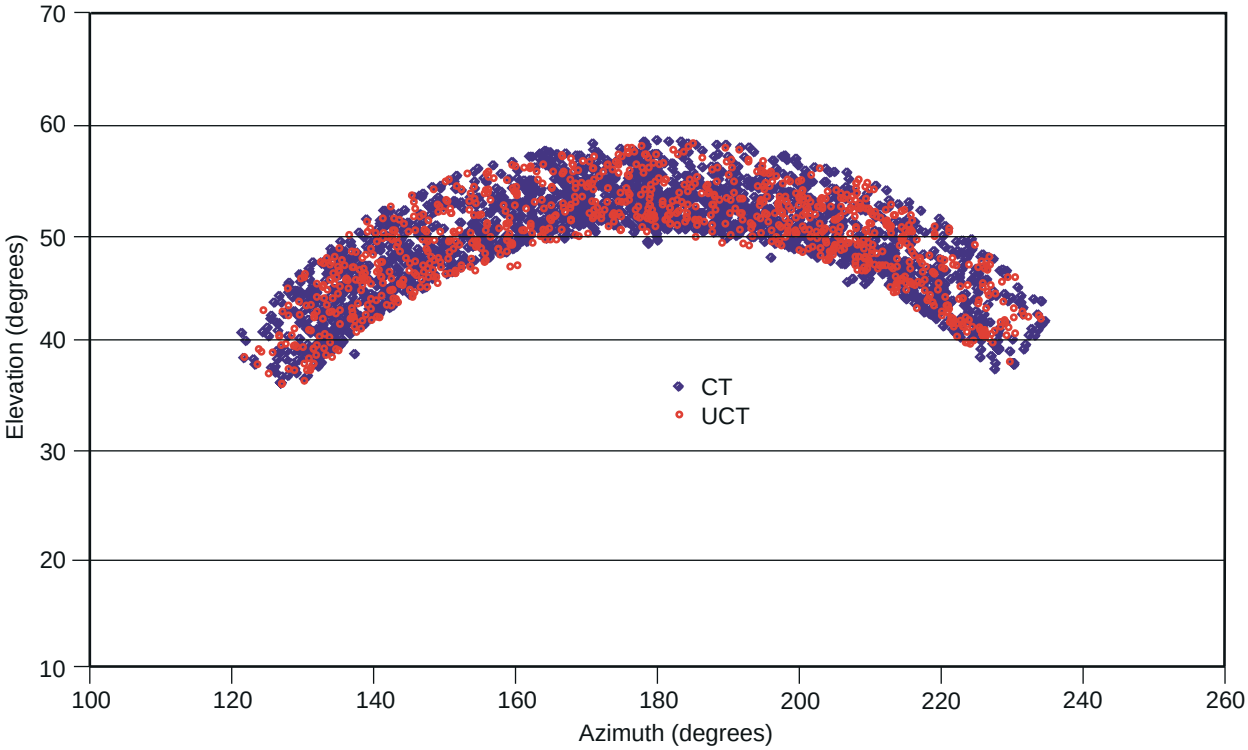

Figure 38: Distribution of detections, CT and UCT for 1998.

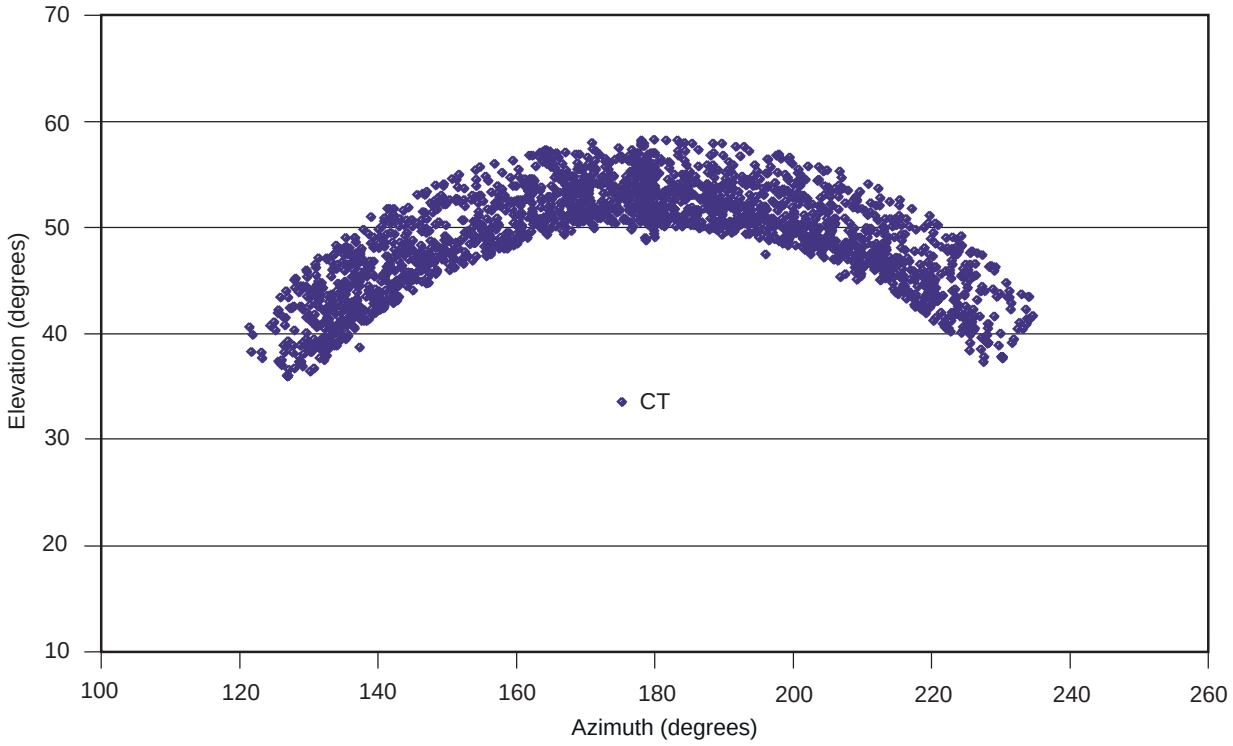

Figure 39: Distribution of detections, CT-only observations.

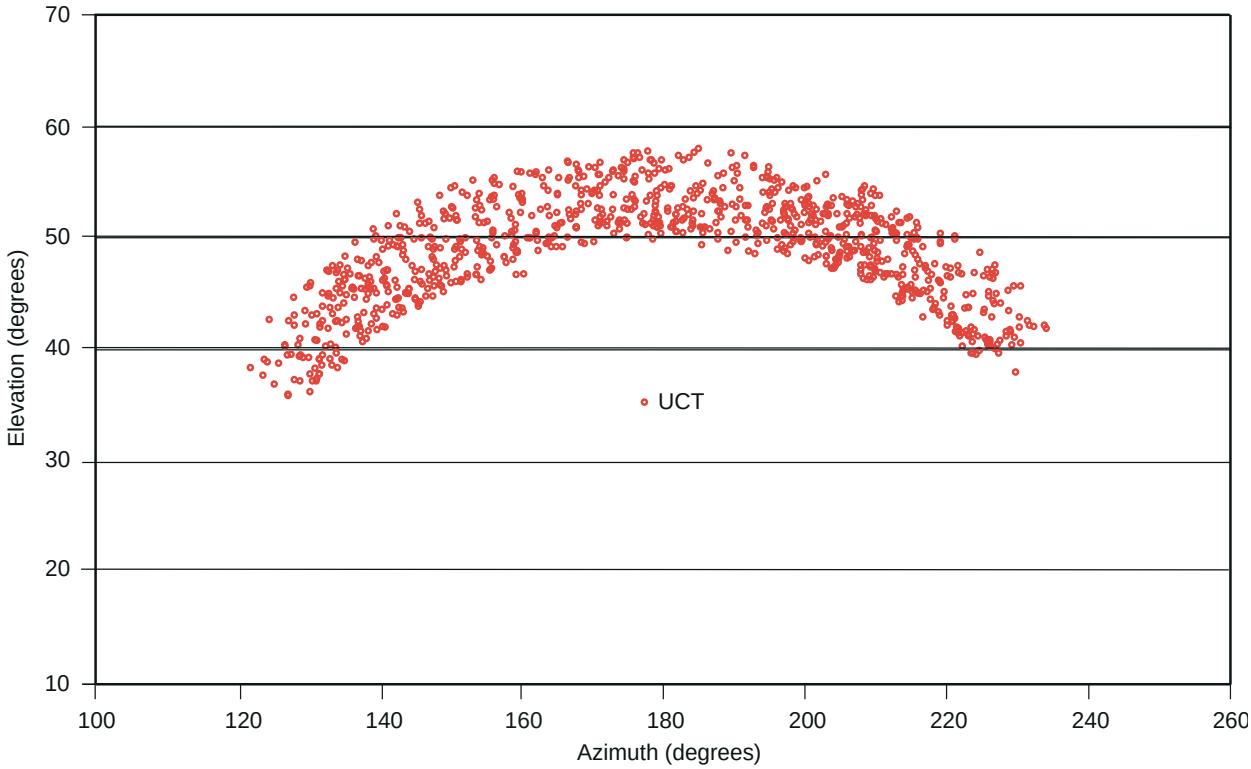

Figure 40: Distribution of detections, UCT-only observations.

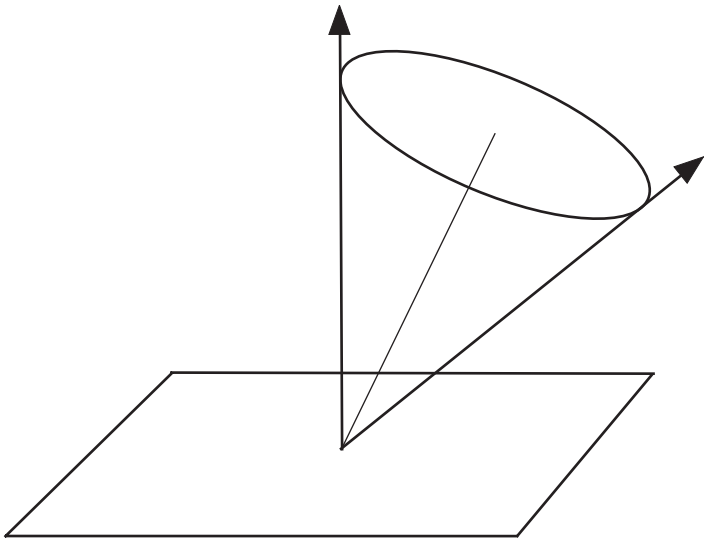

Figure 41: Angular momentum vector of an orbit.

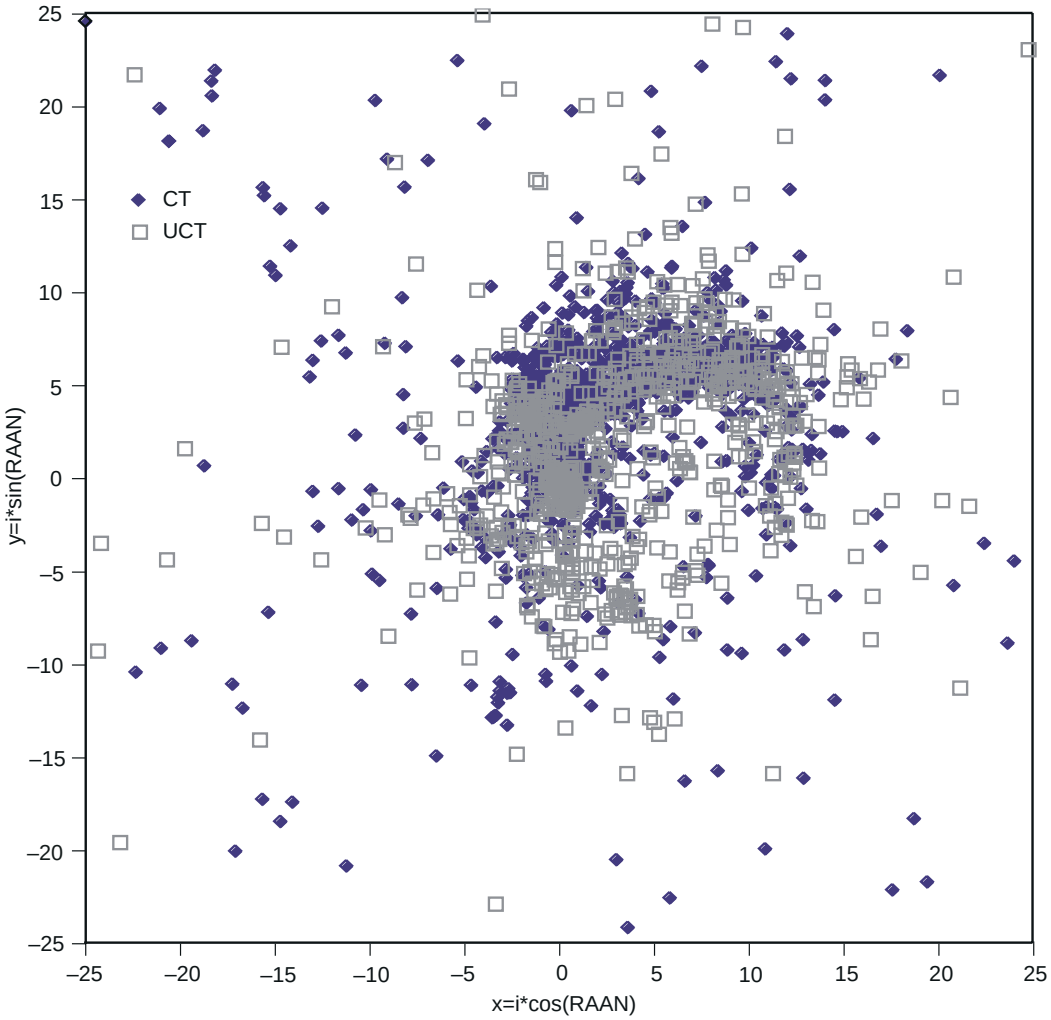

Figure 42: Polar coordinates for objects, entire range.

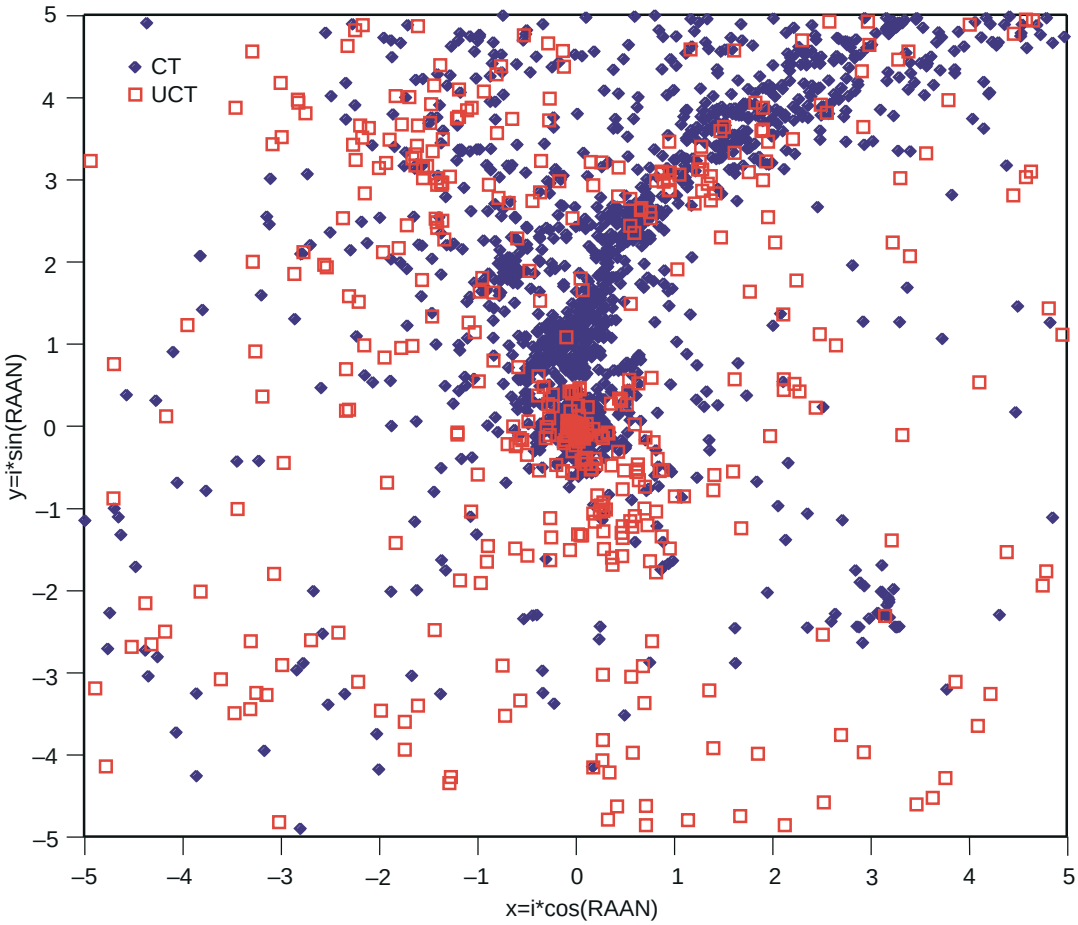

Figure 43: Polar plot, concise range.

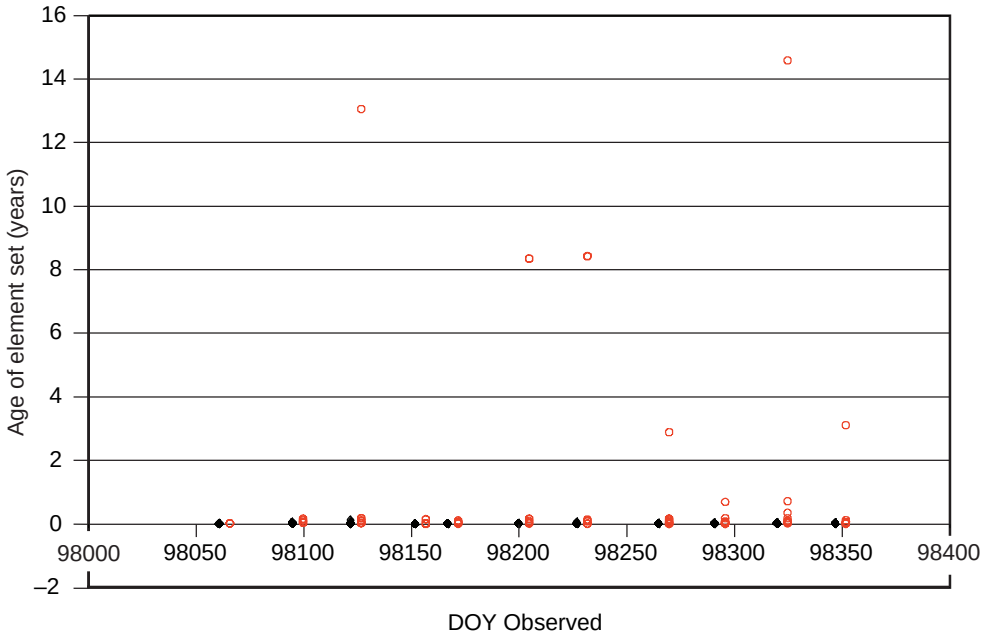

Figure 44: Epoch comparison for CT and nosees, entire range, age in years.

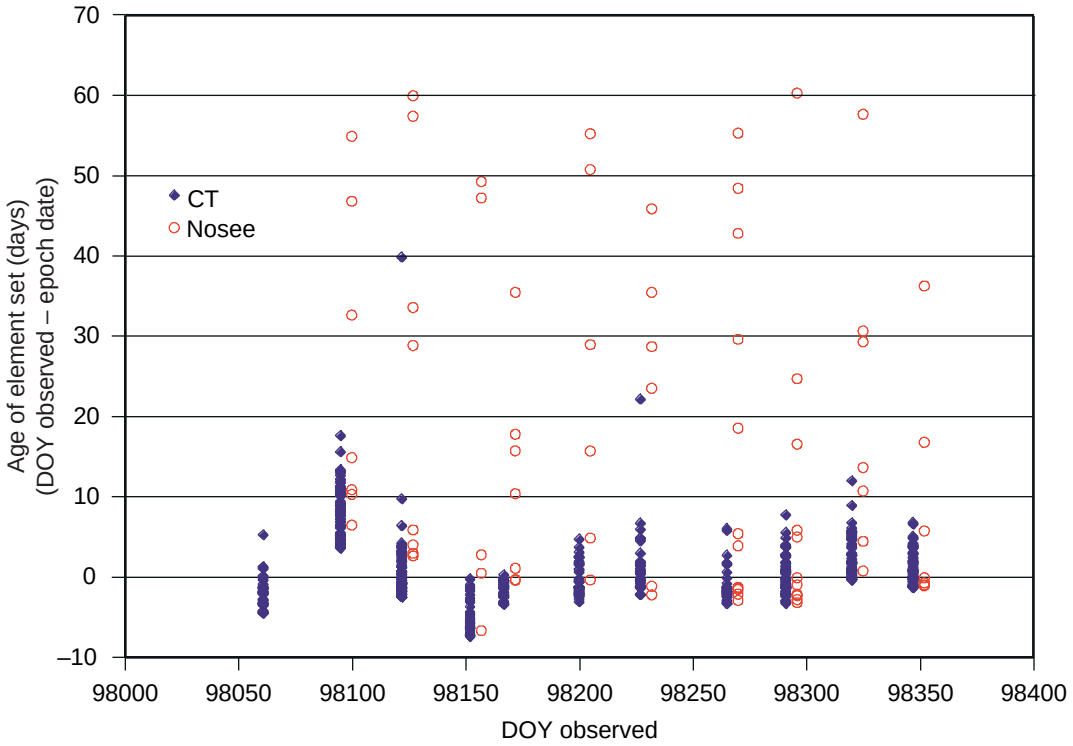

Figure 45: Epoch comparison for CTs and nosees, concise range, age in days.

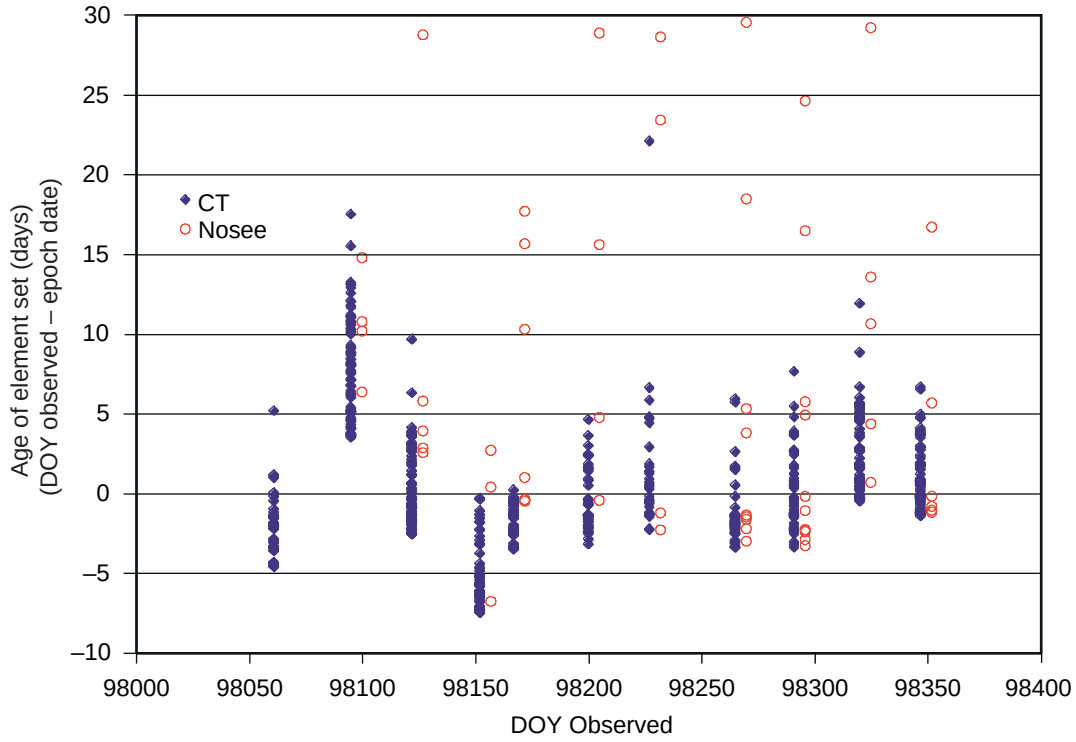

Figure 46: Epoch comparison for CT and nosees, more concise range.

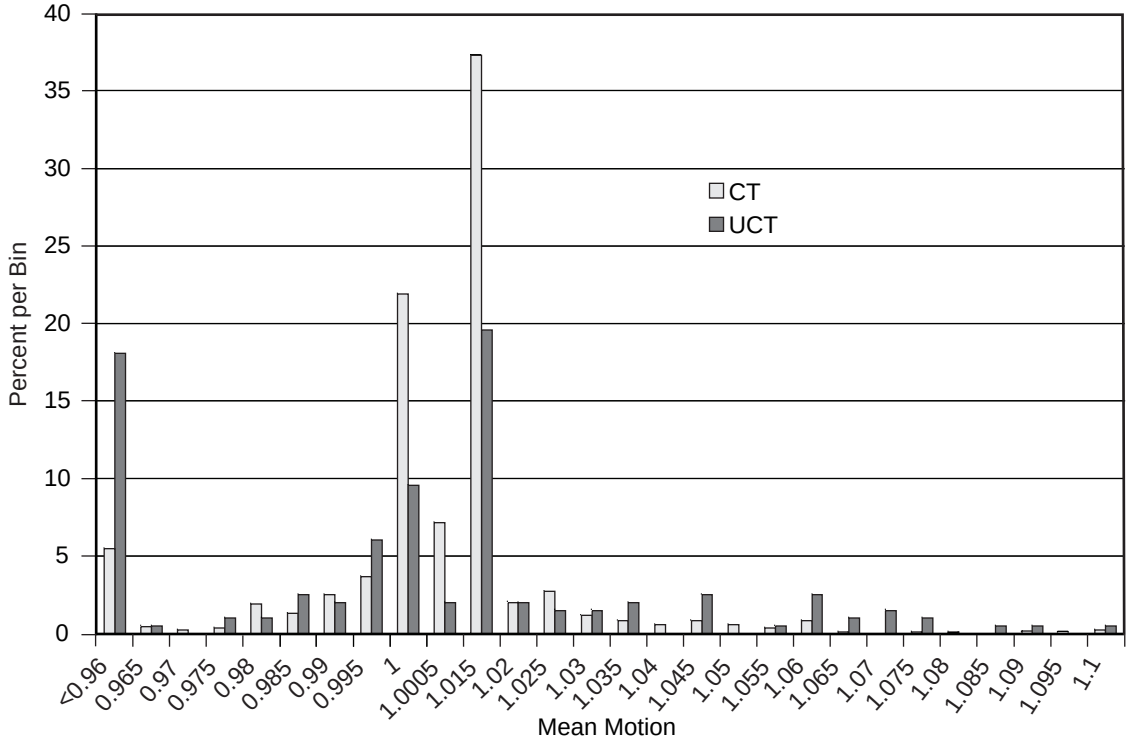

Figure 47: Mean motion distribution for CT and UCT objects.

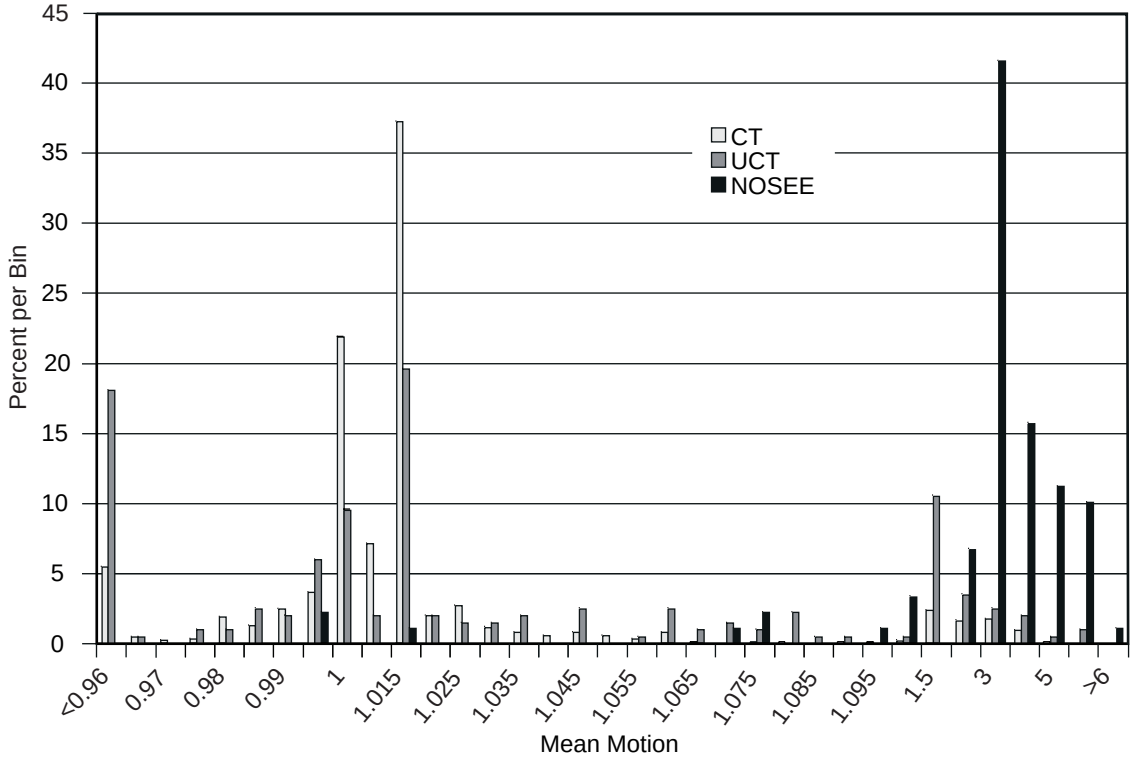

Figure 48: Mean motions for CT, UCT, and nosee objects.

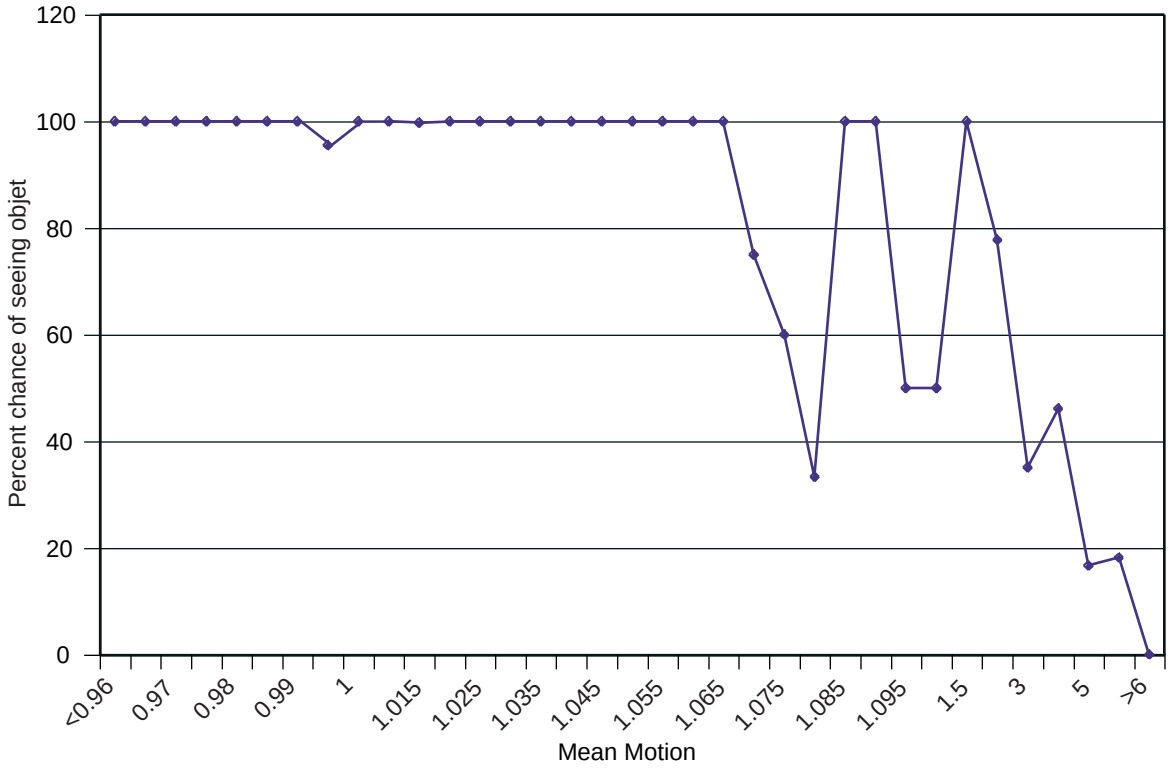

Figure 49: Percent chance of seeing an object at a specific mean motion.

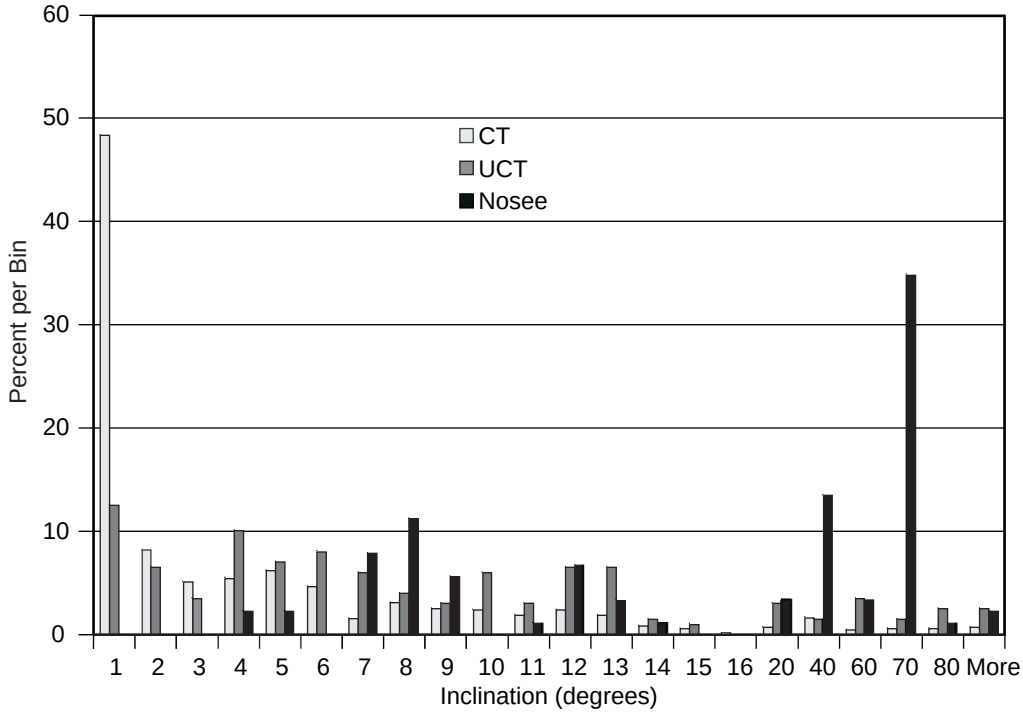

Figure 50: Distribution of inclinations for CT, UCT, and nosee objects, entire range.

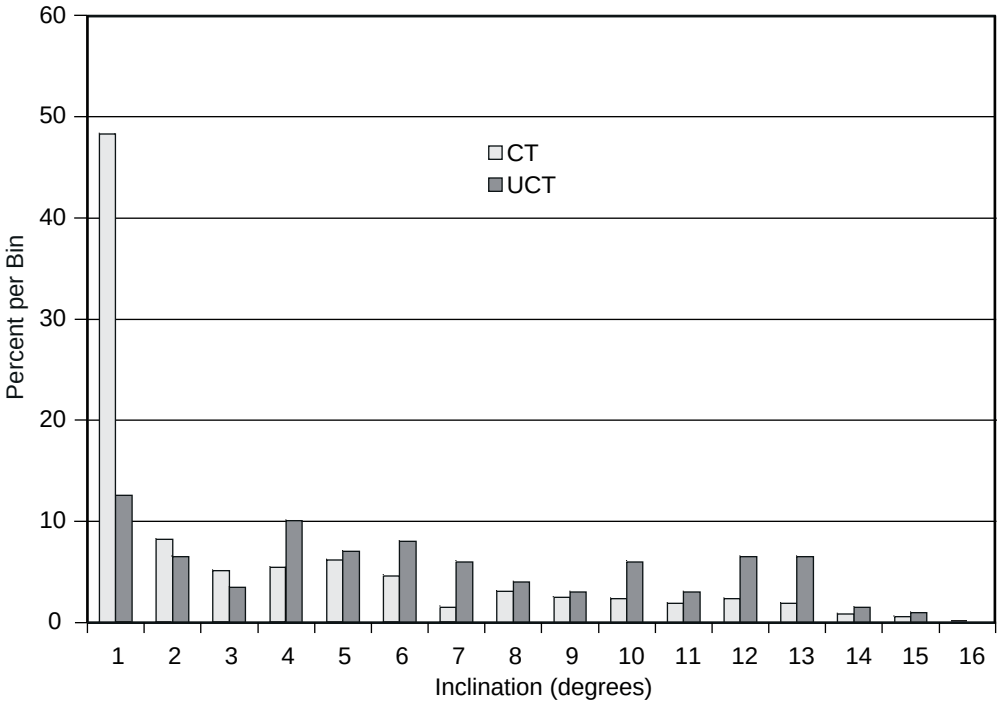

Figure 51: Distribution of inclinations for CT and UCT objects, selected range.

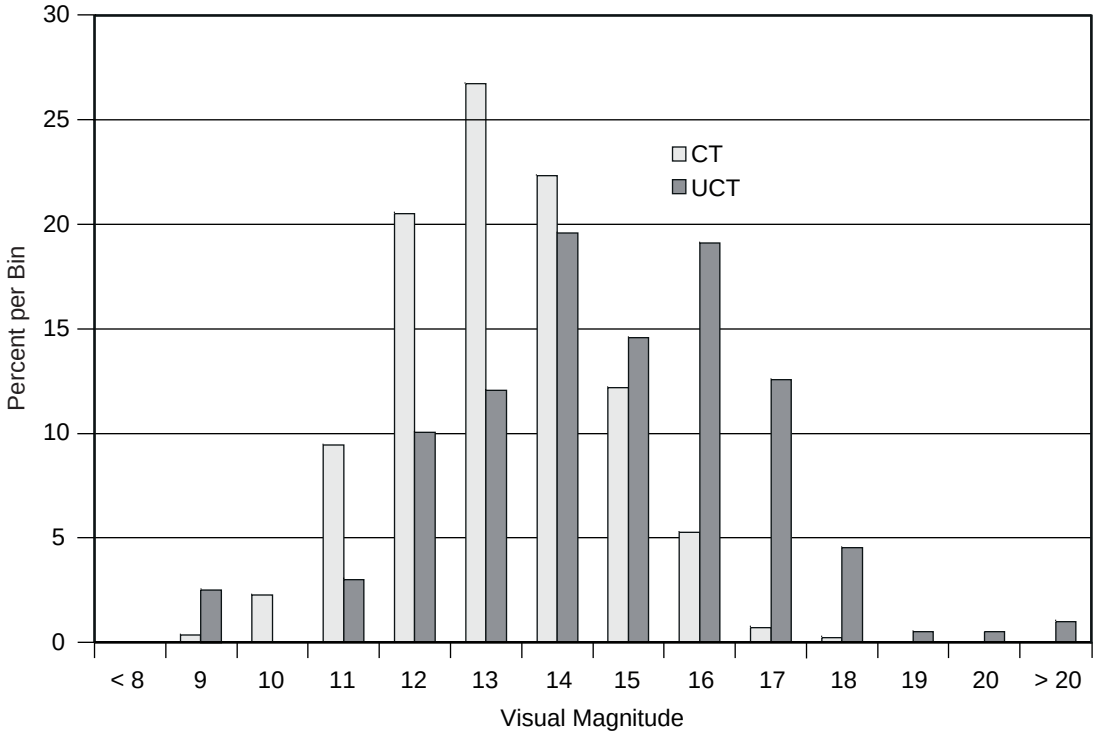

Figure 52: Visual magnitude distribution for detections.

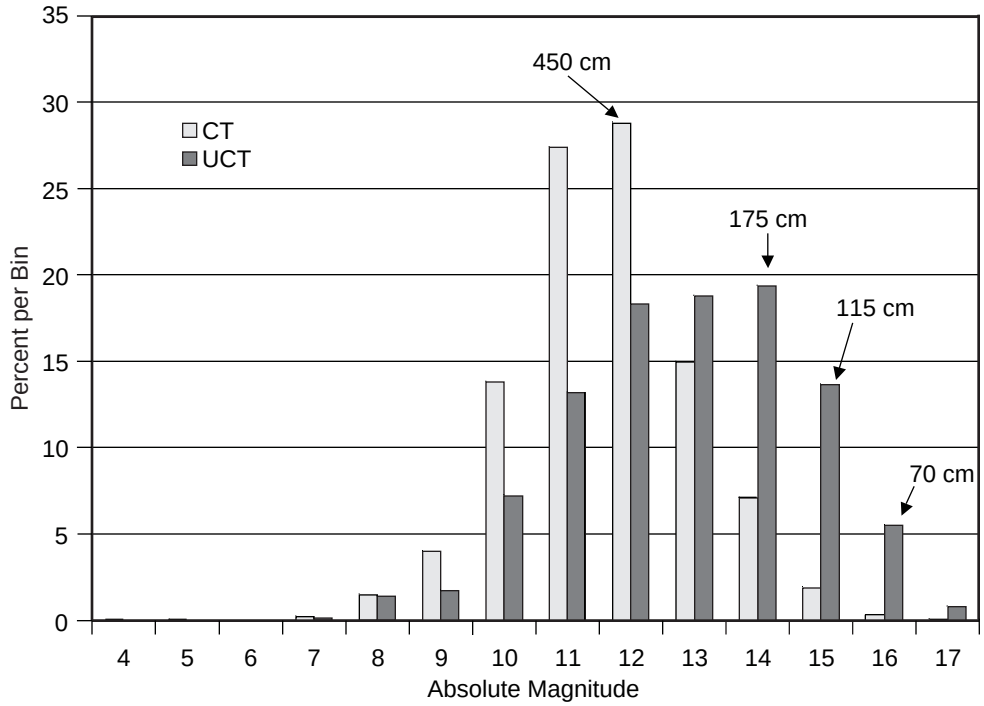

Figure 53: Absolute magnitude and derived size distribution.

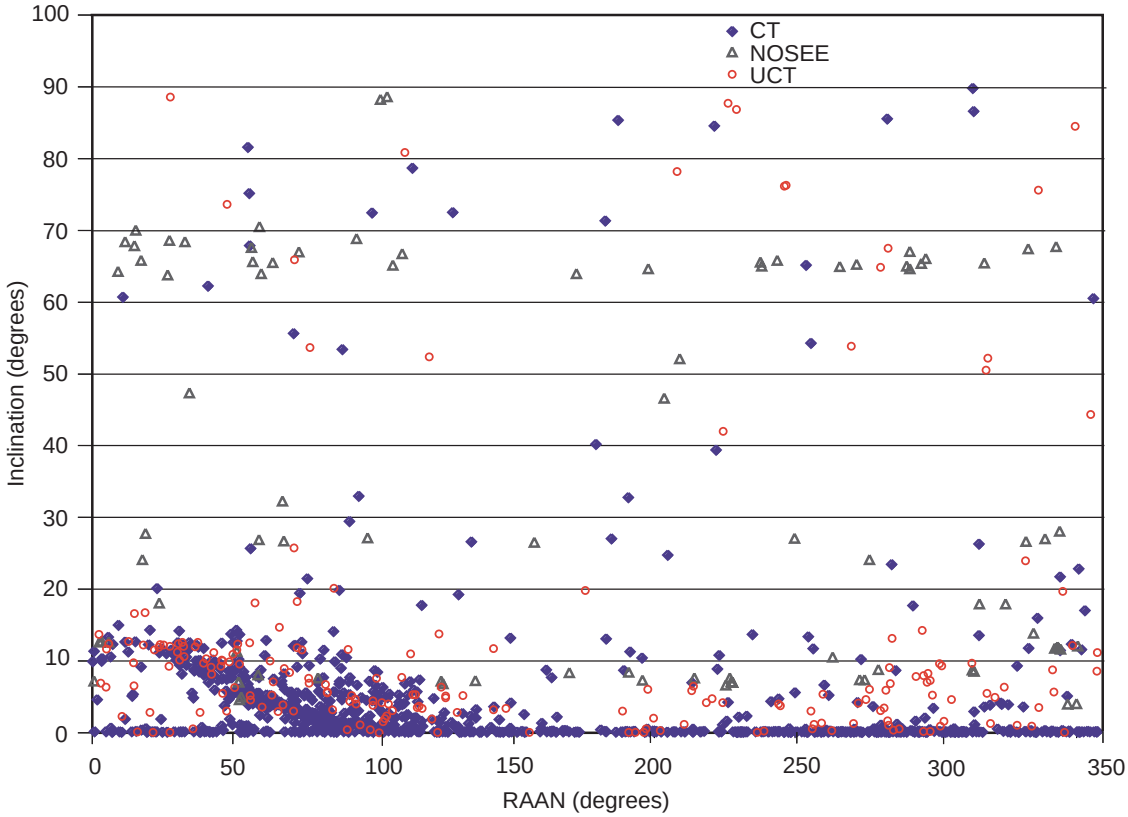

Figure 54: RAAN vs. inclination for CT, UCT, and nosee objects, entire range; 11-day sample.

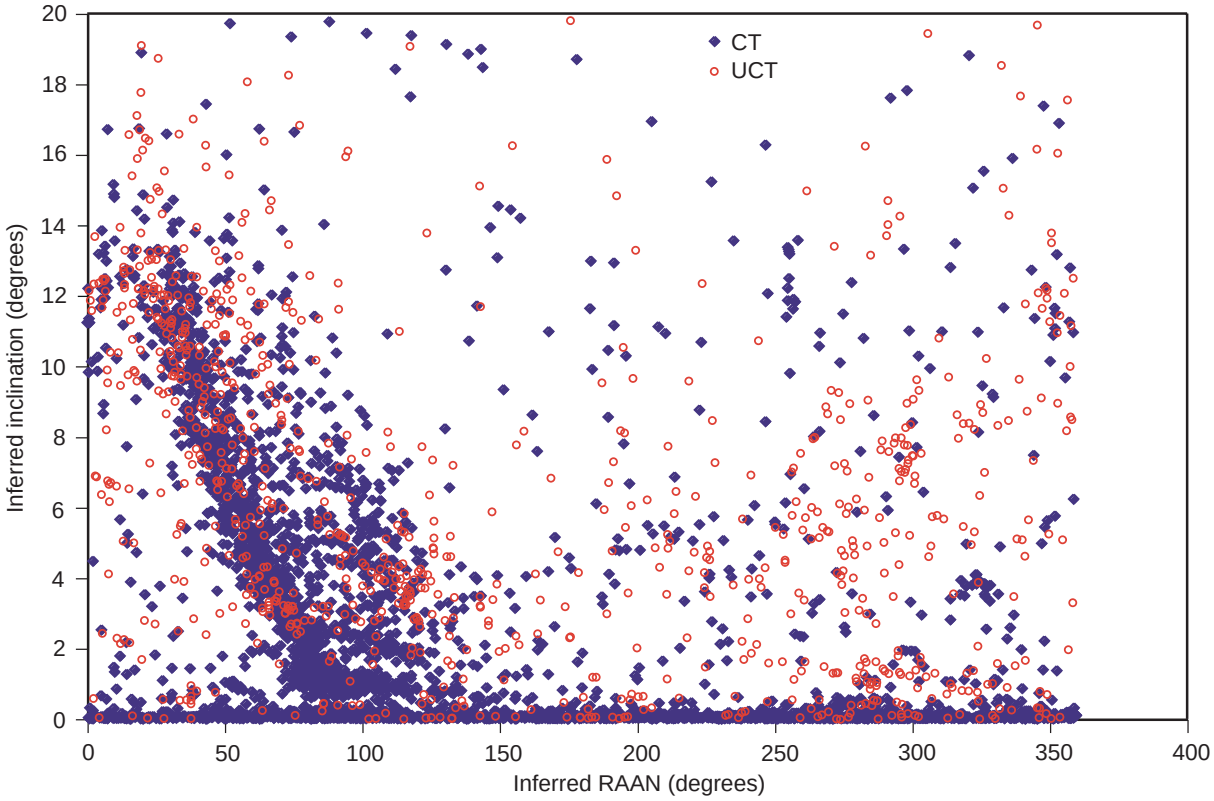

Figure 55: RAAN vs. inclination, CT and UCT observations, concise range; 58 nights.

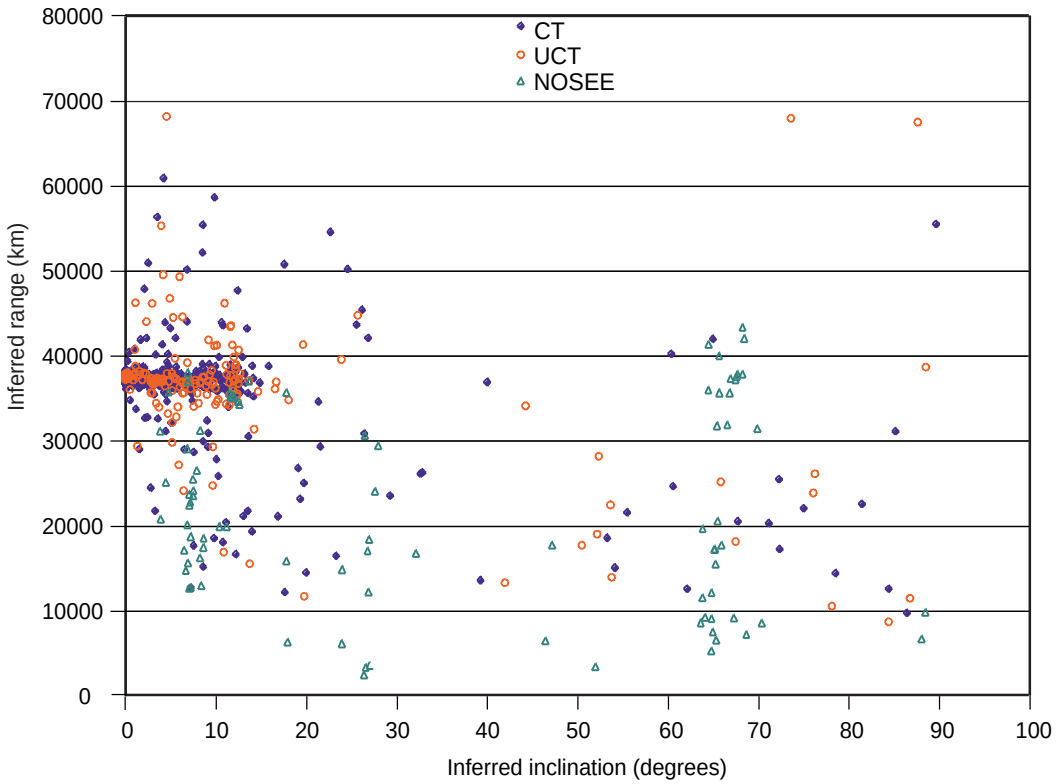

Figure 56: Inclination vs. range, CT, UCT, and nosee observations, entire range; 11-day sample.

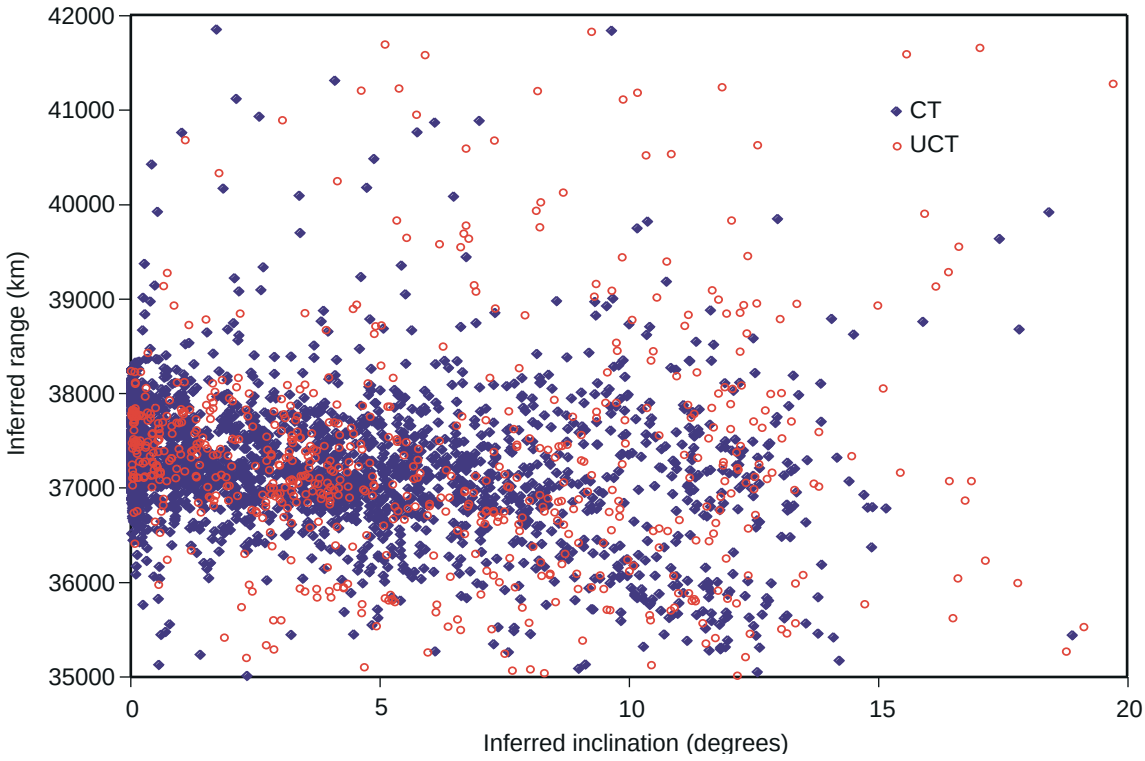

Figure 57: Inclination vs. range, CT and UCT observations, concise range; 58 nights.

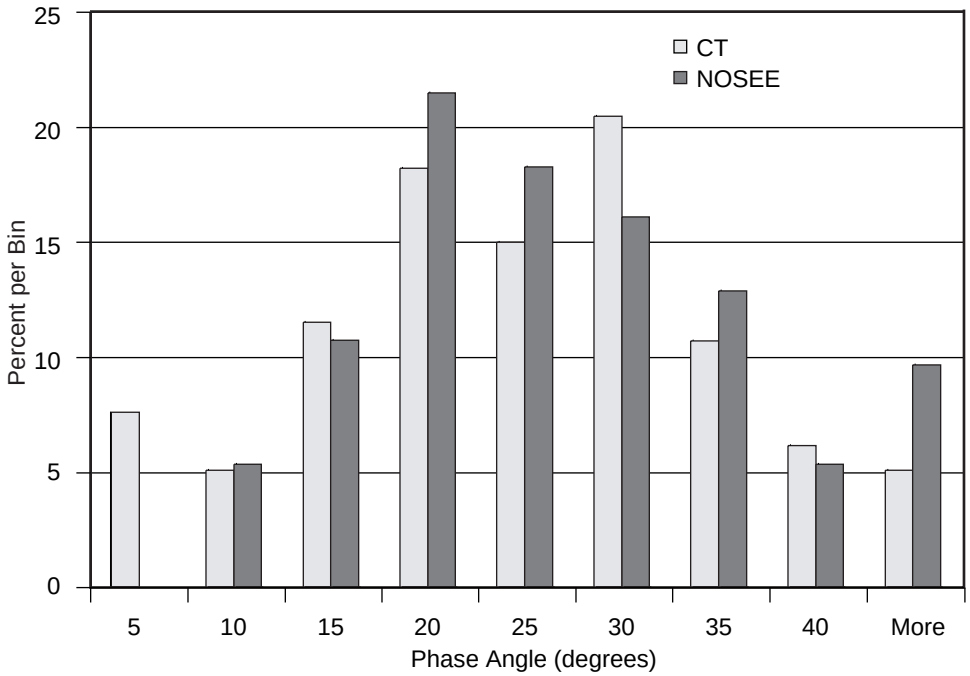

Figure 58: Phase angle for CT and nosee objects.

APPENDIX A
Telescope Control File

HA = Hour Angle (degrees)
DEC = Declination (degrees)
RA = Right Ascension (degrees)
UT = Universal Time (seconds)

HA	DEC	RA	UT
–33.600	–1.600	56.650	19635.9
–33.454	–1.600	56.650	19670.9
–33.454	–1.600	56.796	19705.9
–33.308	–1.600	56.796	19740.9
–33.600	–3.200	57.235	19775.9
–33.454	–3.200	57.235	19810.9
–33.454	–3.200	57.381	19845.9
–33.308	–3.200	57.381	19880.9
–33.600	–4.800	57.820	19915.9
–33.454	–4.800	57.820	19950.9
–33.454	–4.800	57.965	19985.9
–33.308	–4.800	57.965	20020.9
–33.600	–6.400	58.405	20055.9
–33.454	–6.400	58.405	20090.9
–33.454	–6.400	58.550	20125.9
–33.308	–6.400	58.550	20160.9
–33.600	–8.000	58.990	20195.9
–33.454	–8.000	58.990	20230.9
–33.454	–8.000	59.135	20265.9
–33.308	–8.000	59.135	20300.9
–32.000	–1.600	57.974	20335.9
–31.854	–1.600	57.974	20370.9
–31.854	–1.600	58.120	20405.9
–31.708	–1.600	58.120	20440.9
–32.000	–3.200	58.559	20475.9
–31.854	–3.200	58.559	20510.9
–31.854	–3.200	58.705	20545.9
–31.708	–3.200	58.705	20580.9
–32.000	–4.800	59.144	20615.9
–31.854	–4.800	59.144	20650.9
–31.854	–4.800	59.290	20685.9
–31.708	–4.800	59.290	20720.9
–32.000	–6.400	59.729	20755.9
–31.854	–6.400	59.729	20790.9
–31.854	–6.400	59.875	20825.9
–31.708	–6.400	59.875	20860.9
–32.000	–8.000	60.314	20895.9

APPENDIX B

Astro Output File

```
# astro version 1.4 - Automated Astrometry Output
# Created on:  Fri, 25-Jun-99 23:03:47
# Created by:  africano
# Input file:  G0884311fd.98.03.28.1.subset.fits
# Site:  Cloudcroft
# Sensor name:  Cloudcroft
# Sensor ID:  231
# Track Mode:  stare
# Object name:  G0884311fd
# Image start date:  28/03/98
# Image start time:  11:44:31.445988
# Image exposure:  19.99001  seconds
# Image filter: Clear
# Image header RA:  15:19:36.000
# Image header Dec:  –4.800
# Image airmass:  1.
# Star Catalog:  GSC
# Detected Stars in FOV:  201
# Weather:  Green
# Catalog Stars in FOV:  100
# Catalog Stars Matched:  57
# Highest Coeff. Fit:  6
# Objects:  2

[Catalog Star Match Results]

True Center RA:  15:20:09.23          Dec:  –4:37:50.15
Center RA Bias:  8.3090 (arcmin)      Dec Bias:  10.1642
Camera Rotation:  –0.901 (degrees)

[3 Coeff. Plate Solution]

Fit error:  Chi^2_x: 39.11    Chi^2_y:  13.98    Number of stars:  34
No    Term        Xi           Error          Eta          Error
1        x      12.512        0.001467    12.523        0.001919
2        y       0.037605    0.001422    –0.008676    0.001832
3        1      –0.70368      0.1822        0.070259    0.4393

[6 Coeff. Plate Solution]

Fit error:  Chi^2_x: 20.02   Chi^2_y: 14.89   Number of stars: 26
No    Term        Xi           Error          Eta          Error
```

APPENDIX C

1	x	12.481	0.001832	12.526	0.001919
2	y	0.026365	0.001919	–0.007705	0.001832
3	1	0.57041	0.4393	–0.27761	0.4393
4	x2	1.3752E-4	1.6860E-5	–1.011E-4	1.7620E-5
5	xy	1.1352E-4	1.7970E-5	–2.625E-5	1.7970E-5
6	y2	2.5342E-4	1.7620E-5	3.0407E-5	1.6860E-5

[Differential Photometry]

ZeroPoint: 24.014 Std Dev: 0.39979 Photometric Stars: 39

[Catalog Star Astrometry]

Name	X Center	Y Center	
Catalog RA	Image RA	Catalog Dec	Image Dec
Catalog Mag	Image Mag	Catalog Mag Err	Image Mag Err
Xi 3 Error	Eta 3 Error	Xi 6 Error	Eta 6 Error
GSC5010.0405	108.00		204.00
15:22:04.474	15:22:04.423	–4:46:38.35	-4:46:36.29
10.44	9.87	0.00	0.00
–9.57	4.96	–4.91	3.93
GSC5010.0708	383.00	70.00	
15:18:14.599	15:18:15.223	–5:14:34.91	–5:14:36.21
9.66	10.02	0.00	0.00
1.21	3.91	INDEF	INDEF
GSC5010.0835	302.00	334.00	
15:19:22.920	15:19:22.665	–4:19:33.20	–4:19:28.11
10.31	10.19	0.00	0.00
–2.48	1.02	–1.82	0.89
GSC5010.0619	142.00	135.00	
15:21:36.353	15:21:36.004	–5:01:02.10	–5:01:01.68
10.75	10.34	0.00	0.00
–2.37	5.2	-0.46	5.57
GSC5010.0685	122.00	403.00	
15:21:54.110	15:21:53.529	–4:05:10.64	–4:05:06.93
9.71	10.35	0.00	0.00
4.72	0.79	3.05	2.25
GSC5010.0594	147.00	71.00	
15:21:32.570	15:21:31.998	–5:14:34.08	–5:14:24.96
10.48	10.35	0.00	0.00
5.67	–5.43	2.84	–3.12

APPENDIX C (Continued)

GSC5010.0842	393.00	105.00	
15:18:05.916	15:18:06.764	–5:07:19.16	–5:07:16.40
11.27	10.51	0.00	0.00
–5.02	1.24	INDEF	INDEF
GSC5010.0303	271.00	224.00	
15:19:49.349	15:19:48.222	–4:42:30.10	–4:42:25.70
11.09	10.64	0.00	0.00
9.25	1.93	INDEF	INDEF
GSC5010.0774	245.00	399.00	
15:20:10.838	15:20:10.616	–4:05:58.13	–4:05:56.33
11.51	10.67	0.00	0.00
–1.37	2.75	–2.3	4.18
GSC5010.0409	255.00	452.00	
15:20:02.098	15:20:02.677	–3:54:54.14	–3:54:54.35
10.51	10.73	0.00	0.00
–9.04	3.03	INDEF	INDEF
GSC5010.0273	467.00	200.00	
15:17:05.652	15:17:05.078	–4:47:30.91	–4:47:22.23
10.46	10.74	0.00	0.00
INDEF	INDEF	2.94	–2.67
GSC5011.0959	44.00	315.00	
15:22:57.754	15:22:58.359	–4:23:36.38	-–4:23:26.03
10.60	10.94	0.00	0.00
INDEF	INDEF	INDEF	INDEF
GSC5010.0699	229.00	238.00	
15:20:23.657	15:20:23.295	–4:39:39.82	–4:39:30.63
10.39	11.06	0.00	0.00
–3.88	–2.73	–0.25	–3.2
GSC5010.0712	474.00	433.00	
15:16:59.582	15:17:00.046	–3:58:52.82	–3:58:45.86
11.07	11.16	0.00	0.00
0.36	–1.01	INDEF	INDEF
GSC5010.0071	154.00	360.00	
15:21:27.197	15:21:26.449	–4:14:10.61	–4:14:04.22
11.31	11.21	0.00	0.00
3.78	–0.84	5.54	-0.42
GSC5011.0019	33.00	383.00	
15:23:06.835	15:23:07.992	–4:09:20.41	–4:09:16.02
11.39	11.23	0.00	0.00
INDEF	INDEF	INDEF	INDEF

APPENDIX C (Continued)

GSC5011.0357	59.00	228.00	
15:22:45.845	15:22:45.496	–4:41:48.16	–4:41:35.01
11.72	11.28	0.00	0.00
–4.83	–5.45	–0.47	–7.18
GSC5010.0653	83.00	278.00	
15:22:26.314	15:22:25.516	–4:31:12.86	–4:31:09.39
11.37	11.30	0.00	0.00
2.08	3.8	6.26	2.5
GSC5010.0332	156.00	448.00	
15:21:25.819	15:21:25.429	–3:55:50.59	–3:55:45.11
10.87	11.33	0.00	0.00
5.37	–2.69	0.21	0.49
GSC5010.0567	132.00	348.00	
15:21:43.750	15:21:44.795	–4:16:37.42	–4:16:34.19
11.35	11.33	0.00	0.00
INDEF	INDEF	INDEF	INDEF
GSC5010.0543	119.00	82.00	
15:21:56.002	15:21:55.373	–5:12:14.83	–5:12:06.54
10.95	11.40	0.00	0.00
5.04	–3.89	3.7	–2.3
GSC5011.0431	23.00	125.00	
15:23:14.486	15:23:15.659	–5:03:12.20	–5:03:05.19
11.82	11.45	0.00	0.00
INDEF	INDEF	INDEF	INDEF
GSC5010.0725	302.00	132.00	
15:19:23.201	15:19:22.437	–5:01:49.08	–5:01:39.05
11.84	11.58	0.00	0.00
10.	–5.35	5.74	–4.03
GSC5010.0067	112.00	118.00	
15:22:01.090	15:22:01.131	–5:04:39.83	–5:04:34.64
11.61	11.62	0.00	0.00
-7.58	0.36	–6.31	0.8
GSC5010.0393	386.00	358.00	
15:18:11.971	15:18:12.783	–4:14:34.84	–4:14:26.10
12.13	11.70	0.00	0.00
INDEF	INDEF	INDEF	INDEF
GSC5010.0505	183.00	282.00	
15:21:02.882	15:21:01.836	–4:30:21.28	–4:30:19.83
11.36	11.79	0.00	0.00
5.51	5.1	INDEF	INDEF

APPENDIX C (Continued)

GSC5010.0496	234.00	128.00	
15:20:18.262	15:20:19.156	–5:02:32.24	–5:02:29.75
12.20	11.86	0.00	0.00
INDEF	INDEF	INDEF	INDEF
GSC5010.0854	413.00	50.00	
15:17:50.558	15:17:50.387	–5:18:48.20	–5:18:46.84
12.34	11.90	0.00	0.00
INDEF	INDEF	–3.13	4.65
GSC5010.0181	448.00	252.00	
15:17:20.352	15:17:20.879	–4:36:41.15	–4:36:31.09
11.89	12.06	0.00	0.00
-5.03	–2.51	INDEF	INDEF
GSC5011.0323	17.00	392.00	
15:23:22.469	15:23:21.485	–4:07:26.15	–4:07:23.39
12.03	12.07	0.00	0.00
INDEF	INDEF	INDEF	INDEF
GSC5010.0074	97.00	146.00	
15:22:14.246	15:22:13.640	–4:58:49.40	–4:58:43.21
12.43	12.07	0.00	0.00
0.53	0.17	3.37	–0.2
GSC5011.0353	17.00	223.00	
15:23:21.806	15:23:20.700	–4:42:50.04	–4:42:36.85
12.40	12.11	0.00	0.00
INDEF	INDEF	INDEF	INDEF
GSC5011.0463	25.00	54.00	
15:23:14.830	15:23:14.179	–5:18:00.43	–5:17:56.22
11.52	12.14	0.00	0.00
7.32	0.75	INDEF	INDEF
GSC5010.0287	114.00	422.00	
15:22:01.255	15:22:00.380	–4:01:16.10	–4:01:09.66
11.73	12.17	0.00	0.00
INDEF	INDEF	INDEF	INDEF
GSC5010.0834	317.00	344.00	
15:19:10.051	15:19:10.203	–4:17:24.83	–4:17:22.77
12.02	12.19	0.00	0.00
–7.71	3.98	–7.9	3.92
GSC5011.0699	69.00	56.00	
15:22:36.727	15:22:37.314	–5:17:39.95	–5:17:32.14
11.88	12.28	0.00	0.00
11.4	–3.55	INDEF	INDEF

APPENDIX C (Continued)

GSC5010.0800	126.00	380.00	
15:21:50.357	15:21:50.016	–4:10:01.81	–4:09:54.25
12.25	12.31	0.00	0.00
–0.7	–2.39	–0.54	–1.59
GSC5010.0263	136.00	417.00	
15:21:40.454	15:21:41.913	–4:02:22.06	–4:02:12.12
12.11	12.34	0.00	0.00
INDEF	INDEF	INDEF	INDEF
GSC5011.0593	47.00	322.00	
15:22:55.193	15:22:55.877	–4:22:02.75	–4:21:58.54
11.88	12.35	0.00	0.00
INDEF	INDEF	INDEF	INDEF

[Object Astrometry]

Name	X Center	Y Center	
Name	Date	Time	
Name	Image RA	Image Dec	
Name	Image Mag	Image Mag Err	Filter
90001	238.83	345.87	
90001	28/03/98	11:44:31.445988	
90001	15:20:05.452	–4:17:00.44	
90001	12.91	INDEF	Clear
90001	238.83	345.87	
90001	28/03/98	11:44:51.435998	
90001	15:20:25.442	–4:17:00.44	
90001	12.91	INDEF	Clear
90002	386.78	138.80	
90002	28/03/98	11:44:31.445988	
90002	15:18:01.838	–5:00:12.26	
90002	12.83	INDEF	Clear
90002	386.78	138.80	
90002	28/03/98	11:44:51.435998	
90002	15:18:21.828	–5:00:12.26	
90002	12.83	INDEF	Clear

APPENDIX C (Concluded)

Correlation Output File
G0884311fd.98.03.28.1.ast
START TIME =11:44:31 YEAR = 98
TRUE RA and DEC center: 15:20: 9 –4:37:50
NUMBER OF OBJECTS DETECTED = 2
[Object Astrometry]

Name	X Center	Y Center	
Name	Date	Time	
Name	Image RA	Image Dec	
Name	Image Mag	Image Mag Err	Filter
21041	238.83	345.87	
21041	28/03/98	11:44:31.445988	
21041	15:20:05.452	-4:17:00.44	
21041	12.91	INDEF	Clear
21041	238.83	345.87	
21041	28/03/98	11:44:51.435998	
21041	15:20:25.442	–4:17:00.44	
21041	12.91	INDEF	Clear
13637	386.78	138.80	
13637	28/03/98	11:44:31.445988	
13637	15:18:01.838	–5:00:12.26	
13637	12.83	INDEF	Clear
13637	386.78	138.80	
13637	28/03/98	11:44:51.435998	
13637	15:18:21.828	–5:00:12.26	
13637	12.83	INDEF	Clear

SSN 13637 RA = 15:18: 5 DEC = –5: 0:25
SATELITE X AND Y PIXEL POSITION = 396.9 145.8

SSN 13652 RA = 15:16:18 DEC = –4:26:16
SATELITE X AND Y PIXEL POSITION = 525.4 309.7

SSN 21041 RA = 15:19:46 DEC = –4:16:16
SATELITE X AND Y PIXEL POSITION = 276.0 357.7

3 SATELLITES PREDICTED BY SGP4 TO BE IN THE FIELD OF VIEW
********** ********** **********

REPORT DOCUMENTATION PAGE

Form Approved
OMB No. 0704-0188

Public reporting burden for this collection of information is estimated to average 1 hour per response, including the time for reviewing instructions, searching existing data sources, gathering and maintaining the data needed, and completing and reviewing the collection of information. Send comments regarding this burden estimate or any other aspect of this collection of information, including suggestions for reducing this burden, to Washington Headquarters Services, Directorate for Information Operations and Reports, 1215 Jefferson Davis Highway, Suite 1204, Arlington, VA 22202-4302, and to the Office of Management and Budget, Paperwork Reduction Project (0704-0188), Washington, DC 20503.

1. AGENCY USE ONLY *(Leave Blank)*	2. REPORT DATE	3. REPORT TYPE AND DATES COVERED
	April 2002	NASA Technical Paper

4. TITLE AND SUBTITLE
A Log Logistic Survival Model Applied to Hypobaric Decompression Sickness

5. FUNDING NUMBERS

6. AUTHOR(S)
K. S. Jarvis;* T. L. Thumm;* K. Jorgensen;** J. L. Africano;*** P. F. Sydney;*** M. J. Matney;* E. G. Stansbery;** M. K. Mulrooney****

7. PERFORMING ORGANIZATION NAME(S) AND ADDRESS(ES)

Lyndon B. Johnson Space Center
Houston, Texas 77058

8. PERFORMING ORGANIZATION REPORT NUMBERS
S-883

9. SPONSORING/MONITORING AGENCY NAME(S) AND ADDRESS(ES)

National Aeronautics and Space Administration
Washington, DC 20546-0001

10. SPONSORING/MONITORING AGENCY REPORT NUMBER
TP-2002-210773

11. SUPPLEMENTARY NOTES
*Lockheed Martin Space Operations, Houston, TX; **Lyndon B. Johnson Space Center, Houston, TX; ***Boeing North American, Colorado Springs, CO; ****Ariel Research Company, Houston, TX

12a. DISTRIBUTION/AVAILABILITY STATEMENT

Available from the NASA Center for AeroSpace Information (CASI)
7121 Standard
Hanover, MD 21076-1320 Category: 88

12b. DISTRIBUTION CODE

13. ABSTRACT *(Maximum 200 words)*
NASA has been using the charged coupled device (CCD) debris telescope (CDT)—a transportable 32-cm Schmidt telescope located near Cloudcroft, New Mexico—to help characterize the debris environment in geosynchronous Earth orbit (GEO). The CDT is equipped with a SITe 512 x 512 CCD camera whose 24 m2 (12.5 arc sec) pixels produce a 1.7 x 1.7-deg field of view. The CDT system can therefore detect 17th-magnitude objects in a 20-sec integration corresponding to an ~0.6-m diameter, 0.20 albedo object at 36,000 km. The telescope pointing and CCD operation are computer controlled to collect data automatically for an entire night. The CDT has collected more than 1500 hrs of data since November 1997. This report describes the collection and analysis of 58 nights (~420 hrs) of data acquired in 1998.

14. SUBJECT TERMS	15. NUMBER OF PAGES	16. PRICE CODE
charged coupled devices; debris; space debris; telescopes; Earth orbital environments; geosynchronous orbits; Schmidt cameras; Schmidt telescope	68	

17. SECURITY CLASSIFICATION OF REPORT	18. SECURITY CLASSIFICATION OF THIS PAGE	19. SECURITY CLASSIFICATION OF ABSTRACT	20. LIMITATION OF ABSTRACT
Unclassified	Unclassified	Unlimited	Unlimited